

# Baseline Design Summary



**August, 2012**



**Rare Isotope Science Project**

## List of Contributors

Jung Keun Ahn<sup>2</sup>, Dong Hyun An<sup>3</sup>, Kwang-yun Baek<sup>2</sup>, Seung Won Baek<sup>4</sup>, Jung-Bae Bahng<sup>5</sup>, Sang-in Bak<sup>29</sup>, Dae-sik Chang<sup>28</sup>, Byunggu Cheon<sup>21</sup>, Myung-Ki Cheoun<sup>6</sup>, Dong-hyun Cho<sup>8</sup>, Hee-Suk Cho<sup>2</sup>, Bong Hyuk Choi<sup>1</sup>, Chang-il, Choi<sup>39</sup>, Chul Jin Choi<sup>1</sup>, Eun-mi Choi<sup>42</sup>, Han-woo Choi<sup>31</sup>, Hyo-jung Choi<sup>29</sup>, Kwang-Yong Choi<sup>7</sup>, Min Sik Choi<sup>46</sup>, Seonho Choi<sup>9</sup>, Su Yong Choi<sup>8</sup>, Tae-Keun Choi<sup>26</sup>, Yeon Suk Choi<sup>23</sup>, Hyun Tai Chung<sup>9</sup>, Kie Hyung Chung<sup>36</sup>, Yeon Sei Chung<sup>1</sup>, Khalid M.M.Gad<sup>29</sup>, Eun Ja Ha<sup>6</sup>, Bo-young Han<sup>28</sup>, Jae Eun Han<sup>1</sup>, Jaemin Han<sup>28</sup>, Byungsik Hong<sup>8</sup>, In Seok Hong<sup>1</sup>, Wan Hong<sup>31</sup>, In-ho Huh<sup>29</sup>, Min Sup Hur<sup>42</sup>, Churl-kew Hwang<sup>1</sup>, Ji-Gwang Hwang<sup>5</sup>, Sanghoon Hwang<sup>5</sup>, Won Joo Hwang<sup>1</sup>, Chang Ho Hyun<sup>10</sup>, Doh-Yun Jang<sup>28</sup>, Jaeho Jang<sup>13</sup>, Si-Won Jang<sup>5</sup>, Zeehoon Jang<sup>24</sup>, Dong O Jeon<sup>1</sup>, Doo Jeong<sup>29</sup>, Jae Min Jeong<sup>11</sup>, Seung Ho Jeong<sup>28</sup>, Sun-Chan Jeong<sup>37</sup>, Genie Jhang<sup>8</sup>, Kwang-ho Jo<sup>41</sup>, Jong Dae Joo<sup>1</sup>, Mi Joung Joung<sup>1</sup>, Hoe Chun Jung<sup>1</sup>, Yacine Kadi<sup>29</sup>, Byoung Hwi Kang<sup>1</sup>, Jeongsoo Kang<sup>21</sup>, Keon Wook Kang<sup>11</sup>, Sang Mook Kang<sup>21</sup>, A-ram Kim<sup>9</sup>, Byoung Chul Kim<sup>18</sup>, Do Gyun Kim<sup>1</sup>, Do-yoon Kim<sup>29</sup>, Dong-Eon Kim<sup>16</sup>, Dong Lak Kim<sup>23</sup>, Dong Uk Kim<sup>36</sup>, Eun-Joo Kim<sup>14</sup>, Eun-San Kim<sup>5</sup>, Geun Beom Kim<sup>3</sup>, Gi Dong Kim<sup>1</sup>, Hee-kyung Kim<sup>48</sup>, Hong joo Kim<sup>5</sup>, Hye Jin Kim<sup>5</sup>, Hyun-Chul Kim<sup>34</sup>, Hyung Jin Kim<sup>1</sup>, In Gyu Kim<sup>28</sup>, Jae Cheon Kim<sup>1</sup>, Jong Tae Kim<sup>29</sup>, Jong Won Kim<sup>1</sup>, Joon-kon Kim<sup>49</sup>, Kyung Il Kim<sup>1</sup>, Mi Jung Kim<sup>1</sup>, Myeongjin Kim<sup>1</sup>, Sang-ho Kim<sup>45</sup>, Sang-hoon Kim<sup>47</sup>, Seo-hee Kim<sup>29</sup>, Seong Jun Kim<sup>1</sup>, Sun Kee Kim<sup>1</sup>, Yong Kyun Kim<sup>1</sup>, Young Jin Kim<sup>1</sup>, Young Kwon Kim<sup>1</sup>, Yeong-sun Kim<sup>29</sup>, Youngman Kim<sup>1</sup>, Byeong Rok Ko<sup>8</sup>, Jin-a Ko<sup>29</sup>, Seung Kook Koh<sup>36</sup>, Jeong-Won Kwak<sup>15</sup>, Taeg-yong Kwon<sup>18</sup>, Young Kwan Kwon<sup>1</sup>, Byeong-no Lee<sup>28</sup>, Chang-Hwan Lee<sup>2</sup>, Cheol-Woo Lee<sup>28</sup>, Chi-hwan Lee<sup>44</sup>, Chun Sik Lee<sup>7</sup>, Hee-Jung Lee<sup>20</sup>, Hee-Seock Lee<sup>16</sup>, Hoseong Lee<sup>18</sup>, Hyo-Sang Lee<sup>2</sup>, Hyun Su Lee<sup>17</sup>, Jaeyu Lee<sup>13</sup>, Jeong Han Lee<sup>1</sup>, Ju Hahn Lee<sup>1</sup>, Kang Ok Lee<sup>36</sup>, Kang-Seog Lee<sup>27</sup>, Kwang-won Lee<sup>28</sup>, Kyong Sei Lee<sup>8</sup>, Sang-duk Lee<sup>29</sup>, Seok Kwan Lee<sup>46</sup>, Seung kyu Lee<sup>21</sup>, Su Houng Lee<sup>43</sup>, Young-Ouk Lee<sup>28</sup>, Young Sung Lee<sup>20</sup>, Gwon Lim<sup>28</sup>, Satarov Matlabjon<sup>11</sup>, Chang-Bum Moon<sup>19</sup>, Jun-Young Moon<sup>7</sup>, Shinwoo Nam<sup>1</sup>, Soon-Kwon Nam<sup>32</sup>, Won Namkung<sup>16</sup>, Bong Hoon Oh<sup>13</sup>, Byung-Hoon Oh<sup>28</sup>, Jin-hwan Oh<sup>29</sup>, Yongseok Oh<sup>5</sup>, Byung-yoon Park<sup>35</sup>, Gunn Tae Park<sup>1</sup>, Jin-a Park<sup>29</sup>, Jin Yong Park<sup>2</sup>, Junesic Park<sup>21</sup>, Ki Hyun Park<sup>13</sup>, Se-hwan Park<sup>28</sup>, Sung Jong Park<sup>1</sup>, Sung-Ho Park<sup>9</sup>, Tae-sun Park<sup>29</sup>, Wooyoon Park<sup>20</sup>, Yung-ho Park<sup>1</sup>, Chung-Yeol Ryu<sup>21</sup>, Min-Sang Ryu<sup>25</sup>, Chang Seok Seo<sup>1</sup>, Hee Jeong Seo<sup>36</sup>, Ik Jae Shin<sup>1</sup>, Jae-won Shin<sup>29</sup>, SeungWook Shin<sup>29</sup>, Kwang-souk Sim<sup>8</sup>, Woon-Young So<sup>38</sup>, Chang Wook Son<sup>40</sup>, Jae Bum Son<sup>21</sup>, Ho-seung Song<sup>29</sup>, Hye-jin Song<sup>20</sup>, Jong Sog Song<sup>1</sup>, Tae-Yung Song<sup>28</sup>, Byung Jin Suh<sup>22</sup>, Zhou Tong<sup>29</sup>, Kyoungho Tshoo<sup>1</sup>, Takuya Tsukioka<sup>1</sup>, Eun Il Won<sup>8</sup>, Mi Sook Won<sup>23</sup>, Hyung Joo Woo<sup>1</sup>, Ghil-Seok Yang<sup>5</sup>, Haeryong Yang<sup>16</sup>, Youngoo Yang<sup>29</sup>, Sung-Joon Ye<sup>9</sup>, Yeong-Heum Yeon<sup>29</sup>, Won Ju Yi<sup>30</sup>, In-Kwon Yoo<sup>2</sup>, Jaegwon Yoo<sup>28</sup>, Seong-Yeon Yoo<sup>35</sup>, Jin Woo Yoon<sup>1</sup>, Moohyun Yoon<sup>13</sup>, Sato Yoshiteru<sup>11</sup>, Byung-Geel Yu<sup>33</sup>, Dai-Hyuk Yu<sup>18</sup>, and Chong Cheoul Yun<sup>1</sup>

<sup>1</sup>Institute for Basic Science, Daejeon 305-811, Korea

<sup>2</sup>Pusan National University, Busan 609-735, Korea

<sup>3</sup>Korea Institute of Radiological & Medical Sciences, Seoul 139-909, Korea

<sup>4</sup>Korea Institute for Advanced Study, Seoul 130-722, Korea

<sup>5</sup>Kyungpook National University, Daegu 702-701, Korea

<sup>6</sup>Soongsil University, Seoul 156-743, Korea

<sup>7</sup>Chung-Ang University, Seoul 156-756, Korea

<sup>8</sup>Korea University, Seoul 136-701, Korea

<sup>9</sup>Seoul National University, Seoul 110-799, Korea

<sup>10</sup>Daegu University, Gyeongsan 712-714, Korea

<sup>11</sup>Seoul National University, Seoul 151-742, Korea

<sup>12</sup>Advanced Photonics Research Institute, Gwangju 500-712, Korea

<sup>13</sup>Pohang University of Science and Technology, Pohang 790-784, Korea

<sup>14</sup>Chonbuk National University, Jeonju 561-756, Korea

<sup>15</sup>ASAN Medical Center, Seoul 138-736, Korea

<sup>16</sup>Pohang Accelerator Laboratory, Pohang 790-784, Korea

<sup>17</sup>Ewha Womans University, Seoul 120-750, Korea

<sup>18</sup>Korea Research Institute of Standards and Science, Daejeon 305-340, Korea

<sup>19</sup>Hoseo University, Cheonam 330-713, Korea

- <sup>20</sup>Chungbuk National University, Cheongju 361-763, Korea  
<sup>21</sup>Hanyang University, Seoul 133-791, Korea  
<sup>22</sup>Catholic University, Seoul 110-758, Korea  
<sup>23</sup>Korea Basic Science Institute, Daejeon 305-806, Korea  
<sup>24</sup>Kookmin University, Seoul 136-702, Korea  
<sup>25</sup>University of Seoul, Seoul 130-743, Korea  
<sup>26</sup>Yonsei University, Wonju 220-710, Korea  
<sup>27</sup>Chonnam National University, GwangJu 500-757, Korea  
<sup>28</sup>Korea Atomic Energy Research Institute, Daejeon 305-353, Korea  
<sup>29</sup>Sungkyunkwan University, Suwon 440-746, Korea  
<sup>30</sup>Plasma & Energy Technology Corp. ,Seoungnam 464-120, Korea  
<sup>31</sup>Korea Institute of Geoscience and Mineral Resources, Daejeon 305-350, Korea  
<sup>32</sup>Kangwon National University, Chunchon 200-801, Korea  
<sup>33</sup>Korea Aerospace University, Koyang 412-791, Korea  
<sup>34</sup>Inha University, Incheon 402-751, Korea  
<sup>35</sup>Chungnam National University, Daejeon 305-764, Korea  
<sup>36</sup>Korea Accelerator and Plasma Research Association, Cheorwon 269-843, Korea  
<sup>37</sup>High Energy Accelerator Research Organization, Tsukuba, Ibaraki-305-0801, Japan  
<sup>38</sup>Kangwon National University, Samcheok 245-905, Korea  
<sup>39</sup>Korea Institute of Nuclear Safety, Daejeon 305-338, Korea  
<sup>40</sup>PEMTRON, Seoul 153-704, Korea  
<sup>41</sup>Korea Institute of Nonproliferation and Control, Daejeon 305-348, Korea  
<sup>42</sup>Ulsan National Institute of Science and Technology, Ulsan 689-798, Korea  
<sup>43</sup>Yonsei University, Seoul 120-749, Korea  
<sup>44</sup>Uiduk University, Seoul 120-749, Korea  
<sup>45</sup>Oak Ridge National Laboratory, USA  
<sup>46</sup>Dankook University, Yongin 448-701, Korea  
<sup>47</sup>Argonne National Laboratory, USA  
<sup>48</sup>SAMSUNG DISPLAY, Asan 336-840, Korea  
<sup>49</sup>Korea Institute of Science and Technology, Seoul 136-791, Korea

### **Acknowledgements**

We thank authors of the Conceptual Design Report of Korea Rare Isotope Accelerator. Many parts of this work were based on the result of the report. This work was supported by the Rare Isotope Science Project funded by the Ministry of Education, Science and Technology (MEST) and National Research Foundation (NRF) of KOREA (2011-0032011).

## **Table of Contents**

<b>Chapter I. Project Overview</b>	<b>5</b>
I.1 Science goals and beam requirements	7
I.2 Concepts of Accelerators	12
<b>Chapter II Rare Isotope Science</b>	<b>15</b>
II.1 Nuclear astrophysics	17
II.2 Nuclear Matter	20
II.3 Nuclear structure	22
II.4 Study of Fundamental Symmetry	24
II.5 Nuclear theory	28
II.6 Medical and Bio Science	30
II.7 Material Science	32
II.8 Neutron Science	34
II.9 Atomic trap for rare isotope science	37
<b>Chapter III Accelerators</b>	<b>39</b>
III.1 Driver Linac	39
III.2. In-Flight Fragment system	118
III.3 Cyclotron	132
III.4 ISOL system	137
III.5 ISOL Post Accelerator	159

<b>Chapter IV Experimental Apparatus</b>	<b>165</b>
IV.1 KRS (Korea Recoil spectrometer)	165
IV.2 LAMPS (Large Acceptance Multi-Purpose Spectrometer)	167
IV.3 Separator for SHE (Super Heavy Element)	170
IV.4 High Resolution Spectrometer and ZeroDegree Spectrometer	171
IV.5 Neutron science	174
IV.6. Material Science	176
IV.7 Ion trap and Laser spectroscopy	179
IV.8 Medical/Bio Science	182
IV.9 Elemental Particle Physics	183
<b>Chapter V Conventional Facilities</b>	<b>187</b>
V.1 Site	187
V.2 Facilities	188
V.3 Cryogenic System	192
V.4 Electric Power System	196
V.5 Radiation Safety	198
<b>Chapter VI Organization</b>	<b>201</b>
<b>Chapter VII Costs and Schedule</b>	<b>204</b>

## Chapter I Project Overview

As the major research facility of the International Science Business Belt (ISBB) in Korea, construction of the accelerator complex for the rare isotope science was approved by the Korean government in 2009. The Conceptual Design Report written in February of 2011 was reviewed by the International Advisory Committee. The IAC appreciated the soundness of science goals and the unique feature of having both ISOL and IF for the various rare isotope productions. The committee agreed that the cost estimate was reasonable after making a comparison with other similar projects. Also, the committee pointed out that the time schedule was aggressive and stressed the importance of the international cooperation. In November 2011, the Institute for Basic Science (IBS) was established as the main institution of ISBB to host about 50 research centers and other affiliated Institutes. In order to carry out the technical design and the construction of the accelerator complex, the Rare Isotope Science Project (RISP) was established in December 2011, in the IBS. The project will be housed in the IBS affiliated "Accelerator Institute" later, which will be operated independently of the IBS.

The accelerator complex will be located in "Sindong" area in the Northern part of Daejeon City. The goal of the accelerator complex is to produce variety of stable and rare isotopes to be used for researches in basic science and various applications. The complex consists of a heavy ion linear accelerator as the driver, called as Driver Linac, for the IF (In-flight Fragmentation) system, a proton cyclotron as the driver for the ISOL (Isotope Separation On-Line) system and a post-accelerator for the ISOL system. The ISOL and the IF systems will be operated separately and independently. In addition, the rare isotopes produced in ISOL can be injected into the Driver Linac for accelerating the RI beam even higher energies or for use in IF system to produce even more exotic rare isotopes. In the future stage, the proton beam in the Driver Linac can be used for the ISOL system with

higher power. A large number of rare isotopes with high intensity and with various beam energies will be available. The schematic diagram of the complex is shown in Figure I.1.

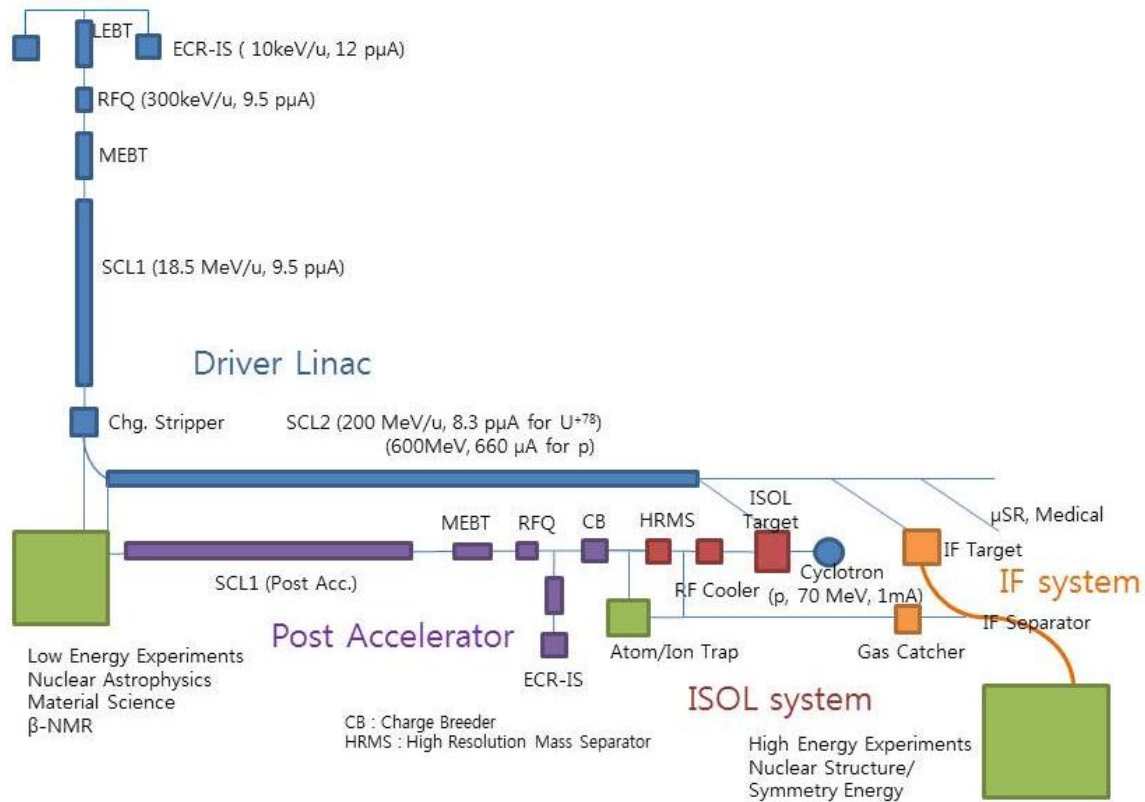


**Figure I.1 Schematic diagram of the accelerator complex of RISP**

Sciences with rare isotopes have been well described by numerous previous studies [I.1] [I.2]. The number of rare isotope accelerator facilities in operation or under construction demonstrating the importance of rare isotope sciences in the world. The science program of the RISP includes nuclear physics, nuclear astrophysics, and applications to material sciences, bio and medical sciences.

This report is to summarize the baseline design of the accelerator system and experimental apparatus to achieve the science goals proposed by various user communities. The baseline design in this report will be used as the base of the technical

design report. It should be noted that the given time limit permits only limited R&D and we need to adapt the known technologies and experiences acquired by other accelerator projects and laboratories in the world.

### **[Reference I]**

[I.1] D. F. Geesaman, C. K. Gelbke, R. V. F. Janssens, and B. M. Sherrill, *Ann. Rev. of Nucl. And Part. Sci.* **56**, 53 (2006)

[I.2] *Scientific Opportunities with a Rare-Isotope Facility in the United States*, Rare Isotope Science Assessment Committee, NRC, The national academies press (2007)

## **I.1 Science goals and beam requirements**

The basic and applied science using the rare isotope (RI) beams is a challenging research. In particular, the production of the RIs near the drip line and their properties are still unexplored compared to those basic elements and proton- or neutron-deficient RIs due to the difficulties of RI production.

Figure I.1-1 shows the high priority studies in the proton- or neutron-rich region on the chart of nuclei by the axes of numbers of protons and neutrons. The RISP accelerator facility has been conceptually designed to produce especially neutron-rich RI beams near the drip line, and to study the basic and applied sciences with challenging ideas and schemes.

By using low and high energy RI beams, the basic science, nuclear physics, astrophysics and atomic physics will be researched. The programs include the study of nuclear structure of very neutron rich nuclei near the drip line, the properties of exotic nuclei and the equation of state (EoS) of nuclear matter, and the attempt to understand the origin of the universe and the process of nucleosynthesis under the various stellar environments.

In addition, one of the aims of the RISP is to discover a new super-heavy element with  $Z > 116$ , which can be named as "Koreanium".

For the applied science, finding new material, mutating the cell or DNA, constructing nuclear data, and developing new medical heavy ion therapy will be fulfilled. The material science with RI beams, whose scale is in femto( $10^{-15}$ ) meter, will give us chance to make new materials, to study their properties, and to see a dynamic image in the nano( $10^{-9}$ ) meter scale. For the medical and biological applications, there is a plan to develop the advanced treatment technology by using energetic RI beams and to study the mutation of DNA. A systematic nuclear data measurement using fast neutrons has been planned for the future nuclear energy development and radioactive waste transmutation research

In order to produce RI beams of high purity and high intensity near the proton- and especially neutron- drip line, the two RI production methods[I.1.1] will be used: isotope separation on-line (ISOL) and in-flight fragmentation (IFF).

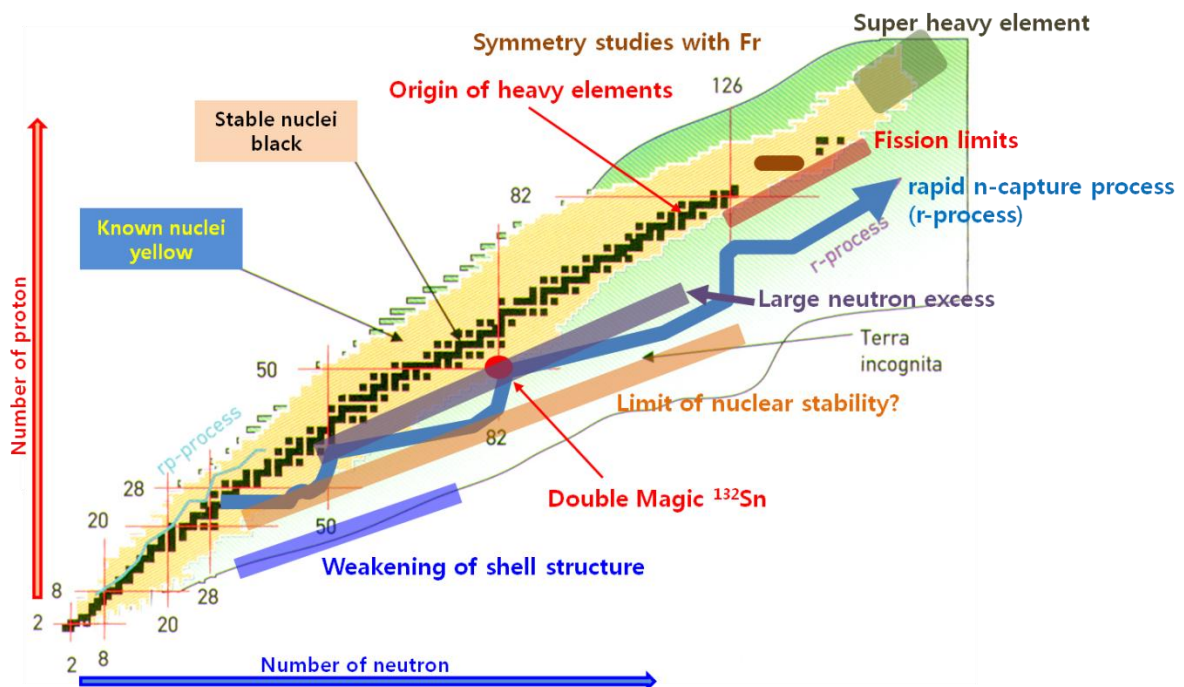


**Fig I.1.1 High priority researches on the chart of nuclei by axes of the numbers of proton and neutron. The stable (solid black square), known (yellow region), undiscovered (green and white region) nuclei are indicated in the region up to neutron and proton drip lines (outermost black lines). The narrow vertical and horizontal lines mean the nuclear magic numbers. The base figure is from [I.1.2].**

The RISP facility can produce exotic proton- or neutron-rich RI beams and has a unique operation mode that nobody has tried before. It will give us more opportunities close to the region near the drip-line by using more exotic RI beams. Thus, the RISP accelerator can be a highly valuable machine for nuclear and other basic sciences, and will bring lots of opportunities for young scientists to see and learn about both scientific and industrial effects.

The various kinds of RI beams of proton- and neutron-rich nuclei which are demanded for research opportunities at RISP are summarized in table I.1.1. The required RI beams are listed by the RISP user community with thorough consideration of perspective and analysis of current research trends for research fields of RI science.

**Table I.1.1 Selected RI beam requirements for RISP research opportunities**

RI Beam species	Energy Range	Desired Intensities [ particles / sec ]	Research fields
$^{80}\text{Ni}$ , $^{76}\text{Fe}$ , $^{132}\text{Sn}$ , $^{144}\text{Xe}$	> 100 A MeV	> $10^9$	Nuclear structure
$^{80}\text{Ni}$ , $^{76}\text{Fe}$ , $^{132}\text{Sn}$ , $^{144}\text{Xe}$	5-20 A MeV	> $10^8$	Nuclear Structure
$^{15}\text{O}$ , $^{14}\text{O}$	< 10 A MeV < 30 keV	> $10^{10-11}$ > $10^8$	Nuclear astrophysics Material Science
$^{26\text{m}}\text{Al}$	5-20 A MeV	> $10^{7-8}$	Nuclear astrophysics

$^{45}\text{V}$	0.613-2.25 A MeV	$> 10^7 - 10^9$	Nuclear astrophysics
$^{39}\text{Si}, ^{36}\text{Mg}$	5-10 A MeV	$> 10^{7-9}$	Nuclear Structure
$^{68}\text{Ni}, ^{106}\text{Sn}, ^{132}\text{Sn}, ^{140}, ^{142}\text{Xe}$	10-250 A MeV	$> 10^9$	Symmetry energy
$^{6,8}\text{He}, ^{12}\text{Be}, ^{24-30}\text{O}$	50-100 A MeV	$> 10^9$	Nuclear study with Polarized target
$^{17}\text{N}, ^{17}\text{B}, ^{12}\text{B}, ^{14-15}\text{B}, ^{31-32}\text{Al}, ^{34}\text{K}$	50-100 A MeV	$> 10^9$	Nuclear study with Polarized RI beam
$^8\text{Li}, ^{11}\text{Be}, ^{17}\text{Ne}$	$< 30$ keV	$> 10^8$	Material science
$^{133-140}\text{Sn}$	$< 60$ keV	$> 1$	Atomic physics
$^8\text{B}, ^8\text{Li}, ^9\text{C}, ^{11}\text{C}, ^{15}\text{O}$	$\geq 400$ A MeV	$>10^7 \sim 10^9$	Medical and Bio science

Based on the beam requirements from users and consideration of conditions for various kinds of experiments, the requests on characteristics of the beam and accelerator are summarized on table I.1.2.

**Table I.1.2 Requests on beam characteristics for experiments**

Characteristics	Requests	Remarks
Maximum Beam Energy	250MeV/nucleon for $^{132}\text{Sn}$	- Symmetry energy
Minimum Beam Energy	$\leq 0.3$ MeV/nucleon (Min E from RFQ $\sim 0.5$ MeV/nucleon)	- Nuclear astrophysics - 0~1 MeV/nucleon is possible?

Energy Variability	0.5% at <18 MeV/nucleon (ex. 50keV/u @ 10MeV/u) 1MeV at >18 MeV/nucleon	- Fast and precise beam energy changes for low energy beams (<5MeV/nucleon)
Beam Energy Definition	0.1% or better	- beam-energy analysis spectrometer
Time Resolution	0.5 ns/bunch (FWHM) upper limit ~ 1 ns	- for TOF measurement - How about energy spread of the beam?
Time Structure: pulse rate and chopping	- 100~200 ns (5~10 MHz) - chopping 12 ns ~ 1 ms	- for TOF measurement, 81.25 MHz (~12.3 ns) is high - for LAMPS experiment
Beam Sharing	- 5 ports for muSR - 2 ports for beta-NMR - low E nucl. phys+material sci.	- to use the beam time efficiently
Stable Beam Operation at post-accelerator	- $10^{11-12}$ pps	- setting up and calibrating instruments - reference points for studies with RIBs - by-pass BT line for high E is required
Beam Purity	single-isotope beams	
Beam Emittance and Spot Size	1~2 $\pi$ mm-mrad 2mm <sup>2</sup>	- for RI beams from ISOL - Is technically feasible?

\* Reference: Task Force reports, EURISOL design study (N. Orr, LPC-Caen, 2006)

### [Reference I.1]

[I.1.1] Min Sang Ryu, Byoung Hwi Kang, Yong-Kyun Kim, Sun-Chan Jeong and Chong Cheoul Yun, J. Korean Phys. Soc. **60**, 19 (2012).

[I.1.2] *RIA Physics White Paper*, RIA Workshop, Durham, North Carolina (2000)

## I.2 Concepts of Accelerators

The accelerator complex is designed to become one of the world's leading facilities in rare isotope science. The rare isotopes can be produced either target spallation, fission in the ISOL system or projectile fragmentation in the IF system. Two methods produce rare isotopes of different characteristics, and thereby provide wider varieties of rare isotopes than other facilities operating only one of the two methods. The science goals described in the last section require high intensity RI beams with various beam energies. The complex has three accelerators; two heavy ion linear accelerators, and one cyclotron. The driver accelerator for IF system (Driver Linac) consists of two ECR ion sources, low energy beam transport (LEBT), RFQ, medium energy beam transport (MEBT), low energy superconducting linear accelerator, charge stripper and high energy superconducting linear accelerator. At the end of the high energy linear accelerator, proton beams are accelerated to 600 MeV and Uranium to 200 MeV/u. The beam current for the Uranium beam is 8  $\mu\text{A}$ . The driver accelerator for the ISOL system is a proton cyclotron with the beam energy of 70 MeV and beam current of 1 mA. The post accelerator is designed to accelerate the rare isotopes produced in the ISOL system up to  $\sim 20$  MeV/u. But the post accelerator can provides the stable isotopes at the same energy with an additional ECR ion source. Therefore, in principle, the post accelerator is a duplicate of driver accelerator up to low energy linear accelerator. Beam specification and components for each accelerator system are summarized in Table I.2.1.

**Table I.2.1 Beam specifications and main components for each accelerator system**

Accelerator	Beam specification	Components
Driver Linac	p, 600 MeV, U+78, 200 MeV, 8 $\mu\text{A}$	ECR-IS, LEBT, RFQ, MEBT, QWR, HWR, Charge Stripper, SSR1, SSR2

Post Accelerator	RI, ~ 18 MeV/u	Charge Breeder, ECR-IS, LEBT RFQ, MEBT, QWR, HWR
Cyclotron	p, 70 MeV, 1mA	Cyclotron, Pulsed ion source, Charge Stripper, Beam line

The energy of ion at the end of the RFQ is 0.3 MeV/u in the base line design. However, higher energy case is also being considered. Various combinations of superconducting cavity structures are considered for the optimal design of the Driver Linac. The optimal beta, RF frequency, and cavity structure for the base line design are explained in detail in Chapter III. In Table I.2.2, cavity parameters and number of cavities for each linac segment are summarized.

**Table I.2.2 Cavity parameters for each Linac Segment**

SCL	Cavity structure	Frequency	$\beta_g$	Number of cavities	Output energy
SCL1	QWR	81.25 MHz	0.047	24	2.5 MeV/u ( $U^{+33}$ )
	HWR	162.5 MHz	0.12	138	18.5 MeV/u ( $U^{+33}$ )
SCL2	SSR	325 MHz	0.3	88	70.9 MeV/u ( $U^{+79}$ )
	SSR	325 MHz	0.53	136	200 MeV/u ( $U^{+79}$ )

Since the ISOL post-accelerator is a duplicate of the low energy sections of the driver linac, we are planning to share the same doublet lattice as the SCL1, which minimizes

types of accelerator components and reduces cost and R&D efforts. Cavities of the same types and betas will be used as well as the same type of cryomodules.

## Chapter II Rare Isotope Science

A variety of basic and applied science can be studied with RI beams. Especially high intensity and high purity RI beams near the drip lines can give us tremendous opportunities to explore the entire universe from microscopic to macroscopic world. The research subject is categorized into four science fields as follows.

**Nuclear Science:** Research programs in nuclear physics can be roughly divided into: search for drip lines, investigation of shell gaps, study of deformed nuclei, study of charge exchange reaction on various nuclei, study of single particle wave functions, study of asymmetric nuclear matter, and investigation of breaking of fundamental symmetries. The main issue of nuclear astrophysics is to understand key nuclear reactions that synthesize the elements and are responsible for energy generation in stars with different temperatures and densities. The Symmetry Energy in nuclei, which accounts for the asymmetric nature of the strong interactions in nuclear medium, is one of main research topics in nuclear physics program.

Nuclear data is a part of nuclear physics and a basic element in the research and development of nuclear engineering. Research related to nuclear data is divided into two categories: experimental measurement and theoretical research, such as the evaluation and development of nuclear models. Experimental measurements can provide nuclear data directly and be the basis of model evaluation and development at the same time.

**Atomic & Molecular Science:** Precise mass measurements enable the study of the fine structure of the mass surface and clarification of discontinuities in order to extract nuclear structure information from binding energies. Data far from the valley of  $\beta$ -stability represent well-suited test cases for the predictive power of mass models. High-precision measurements of masses, spins, and moments provide important ingredients

for reliable nuclear astrophysical calculations, and help us understand the composition of matter in the universe in general.

**Material Science:** RI material science facilities at RISP involve the  $\beta$ -NMR, PAC, EC, and  $\mu$ SR, and can be a part of the world-leading material research facility. New semiconductor materials, spintronics, and superconducting phenomena could be studied with the RISP RI material science facilities.

**Medical & Bio Science:** With RISP facility, we will find new ways to improve the effect of heavy ion therapy by studying the physical methods, radio-resistant mechanism of cancer cells to heavy ions, new targets and drugs, and normal tissue damage to heavy ions. In the bioscience field, the RISP facility can provide the most current information on the biological effects of heavy ion beams to be used in all biological fields, including radiation biology, microbiology, cancer biology, and radiation oncology.

And the high priority research subjects are summarized in Table II.1.

**Table II.1 High priority research subject at RISP**

Nuclear Science	Nuclear Astrophysics & Nucleosynthesis	- Direct measurements of proton and alpha capture reactions - Search for Super Heavy Elements beyond Z=113
	Nuclear Structure & Matter	- RI nuclear structure of neutron rich nuclei near N=126 - Symmetry energies at sub-saturation density
	Nuclear Data	- Neutron capture cross section measurements by using n-TOF
	Nuclear Theory	- Development of RI nuclear theories
Atomic & Molecular Science	Precision Mass Measurement & Laser Spectroscopy	- Hyperfine structure and characteristics of element and nuclei
Material Science	RI Material Research	- Search for new material and its properties with $\beta$ -NMR/ $\mu$ SR and RI beam
Medical & Bio Science	Medical & Bio application	- Development of new cancer therapy - Biological effect of tissue and DNA by RI beam

## II.1 Nuclear astrophysics

The main purpose of nuclear astrophysics is to understand key nuclear reactions that synthesize the elements and are responsible for energy generation in stars with different temperatures and densities. Because a lot of thermonuclear reactions in explosive stellar sites involve radioactive isotopes, the proposed RISP facility is expected to play an important role in nuclear astrophysics. Various experiments with RI beams by the RISP accelerator have been discussed and proposed to further understanding of element formation following fusion reactions and neutron captures inside and on the surfaces of stars. Important nucleosynthetic processes in various stellar sites are hydrogen-helium

burning thermonuclear reactions, CNO cycle, HCNO cycle, rapid proton capture reactions (rp-process), slow neutron capture reactions (s-process), and rapid neutron capture reactions (r-process).

We give special emphasis to measuring the reaction rates that create and destroy long-lived nuclei such as  $^{22}\text{Al}$ ,  $^{26}\text{Al}$ , and  $^{44}\text{Ti}$  that are targets for gamma-ray astronomy. We also focus on the r-process that creates neutron-rich nuclei with neutron magic numbers of 82 and 126.

We expect to lead the way to solving key issues in astrophysics, such as the structure and evolution of stars (neutron stars, pulsars, and supernovae), the generation of energy in stars, the synthesis of the heavy elements in stars, and the structure and formation of the solar system and our galaxy.

The accurate reaction rates for astrophysical nuclear reactions are critical inputs for stellar models. We have experiences for determination of reaction rates with RI beam via indirect methods like elastic resonant scattering [II.1.1.1]. But the best way to decide reaction rates is the direct measurement of reaction. We expect that cross sections for important nuclear reactions such as proton- or alpha-capture reactions can be measured directly with intense RI beam and recoil spectrometer system at the RISP. These results are going to be essential information for better understanding for nucleosynthesis and energy generation in explosive hydrogen burning environments such as novae and X-ray bursts. One of main research topics is the direct measurement of reaction rate for  $^{15}\text{O}(\alpha,\gamma)^{19}\text{Ne}$  reaction. In the rp-process under a condition of novae, the CNO material would be transmuted to heavier elements. The first step of the process is considered to be  $^{15}\text{O}(\alpha,\gamma)^{19}\text{Ne}$  reaction – break-out reaction from CNO cycle to rp-process. For the direct measurement of  $^{15}\text{O}(\alpha,\gamma)^{19}\text{Ne}$  reaction, recoil separator with high background suppression and high intense  $^{15}\text{O}$  RI beams ( $>10^{11}$  pps) are essential. We expect that the

KRS (Korea recoil spectrometer) and 70 kW ISOL system at the RISP should fulfill experimental requirements.

Investigations of the abundances of the elements found on Earth and in meteorites are essential to understanding the production of stars as well as the formation of the solar system. Measurements of the cross section through the nuclear reactions are important to this study, and RIBs are especially essential for searching the unexplored territory (**Terra Incognita**).

Major research topics which will be performed with RI beams at the RISP facility are summarized as follows:

- The production and extinction of galactic gamma-ray line
- Abundance of important elements by the CNO cycle and the formation of the solar system
- Nucleosynthesis of proton rich nuclides by rapid proton capture process (rp-process)
- Reaction rates of astrophysically important proton and alpha capture reactions
- Determination of the abundances of stable nuclides and around isotopes by the slow neutron capture process (s-process), and neutron rich nuclides by the rapid neutron capture process (r-process)

**[Reference II.1.1]**

[II.1.1.1] H. S. Jung, Y. K. Kwon, C. C. Yun, Y. K. Kim et al., Phys. Rev. C **85**, 045802 (2012).

## II.2 Nuclear Matter

There are more neutrons than protons in heavy stable nuclei. The semi-empirical mass formula successfully explains the masses of stable nuclei from light ones to heavy ones, but the structure of neutron-rich nuclei beyond the limit of stability is not yet fully understood. Symmetry energy is the energy that requires converting a proton to a neutron inside a nucleus. Therefore, understanding the nature of symmetry energy will offer clues to fundamental questions about the asymmetric constitution of nucleons in heavy nuclei, isospin asymmetry in nucleon-nucleon interactions, their modifications in a nuclear medium, etc. In addition, recent research shows that symmetry energy plays a critical role in the properties of a neutron star, such as its cooling rate, mass, and radius. The goal of the proposed investigation is to understand the nature of symmetry energy in nuclei and in nuclear matter with nuclei from stable ones to those far from the stability valley, and to apply our knowledge to related phenomena from a microscopic scale to stellar objects.

Symmetry energy is the strong interaction caused by the difference in the number of the neutron and the proton. Figure II.1.2.1 shows the energy per nucleon in nuclear matter as a function of density. For the normal nuclei in which the number of the neutron is approximately equal to that of the proton, the volume term of the binding energy is represented by the lowest thick solid line. However, if a nucleus is composed of only neutrons, the symmetry energy has to be added to the binding energy, and as a result the binding energy shown by the black solid line predicts an unstable state. As the mass number increases, the ratio of the neutron number to the proton one,  $N/Z$  deviates from 1 substantially. Therefore, it is important to understand the behavior of symmetry energy to figure out the origin of  $N/Z > 1$  in heavy nuclei.

For science, the RISP facility will provide high-intensity RI beams with unprecedented neutron-to-proton ratios. The operation of the RISP at high energies will provide an ideal

environment for studying the stability of nuclear matter with extreme neutron-to-proton ratios. The stability of the neutron-rich matter depends directly on the equation of state of the isospin asymmetric energy term, which is determined by the isoscalar and isovector potentials. However, our knowledge about these potentials is limited, especially at high densities. In a dense medium, the mass modification of hadrons and the three-body interactions can also alter the density dependence of the equation of state for the isospin asymmetric energy term. RISP will enable us to describe the quantitative distinction of various sources for the modification of the isospin-dependent equation of state by measuring the energy (or density) dependence of several observables.

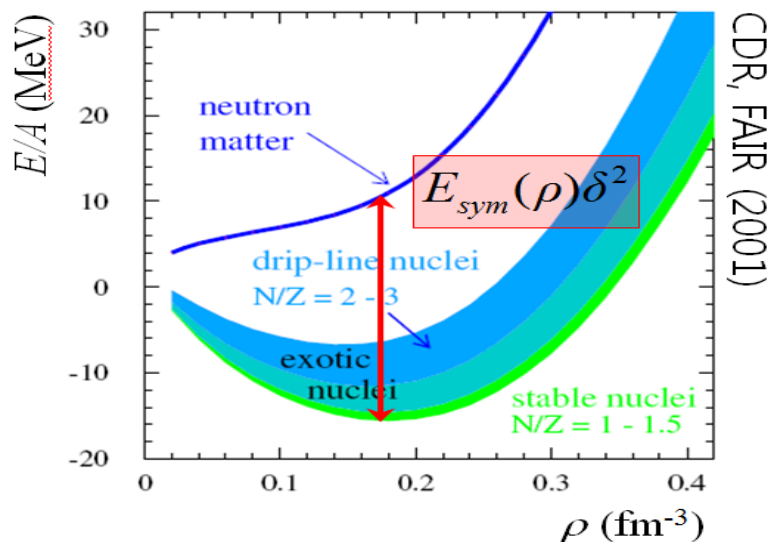


**Fig II.1.2.1 Theoretical model of nuclear symmetry energy. Normal nuclear density =  $0.16 \text{ fm}^{-3}$ . [II.1.2.1]**

**[Reference II.1.2]**

[II.1.2.1] F. de Jong and H. Lenske, Phys. Rev. C **57**, 3099 (1998); F. Hofman, C. M. Keil and H. Lenske, Phys. Rev. C **64**, 034314 (2001)

### II.3 Nuclear structure

Research programs in nuclear physics can be roughly divided into 7 subjects: search for drip-lines, investigation of shell gaps, study of deformed nuclei, study of charge exchange reaction on various nuclei, study of single particle wave functions, study of asymmetric nuclear matter, and investigation of breaking of fundamental symmetries.

It is highly likely that the search for new isotopes will be the first experiment once the facility is completed. During this process, it is also possible to find new isomer states by detecting delayed gamma rays. The new isotopes or isomers near the drip-lines require more detailed investigation of their properties. Interesting phenomena include halo nuclei, two-neutron (or two-proton) emitters, beta-delayed neutron emission, and neutron skins.

Information on the properties of various nuclei near the neutron magic number,  $N \sim 126$ , is critical for new isotopes search, and for changes in nuclear shell structure of very neutron rich nuclei. And also because nuclei along the  $N \sim 126$  are waiting points of  $r$ -process, basic properties such as masses and  $\beta$ -decay half-lives are important for understanding nucleosynthesis under the extreme stellar environments. Recently measured half-lives of these nuclides near  $N \sim 126$  are found to be very different from the previous theoretical values. These results show clearly that theoretical predictions on the basic physical parameters, mass and half-life, about unknown nuclides have limitations. As a primary goal, we focus on the measurements of their half-lives. We also pay attention to the production methods for super neutron rich isotopes by the secondary nuclear reactions using the neutron rich RI beams as building up online separation methods.

The modification of shell gaps with increasing neutron numbers is another important research program for neutron-rich isotopes. It has been discovered that the conventional

magic numbers (or shell gaps) are modified as the number of neutrons increases toward the drip-line. This requires precise mass measurement and measurement of excitation energy to the first  $2^+$  states.

While stable nuclei are spherical, neutron-rich isotopes can have deformation even at their ground states. The study of the degree of deformation as a function of the number of neutrons is another interesting topic. Deformed nuclei produced in the reaction often carry high angular momentum, and will be a unique laboratory to study the interplay between collective and single-particle motion.

Charge-exchange reactions on nuclei are another versatile method to measure Gamow-Teller strength compared to the usual beta-decay study. While measurement of the beta-decay is limited with  $Q$  value, charge exchange reactions do not have such a limit. Charge-exchange reactions will play another important role in studying the properties of various unstable isotopes produced by the facility.

Transfer reactions or knock-out reactions can study wave functions of a single particle or correlated pair of nucleons. With the capability to adjust the number of neutrons, transfer and knock-out reactions can study the evolution of these wave functions over a wide range of isotopes.

Compared to stable isotopes, for which the numbers of protons and neutrons are more or less symmetric, these neutron-rich isotopes have large asymmetry between these two nucleons. In nature, such asymmetric nuclear matter can be found in neutron stars, for example. Thus, neutron-rich isotopes can be a unique access point for asymmetric nuclear matter, providing important clues to understanding neutron stars.

## II.4 Study of Fundamental Symmetry

If the same equations of motion describe the system after the transformation of some of the variables, then the transformation is said to be symmetry. Note that the transformation may change the solution to the equations of motion, because we have different initial conditions. However, a transformation is asymmetric only if a new set of equations are required to describe the evolution of the system, and not just a change in the initial conditions. The symmetry is said to be violated when the transformation does not reserve the equations of motion for the system of interest. Familiar symmetries include:

1. Proper symmetries (can be carried out continuously in infinitesimal steps)

- Spatial translation
- Rotation

2. Improper or discrete symmetries (cannot be built up from infinitesimal steps; they are all or nothing)

- Parity (P)
- Time reversal (T)
- Charge conjugation (C)

Over the past fifty years, there have been considerable works done studying violations of C, P and T.

- CP violation has been well established that parity (P) symmetry is violated in weak interactions, and the experiment of Christenson, Cronin, Fitch, and Tuylay in 1964 demonstrated that the combined charge-parity (CP) symmetry is violated in the decay of neutral kaons.

- T violation. Recently, the CPLEAR collaboration at CERN has shown direct time reversal invariance (T) violation, again in the neutral kaon system.

This had long been expected, because of the powerful CPT theorem. This theorem requires that acting on any state with all three operations C, P, and T must return the original state. It has been rigorously proven for any local theory which satisfies Lorentz invariance. Thus a CP violation should be synonymous with a T, or time reversal, violation. Numerous searches have been made for either CP or T violation in other systems. So far, the baryon asymmetry of the universe is the only other evidence of such a violation, and that evidence is rather hard to quantify. However, the continuing experiments have succeeded in pushing down the upper limits on time reversal violating effects by many orders of magnitude in the past four decades.

Clearly an impressive amount of effort has gone into observing CP violation in the neutral kaon system. However, many proposed CP violating processes, including the baryon asymmetry of the universe, are not flavor changing and so would have to arise from a separate mechanism. Electric Dipole Moment (EDM) measurements are one of the best ways to set limits on many of the mechanisms that theorists have proposed.

A measurement of EDM is important because an EDM violates parity and time reversal. Take a particle with some net spin, and imagine that it also has a separation of charge. The Wigner-Eckhart theorem requires that the charge separation must lie along the spin axis. Under a time reversal operation, the orientation of charge remains the same, but the direction of spin changes: thus time reversal is violated. The case for parity is completely analogous.

An atomic EDM would either arise from an intrinsic fermion EDM or the elementary particle interactions among the atom's constituents. The Standard Model and its various extensions have different CP violating parameters that could lead to an EDM. Searches

that can set new limits on T violation thus provide much needed evidence to determine which of the theories are physically permissible.

Some specific isotopes can amplify the effect of broken fundamental symmetry, such as the electric dipole moment, and can be used to test more easily the fundamental symmetry of the universe. The impact of such a finding would be enormous, and would require new theory to replace the current Standard Model. If it is successful, experiments on these rare isotopes can produce results that cannot be obtained with large accelerators, such as LHC at CERN.

As discussed above, an EDM cannot exist unless both P and T invariance are violated. This can be easily seen from the non-relativistic Hamiltonian for the interaction of an EDM  $\mathbf{d}$  with an electric field  $\mathbf{E}$ , which is  $H_{EDM}^{NR} = -\mathbf{d} \cdot \mathbf{E}$ . Now, a fundamental particle or nucleus in a non-degenerate state, the spin angular momentum  $\mathbf{J}$  is the only 3-dimensional vector available to define a direction of the system. Thus,  $\mathbf{d}$  must be collinear with  $\mathbf{J}$ , and

$$H_{EDM}^{NR} = -\mathbf{d} \cdot \mathbf{E} = -d \frac{\mathbf{J}}{J} \cdot \mathbf{E}.$$

But  $\mathbf{E}$  is a T-even polar vector while  $\mathbf{J}$  is a T-odd axial vector, and therefore  $H_{EDM}^{NR}$  is odd under P and T transformations. The identical conclusion is of course true for the relativistic generation of  $H_{EDM}^{NR}$  [II.1.4.1], with subtle minor changes due to a relativistic effect.

So far, no EDM has been observed, and it is obvious from the present experimental upper limits, that EDMs predicted by Standard Model must be extremely small. For example, the upper limit on the electron EDM  $|d_e|$  is  $10.5 \times 10^{-28}$  e cm [II.1.4.2]. Nevertheless, EDMs may be non-zero, because P and T are in fact violated in nature. Parity non-conservation as well as the violation of charge conjugation invariance occurs

in the weak interaction. Furthermore, combined CP violation is observed in neutral K meson and B meson decays [II.1.4-3]. If we assume CPT invariance, for which we have very strong confidence, then this CP violation is equivalent to T violation. Thus the weak interaction and the mechanism or mechanisms causing CP violation could act jointly to generate EDMs by P, T-odd radiative correction to the P, C, T conserving electromagnetic interaction with the Standard Model of particle physics phenomenology.

However, there are good reasons to think that additional mechanisms exist for CP violation. It is generally accepted that if the universe initially was symmetric in baryon-antibaryon number, the presently observed baryon-antibaryon asymmetry could not have developed without a much larger CP violation than is predicted by the Standard Model [II.1.4-4]. Furthermore, in many theories that attempt to go beyond Standard Model, predicted EDMs are relatively large, for example, in various supersymmetric theories, many new hypothetical particles and coupling appear, and along with them exist new CP violating phases. Thus in many such models the electron and neutron EDMs already appear at the one-loop level, and as a result prediction of electron and neutron EDMs are closed to present experimental limits. Thus discovery of an EDM by practical experimental methods is a real possibility within the foreseeable future, and such a discovery would provide definite evidence for physics beyond the standard model.

Together with EDM, lepton number conservation is another prediction that is strongly supported by Standard Model. In particular, search for lepton violation in decays such as  $\mu \rightarrow e\gamma$ ,  $\mu A \rightarrow eA$ ,  $\mu \rightarrow eee$  has been carried out extensively over past years. The prediction from Standard Model branching fraction of  $\mu \rightarrow e\gamma$ , for example is less than  $10^{-54}$ , that is approximately 30 order of magnitude smaller than present experimental sensitivity [II.1.4-5]. This translates into the fact that there are plenty of rooms for new physics beyond Standard Model can enhance (if theoretically possible) the effect so that experimental search for new physics potential is extremely rich.

## **[Reference II.4]**

[II.1.4.1] E. D. Commins, Journal of Phy. Soc. Of Japan 76 111010 (2007)

[II.1.4.2] J. J. Hudson, et. Al., Nature, 473, 493 (2011)

[II.1.4.3] D. Kirkby and Y. Nir, J Physics G 33, 1 (2006).

[II.1.4.4] See, for example, W. Bernreuther: in CP violation in Particle, Nuclear and Astrophysics, et. M. Beyer (Springer Berlin, 2002) p. 237.

[II.1.4.5] J. Adam, et al., Phys. Rev. Lett. 107, 171801 (2011)

## **II.5 Nuclear theory**

Our goal is basically to understand the origin of matter created through nucleosynthesis that includes all reactions such as the capture by neutrons and protons, the scattering by leptons, the fusions by finite nuclei and so on. To describe them, we divide our works into five parts.

First, the study of exotic nuclear structure includes the structure of all spherical and deformed nuclei. To do that, our group has developed deformed quasi-particle random phase approximation (DQRPA) model to describe the structure of deformed nuclei. The unstable nucleus is usually deformed so that we use Nilsson basis to calculate deformed nuclei. In this model, when deformation parameter is equal to zero, it means that the nucleus is spherical shape. Thus, we can calculate all spherical and deformed nuclei by using DQRPA model.

Thermal nuclear reactions and nuclear processes in the cosmos are for nuclear reactions by neutrons and protons. In nucleosynthesis, main processes are slow neutron capture(s-

process) and rapid neutron capture (r-process). Since the reactions in s- or r-process are capture reactions by a neutron, the situation is involved in nuclear structure of finite nuclei with an excited neutron which can be described by DQRPA model. In addition, the nucleus emits gamma ray when the excited neutron goes down into ground state. Thus this calculation includes both processes; one is nuclear structure by DQRPA and the other is gamma ray emission. Proton process and thermal nuclear reactions are very sensitive on nuclear density and temperature. In the environment with high density and high temperature, the capture reaction by proton is possible and new channels can be opened. The model for proton capture reaction is similar with neutron capture reaction except for Coulomb potential. Thus DQRPA and gamma ray emission are employed to calculate proton process and thermal nuclear reactions.

The study for the sites for nuclear processes is to describe the environment that nucleosynthesis occurs. For instance, when nuclear reactions take place in BBN at early universe, the universe expands with time. Thus, nucleosynthesis is combined with hydrodynamics which describes the expansion of the universe. The situation is similar to nucleosynthesis inside stars because nuclear reactions depend on density and temperature. One of issues in nuclear astrophysics is to describe the process from supernovae explosion to neutron star. Theorists group has studied the infinite matter and the structure of neutron star by using relativistic mean field models and wants to expand our models.

Finally, the study of nuclear abundances in the universe is for nuclear reactions with leptons, especially neutrinos. In the simulation of nucleosynthesis, s-, r- and rp-processes are included but the results still show some incompatibility as compared with observed data. As the solution, neutrino process is proposed in some reactions. When a supernovae explodes, huge amount of neutrinos are emitted so that neutrinos can affect nucleosynthesis although the cross section by neutrinos is very small. We thus have

studied the nuclear scattering by neutrinos, considering charged and neutral currents. We also expect that this work can give the explanation of nuclear abundance in the universe.

Major research topics can be summarized as follows:

- The study of exotic nuclear structure
- Thermal nuclear reactions in the cosmos
- Nuclear processes in the cosmos (slow and fast processes and proton processes)
- Research of cosmological sites for nuclear processes
- Study of nuclear abundances in the universe

## **II.6 Medical and Bio Science**

Due to higher biologic effects compared with x- or gamma-rays, heavy ion beams can be used to treat intractable cancers and to study life science, such as the change of genes, proteins, cells or organs to heavy ions [II.1.6.1].

The primary rationale for radiation therapy (RT) with charged particles is the sharp increase of dose in a well-defined depth (Bragg peak) and the rapid dose falloff beyond that maximum [II.1.6.2]. The ratio of Bragg peak dose to entrance region dose is larger for heavy ions than for protons. Therefore, heavy ions offer an improved dose conformation compared with photon and proton RT, with better sparing of normal tissue structures close to the target. In addition, heavy ions exhibit a strong increase of the LET in the Bragg peak compared with the entrance region. Equal doses of different types of radiation do not produce equal biological effects. The key difference resides in the pattern of energy deposition at the microscopic level. The relative biological effectiveness

of heavy ions is several times greater than that of photons. Heavy ions are less affected by oxygen status than photons [II.1.6-3], and are able to kill cells nearly equally well in all phases of the cell cycle. As the linear energy transfer increases, the relative biological effectiveness also increases. As the oxygen enhancement ratio falls, the relative biological effectiveness of radiation rises. With the RISP facility, we will find new ways to improve the effect of heavy ion therapy by studying the physical methods, radioresistant mechanism of cancer cells to heavy ions, new targets and drugs and normal tissue damage to heavy ions.

The research goal in the bioscience field at the RISP facility is to provide the most current information on the biological effects of heavy ion beams to be used in all biological fields, including radiation biology, microbiology, cancer biology, and radiation oncology. Information about genomic and proteomic responses to heavy ion beams can reveal the subsequent biochemical and physiological function in living cells [II.1.6.4]. This may have a major impact on advances in cellular and molecular radiation biology, as X-ray resulted in the discovery of the double helix model of DNA structure [II.1.6.5]. In conclusion, the purpose of biological study using heavy ion beams is to increase our knowledge of the mechanism of heavy ion induced changes on cellular and molecular levels, and to conjugate a variety of biological fields. The goals of biological research include the study of the following:

- Linear energy transfer, cellular heavy ion damage, and its modification
- Genomic and proteomic response to heavy ion beams and identification of their biological functions
- Heavy ion induced damage, cell death, and repair
- Heavy ion induced cellular senescence and its mechanism

- Epigenetic changes induced by heavy ion beams, and their biological importance
- Heavy ion beam-induced mutation, variant microbes and plants, and their applications
- Basic cancer biology using heavy ion beams.

### **[Reference II.1.6]**

[II.1.6.1] M. Durante, J. S. Loeffler, *Nat Rev Clin Oncol* 7, 37 (Jan, 2010).

[II.1.6.2] E. Fokas, G. Kraft, H. An, R. Engenhart-Cabillic, *Biochim Biophys Acta* 1796, 216 (2009)

[II.1.6.3] O. Jakel, C. P. Karger, J. Debus, *Med Phys* 35, 5653 (2008)

[II.1.6.4] O. Jakel, *Radiat Prot Dosimetry* 137, 156 (2009)

[II.1.6.5] T. Terasawa et al., *Ann Intern Med* 151, 556 (2009)

## **II.7 Material science**

So far a number of nuclear experimental techniques have been introduced to material science, and then have left behind remarkable achievements. Rare isotope beam (RIB) is a very useful tool for looking at the inside nature of condensed matters. It can straightforwardly be used as tracer for diffusion studies. Moreover, due to its high sensitivity to electric and magnetic feature within materials, it is capable of providing microscopic information on the structural and dynamical properties of solids by using the conventional nuclear techniques such as Mössbauer spectroscopy (MES), perturbed angular correlation (PAC),  $\mu$ SR,  $\beta$ -NMR, emission channeling (EC), and conversion electron spectroscopy (CES). Among them,  $\mu$ SR and  $\beta$ -NMR are very unique and promising

techniques to investigate nano-scale electric and magnetic structures and properties of material by using RIBs.

The basic physics of  $\mu$ SR and  $\beta$ -NMR technique is identical to the one of the conventional NMR. The resonance frequency is a measure of local magnetic field and the spin relaxation times provide information on the spin dynamics on the energy level of the resonance frequency (Larmor frequency). However, there are also significant differences which influence the specific applications. In conventional NMR, the resonance signal is detected by using an inductive pickup coil, whereas in  $\mu$ SR and  $\beta$ -NMR technique, the change of spin polarization at resonance frequency is monitored with anisotropic decay properties of the nucleus. In order to obtain a measureable signal in conventional NMR, an appreciable number of probe nuclei are necessary (typically  $10^{18}$  or more). If one uses highly polarized radioactive nuclei and muons, one can investigate the important properties of the material with fewer nuclei (as few as  $10^6$ ). The conventional NMR is mostly a bulk probe of a matter, whereas  $\mu$ SR and  $\beta$ -NMR could be a probe of the microscopic structure of the matter and a depth dependence of physical properties. So far the  $\mu$ SR technique has been more generally applied to investigate the microscopic electric and magnetic properties of a condensed matter due to the relatively easy production of muons and its higher signal to noise ratio than that of radioactive nuclei. However, after the recent success in generating intensive and highly polarized radioactive nuclei beam at several facilities (ISOLDE at CERN and ISAC at TRIUMF), one can realize the potential application of  $\beta$ -NMR technique is significant. The  $\beta$ -NMR facility at ISAC of TRIUMF is the only currently working. Therefore the run time for condensed matter physicist is far from enough.

The  $\mu$ SR is primarily applied to basic studies in condensed matter physics and chemistry. In condensed matter physics research, the muon is a sensitive probe of internal magnetic fields and electron configurations of materials. In chemistry or in semiconductor physics,

the muon plays a role as an isotopic substitution for a proton. In general,  $\mu$ SR gives information that is complementary to that provided by neutron scattering and conventional NMR. There are of course significant differences between these techniques. Some of the unique capabilities of  $\mu$ SR are as follows:

- Due to the extreme sensitivity to small internal magnetic fields ( $\sim 0.1$  G), the  $\mu$ SR is often only method available for detection of the very small and/or dilute moments
- The  $\mu$ SR technique can measure magnetic fluctuations rates in the range  $10^4$  to  $10^{12}$  Hz, which bridges the gap between fluctuation rates sensed by the NMR and neutron scattering technique.
- Muons can be implanted into any material (gas, liquid or solid) and the  $\mu$ SR method can be applied to samples in a large variety of environments (any temperature, magnetic fields, electric fields, high pressure, irradiated with light, applied RF pulse and so on).

## **II.8 Neutron science**

Nuclear data is a part of nuclear physics and a basic element in the research and development of nuclear engineering. Nuclear data is the basic and key element in developing nuclear technologies. A set of nuclear data form a data library, which is implemented in the simulation code. Simulation codes are essential tools in designing and analyzing nuclear reactors. Nuclear data is important in the development of not only nuclear reactors, but also of radiation technology. Decay data and transportation information for radiation play an essential role in developing radiation technologies.

Research related to nuclear data is divided into two categories: experimental measurement and theoretical research, such as the evaluation and development of nuclear models. Experimental measurements can provide nuclear data directly and be the

basis of evaluation and model development at the same time. Experimental measurements include those of reaction cross sections, properties of reaction products, and nuclear structure and decay data. Most importantly, nuclear data includes the cross sections of neutron-induced reactions, such as capture, elastic scattering, inelastic scattering, and fission, since those data are necessary in the development of nuclear reactors. The main goal of RISP is to produce RI beams by stable beams, and to use such RI beams for nuclear physics and astrophysics. The research goal of the nuclear data area is to use the stable beams of RISP facility for nuclear data measurements. Various types of stable beams can be used for measurements related to the reactions induced by charged particles. In addition, proton and deuteron beams among charged particles can be used to produce neutrons by irradiating appropriate target materials. Those neutrons are used to measure the cross sections and other nuclear data related to neutron-induced reactions. The short-term goal is to produce fast neutrons and use those neutrons for measurements. The long-term goal is to produce spallation neutrons and use those neutrons and charged particles for measurements.

The nuclear data of fast neutrons is needed to develop fast reactors, fusion reactors, accelerator-driven systems, and some industrial technologies. The nuclear data of charged particles is also needed in the medical industry, radiation damage research, and other industries. RISP facility can be used to produce various kinds of nuclear data. Three research topics are suggested for the measurements of nuclear data using RISP. Topic 1 is measurements of nuclear data related to the fast neutron. The cyclotron of RISP can provide 70 MeV proton beams. Fast neutrons are produced when a proton or deuteron beam on the order of 10-100 MeV bombards a light nuclei target such as Li, Be, or C. Those fast neutrons have energies almost as high as those of cyclotron beams. Therefore, measurements of fast neutron related data are possible. Topic 2 is measurements of nuclear data using spallation neutrons. The driver linac of RISP provides more than 600 MeV protons, which can produce spallation neutrons when the protons irradiate a heavy

nuclei target, such as W, Ta, Pb, U, etc. The spallation source consists of a wide energy range of neutrons. High flux thermal neutrons are available with the moderator installed around the spallation source target. Topic 3 is the measurements using charged particles. The driver linac provides a variety of stable particles from proton to Uranium with the energy of 200 MeV/u. Heavy ion beams can be accelerated to the proton or deuteron target to study nuclear reaction models based on the inverse kinematics. Proton, deuteron, and He beams can be used to measure cross sections of a sample using surrogate reactions.

The nuclear data measurement system at RISP will be constructed to produce a neutron total cross section, neutron induced-fission cross section, neutron capture cross section, elastic scattering cross section, and inelastic scattering cross section on the structural materials of new nuclear power plants and fuel materials.

Measurements of the neutron cross section are performed by using an n-TOF system with a plastic detector, liquid scintillators, and gamma-ray detecting system with HPGe and C<sub>6</sub>D<sub>6</sub> detectors, and fission chamber.

## **II.9 Atom trap for rare isotope research**

Measurement of the mass of an atom gives us the information on the binding energy of the atoms. Since the binding energy comes from the various physical forces integrating the building blocks, the mass measurement can reveal the fundamental interactions and their effects on static and/or dynamic structure of an atom. High-accuracy mass measurements and mass comparisons of stable or radioactive nuclei on the level of 10<sup>-8</sup> and better have a wide variety of fundamental applications in physics and metrology.

Mass measurements allow the study of the fine structure of the mass surface and clarification of discontinuities in order to extract nuclear structure information from binding energies. Data far from the valley of  $\beta$ -stability represent well-suited test cases for the predictive power of mass models. High-precision measurements of masses, spins and moments, provide important ingredients for reliable nuclear astrophysical calculations and for the understanding of the composition of matter in the universe in general. It is also possible to determine the sequence of isomeric states or to prepare an isomerically pure beam. By investigating the isomeric states, we can get more information on the nuclear structure. High precision mass measurement can also be used to test Standard Model by testing the unitarity of CKM. Precision laser spectroscopy reveals the magnetic and electrostatic hyperfine structure (spin, magnetic moment, quadrupole moment), as well as the influence of the changes in nuclear charge radii on the isotope shifts between different isotopes of a given element. These valuable data can be measured with high accuracy and the nuclear parameters can be extracted model-independently which constitutes a stringent test for nuclear theory.

Another important research area we must consider is the neutral atom trap assisted Standard Model test experiments. Electric dipole moment measurements using for example Fr, and  $\beta$ - $\nu$  correlation measurement using K are the well-known cases. We are also considering the neutral atom trap but the discussions are still underway. The detailed design may be carried out at the next technical design phase.

Major research topics are as follows;

- Precision mass measurement for rare isotopes
- Precision laser spectroscopy for rare isotope research

The purpose of research is to offer the precise mass values and spectroscopic information of rare isotopes so that it can contribute to the research field of particle physics, nuclear physics, astrophysics and verification of standard model etc.

For the science, extensive mass measurements along isotopic and isotonic chains have allowed to study the complex nuclear structure with its shell and sub-shell closures. Combination of mass spectrometry, laser spectroscopy, and nuclear spectroscopy is used to determine the isomer states which have not found before. Masses of nuclides even far away from the valley of stability are important input parameters to calculate the rate and energetics of the nuclear transformations. The Standard Model demands the unitarity of the Cabibbo-Kobayashi-Maskawa (CKM) matrix and mass measurements can give an important test parameter for the unitarity, hence the Standard Model. High-precision mass measurements at  $10^{-8}$  level are used for the determination of the fine structure constant, a new definition of the kilogram, the provision of input data for the determination of the neutrino mass, and the search for neutrinoless double beta decay.

## Chapter III Accelerators

### III.1 Driver Linac

Driver Linac, the main heavy ion linear accelerator, is designed to accelerate ions from proton to Uranium to be used as the driver for 400 kW IF system. It can be also used as the driver for 400 kW ISOL system with the proton beam. In addition, it can be used as a post accelerator for the rare isotopes produced by the ISOL system to be accelerated up to 250 MeV/u. The accelerator can be segmented into injector, low energy linac (SCL1), high energy linac (SCL2) sections. The injector part includes two ECR ion sources, low energy beam transport (LEBT), Radio Frequency Quadrupole (RFQ) and Medium Energy Beam Transport (MEBT). ECR ion source generates various charge states of ions from proton to Uranium. For example, Uranium ions are generated with the charges 33+, 34+, 35+ etc. LEBT delivers these ion beams to the RFQ efficiently. Possibility of bunching at the LEBT is considered. RFQ accelerates the Uranium beam up to 300 keV/u. The MEBT matches the beam from the RFQ to the SCL1. All the accelerating structures in SCL1 and SCL2 are superconducting cavities and focusing elements are quadrupole doublets (QDs). SCL1 accelerates the U33+ beam up to 18 MeV/u. SCL1 consists of SCL11 and SCL12. SCL11 has 24 Quarter Wave Resonators (QWRs) and 24 QDs, while SCL12 has 138 Half Wave Resonators (HWRs) and 30 QDs. The charge stripper section is located between SCL1 and SCL2 to further strip ions for the more efficient acceleration at SCL2. SCL2 accelerates U78+ up to 200 MeV/u. SCL2 consists of SCL21 and SCL22. SCL21 has 88 Single Spoke Resonator (SSR) and 22 QDs and SCL22 has 136 SSR and 17 QDs.

### III.1.1 ECR Ion source

The electron cyclotron resonance (ECR) ion source (IS) is used as ion sources for the main linear accelerator. The design goal of the ECR-IS is to produce various ions with the kinetic energy of 10 keV/u and normalized rms emittance of  $0.1 \pi$  mm-mrad.

The performance of ECR ion source depends on the magnet design, RF frequency and its power. Superconducting (SC) magnets and a high frequency RF source more than 18 GHz are used to improve its ability. RISP employs the 28 GHz SC ECR ion source to produce the highly charged heavy ions like  $^{238}\text{U}^{33+}$ . The Main design parameters are summarized in Table III.1.1.1.

**Table III.1.1.1: Summary of main ECR-IS design parameters**

Frequency (GHz)	28 + (18)
RF Power (kW)	10
Plasma Chamber Diameter (mm)	150
Plasma Chamber Material	Aluminum
Mirror Length (mm)	500
$V_{\text{ext}}$ (kV)	30
SC Wire	NbTi
Number of Solenoid Coils	5
Sextupole Winding Type	Race track type
$B_{\text{inj}}$ (T)	3.5
$B_r$ (T)	2
$B_{\text{ext}}$ (T)	2
$B_{\text{min}}$ (T)	0.4 ~ 0.8

The design of the SC magnets is the most important part of the ECR ion source design. RISP model is to use five solenoids for adjusting ECR zone efficiently. The racetrack

winding technique is used for sextupole coils. The nominal axial fields of the magnets are 3.5 T at the injection side and 2 T at the extraction side while the minimum axial field is variable between 0.4 T and 0.8 T. The nominal radial field strength is 2 T at the plasma chamber wall. Figure III.1.1.1 shows the SC magnet design and typical axial field strength.

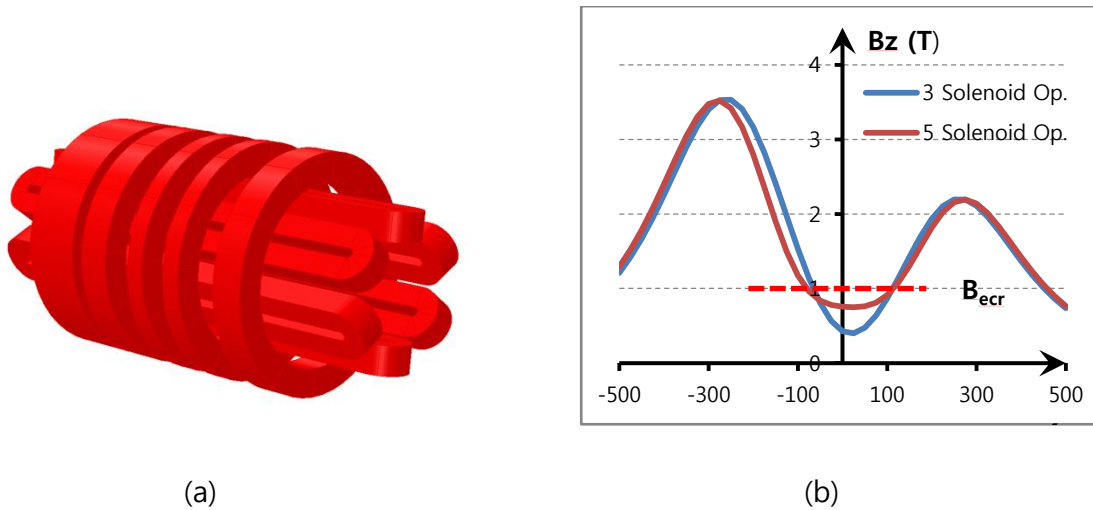


**Figure III.1.1.1: (a) SC magnets design, (b) Axial B Field.**

For the SC magnets, 4 K cryogenic system has to be prepared. The ECR ion source requires more than 10 W cooling powers at 4 K during the operation because X-rays from the plasma chamber could be an extra heat load to the cryostat. Therefore reducing the X-rays is also an important design factor for the SC ECR ion source.

The RF system consists of a 28 GHz gyrotron, an arc detector, a dual directional coupler, a mode converter from TE02 to TE01, a mode filter, corrugated waveguide with 90° bend, high voltage DC break, and a RF window. Because dual frequency operation improves the overall performance, an additional 18 GHz RF source is adapted to produce high charge states and high current ions.

The plasma chamber has a length of 500 mm and an inner diameter of 150 mm. Tantalum sheet with a thickness of 3 mm is used for the x-ray shielding and Kapton

sheet is used for electrical insulation of the plasma chamber wall. The isolated water cooling system is connected to a pipe surrounding the plasma chamber wall. Two turbo molecular pumps are installed below the injection and extraction boxes in order to make UHV environment. The extraction electrode can be movable to maximize the beam current and both sides of the plasma chamber are designed to move for the cryostat installation and the maintenance. Additionally, a high temperature (2000 °C) oven for solid isotopes and a high voltage platform for heavy ions will be necessary.

### **III.1.2 Low Energy Beam Transport (LEBT)**

The LEBT consists of two bends and quadrupoles for achromatic optics, solenoids for beam matching between ECR-IS and RFQ, two bunchers, steering magnets, collimation systems, and diagnostics. Figure III.1.2.1 shows the layout of the LEBT in the Front-End. Figure III.1.2.2 shows designed optics and envelopes for the LEBT beam line. The optics design is optimized by TRANSPORT code.

The dc beam from the ECR-IS is bunched before injection into the RFQ. For a short bunch length with high bunching efficiency, two bunchers are applied. Beam simulation code of IMPACT-Z is utilized for 6-dimension tracking that includes space charge force. A normalized rms emittance of 0.1 pi mm-mrad and intrinsic energy spread of 0.05% are considered. 20,000 macro-particles initially generated in 4-dimensional water-bag transverse distributions with a uniform longitudinal distribution in phase space are tracked in the beam simulation.

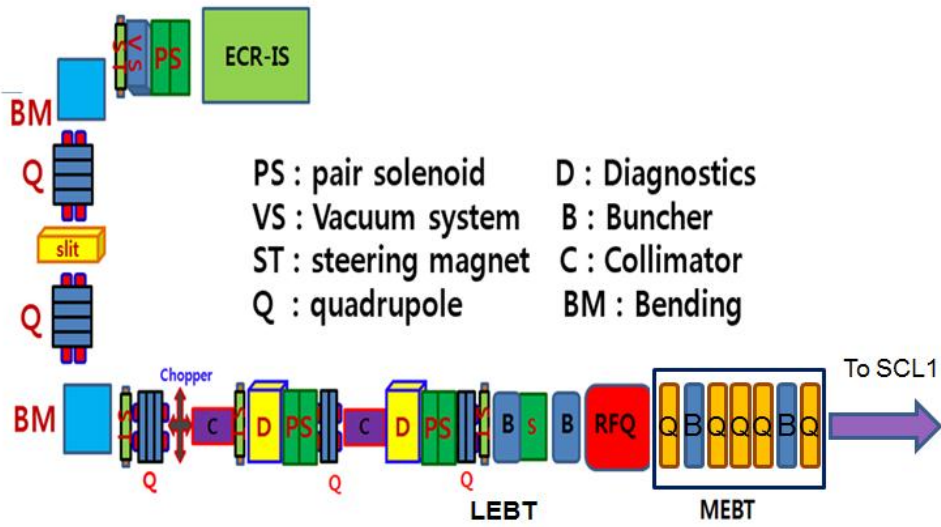


Figure III.1.2.1: Layout of the LEPT in the Front-End

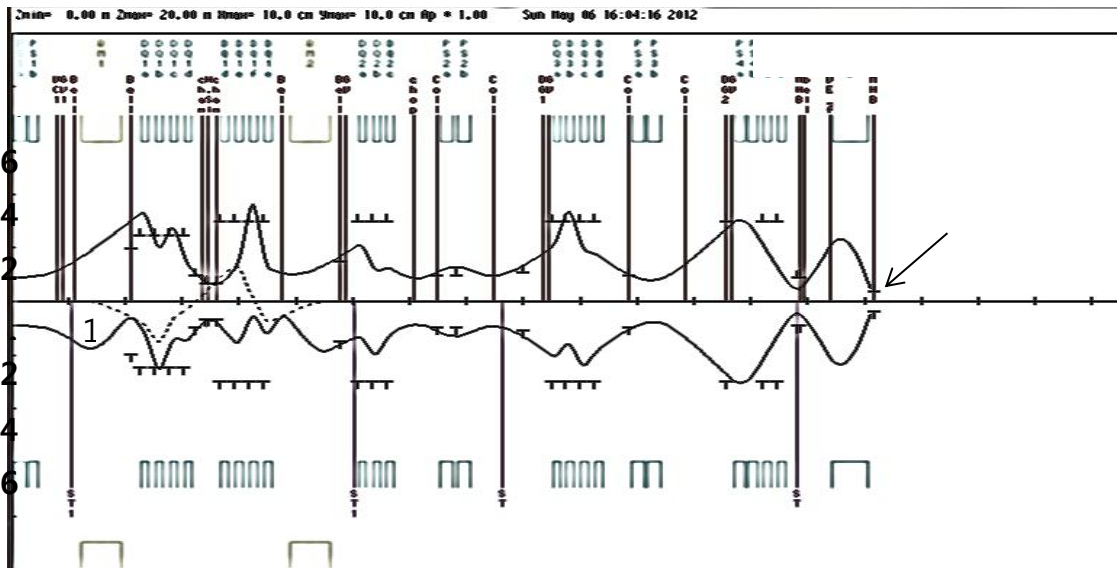
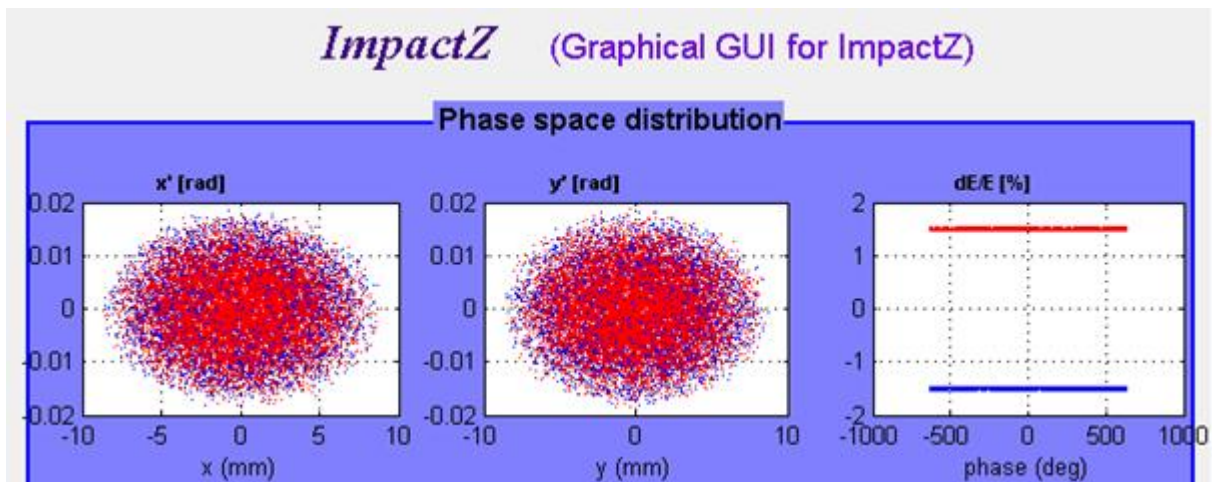


Figure III.1.2.2: Designed optics and envelopes of the LEPT

Figure III.1.2.3 shows the initial beam distributions of two-charge state beam of  $^{238}\text{U}^{33+}$  and  $^{238}\text{U}^{34+}$  in the LEPT. Figure III.1.2.4 shows the beam distributions before and after the

first buncher. Figure III.1.2.5 shows the beam distributions before and after the second buncher. Figure III.1.2.6 shows longitudinal beam distributions at the entrance of the RFQ. It clearly shows that two-charge state beam can be accelerated at the same time in the RFQ by matching phase space. The second buncher of 40.625 MHz is also used to match the energy of two-charge state beams at the RFQ entrance. A distance between the first buncher and the second buncher is 1.18 m for the two-charge state beam of  $^{238}\text{U}^{33+}$  and  $^{238}\text{U}^{34+}$

The beam simulation shows that the designed LEBT provides a good beam matching and bunching for the two-charge state beam. Expected transverse and longitudinal emittances are also obtained at the entrance of RFQ and the space-charge effects with the U beam current of 400 euA in the LEBT is small.



**Figure III.1.2.3 Initial beam distributions in the LEBT**

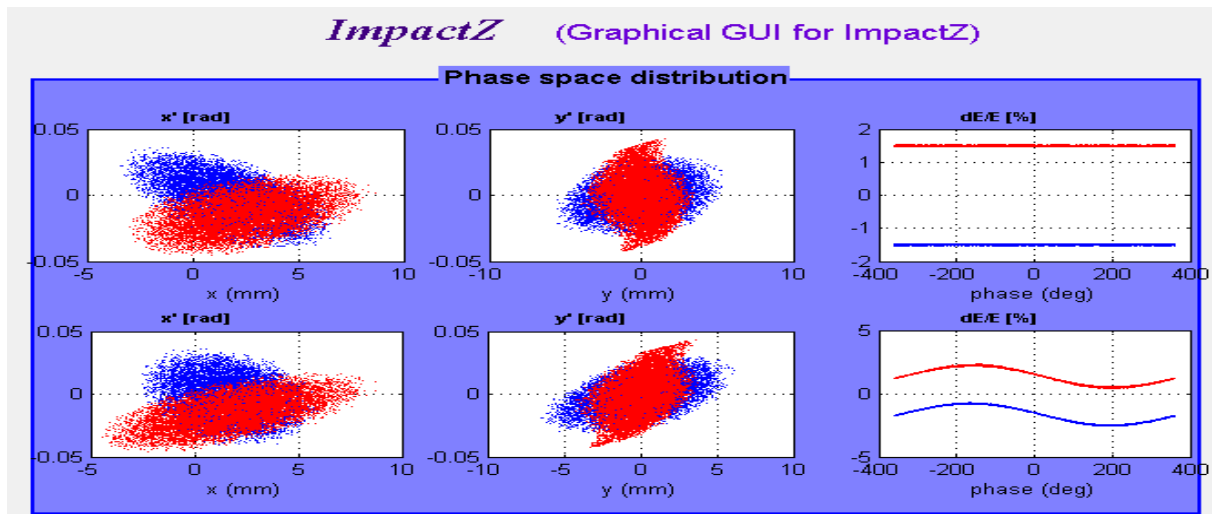


Figure III.1.2.4 Beam distributions before and after 1<sup>st</sup> buncher in the LEBT

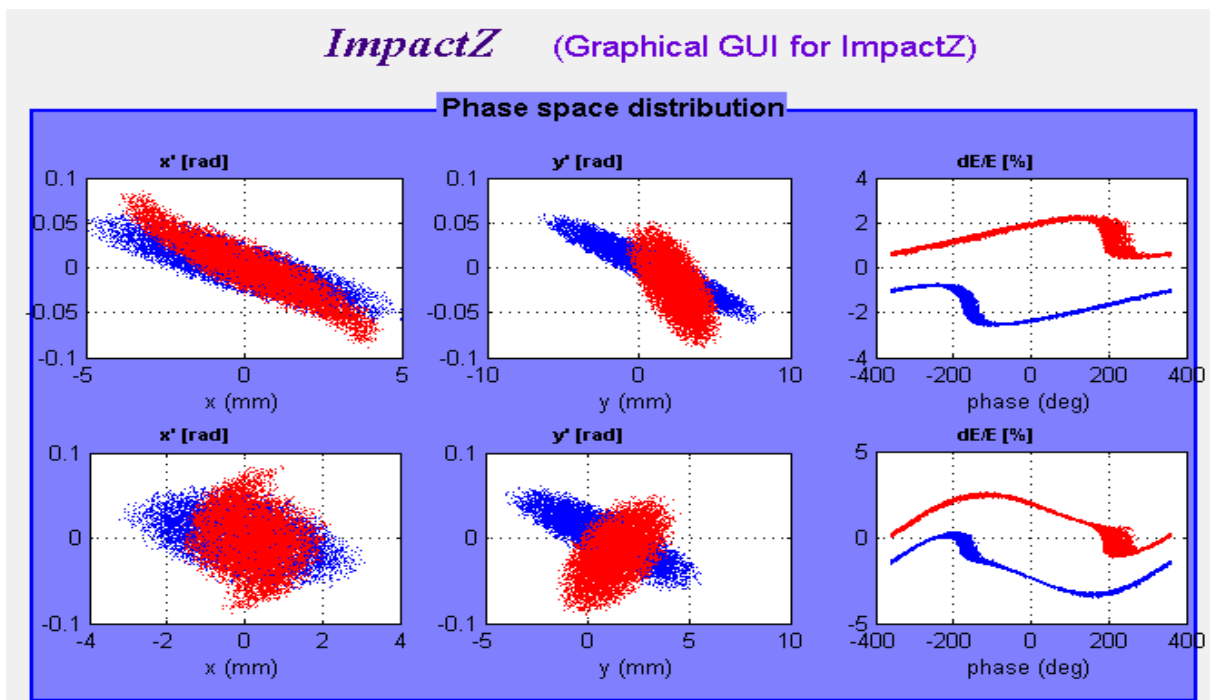


Figure III.1.2.5 Beam distributions before and after 2<sup>nd</sup> buncher in the LEBT

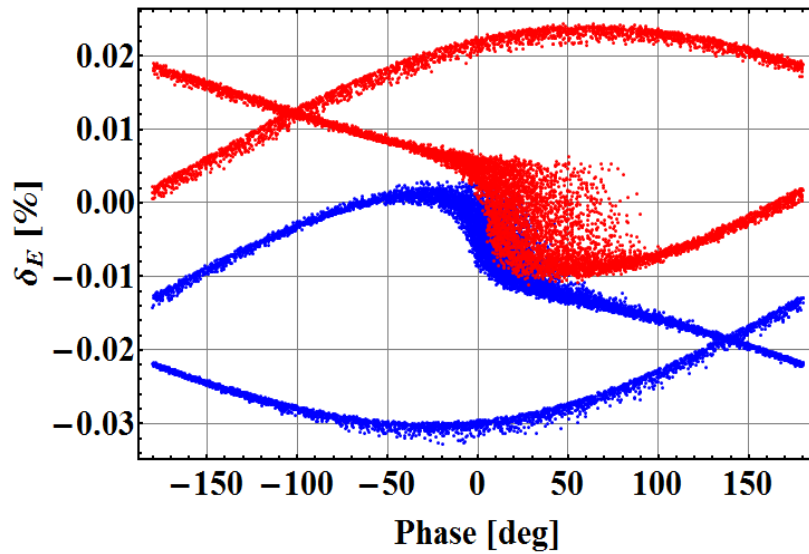


Figure III.1.2.6 Longitudinal beam distribution at the entrance of RFQ

### III.1.3 RFQ

Radio Frequency Quadrupole (RFQ) is to bunch and accelerate beams transported from the LEBT. It consists of a radial matching section, shaper, gentle buncher, and accelerating section. The RFQ is designed to accelerate two-charge state ( $^{238}\text{U}^{33+}$  and  $^{238}\text{U}^{34+}$  of  $12\mu\text{A}$ ) beams from 10 keV/u to 300 keV/u. The PARMTEQ is used to obtain the RFQ design parameters. Table III.1.3.1 shows the main input parameters of RFQ. A charge state of 33.5 for the U beam simulation is used to mimic a multi-charge state beam.

Table III.1.3.1: Main parameters for RFQ

Reference Particles	$^{238}\text{U}^{33+}$ and $^{238}\text{U}^{34+}$
RF Frequency	81.25 MHz
Input charge state	33.5
Input Energy	10 keV/u
Output Energy	300 keV/u

Beam Current	12 $\mu\text{A}$
Input Transverse Emittance	0.1 $\pi$ mm-mrad (normalized rms)
Vane Voltage	70 kV

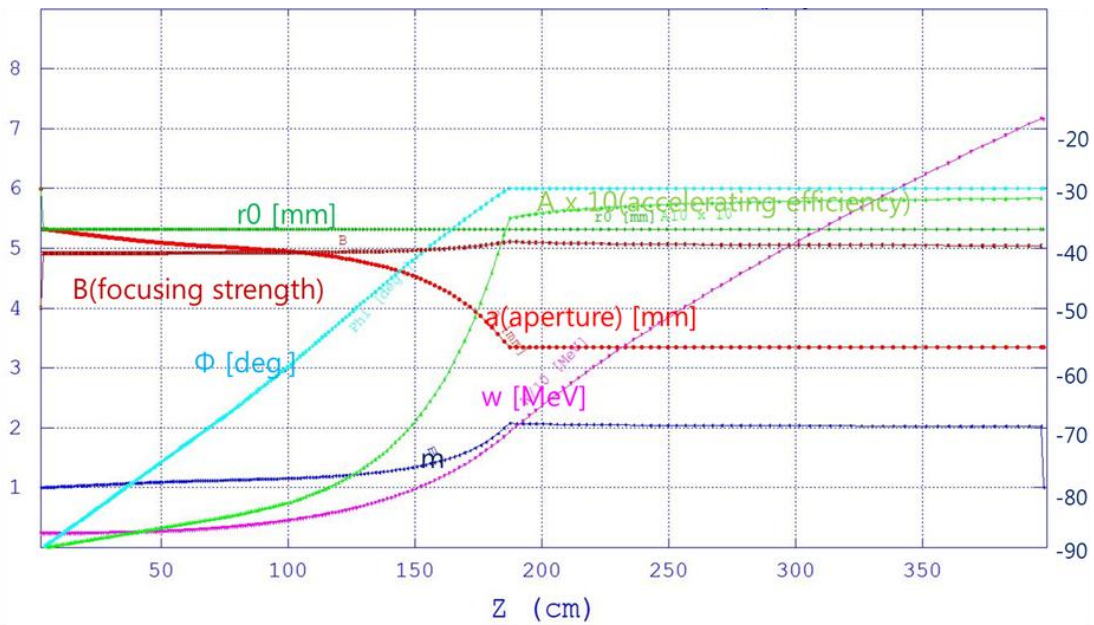


**Figure III.1.3.1 Synchronous phase, modulation factor, focusing strength and radius**

Figure III.1.3.1 shows the behavior of the physical quantities of the RFQ as a function of length. The vane voltage is fixed to be 70 kV. The focusing strength is adopted as a constant ( $B \sim 5.08$ ) along the RFQ. The accelerating efficiency is fixed to be 0.55 in order to reduce the total length of the RFQ. The synchronous phase becomes -30 degrees at the end of gentle buncher from -90 degrees at the entrance of the RFQ. The modulation factor increases from 1 to about 2 and the average radius is 5.32 mm. The total length of the RFQ is 3977.87 mm and total number of cells is 220. The maximum peak surface electric field ( $E$ ) that occurs at cell number of 218 is 17.7659 MV/m and the value  $E$  corresponds to  $1.69E_k$ , where  $E_k$  is the Kilpatrick criterion. Ten thousand particles are generated to simulate the beam current of 12  $\mu\text{A}$ .

Figure III.1.3.2 shows the input and output particle distributions in the transverse and longitudinal planes. Simulation used 4D water bag model for input transverse particles and 2D uniform model for longitudinal particles. The Twiss parameters are  $\alpha_{x,y} = 0.7445$ ,  $\beta_{x,y} = 4.7536$  cm/radian. Figure III.1.3.3 shows the particle distributions in the transverse (horizontal, vertical) positions, phase deviation and kinetic energy deviation as a function of cell number. Transmission rate in the RFQ is 90.8%.

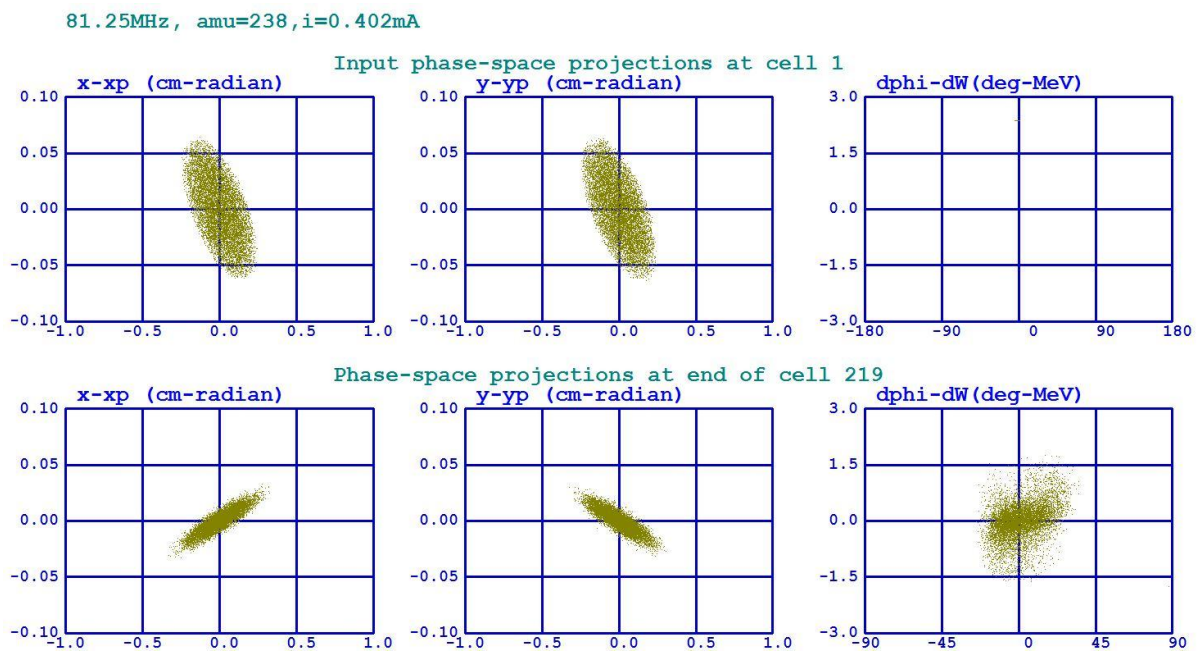
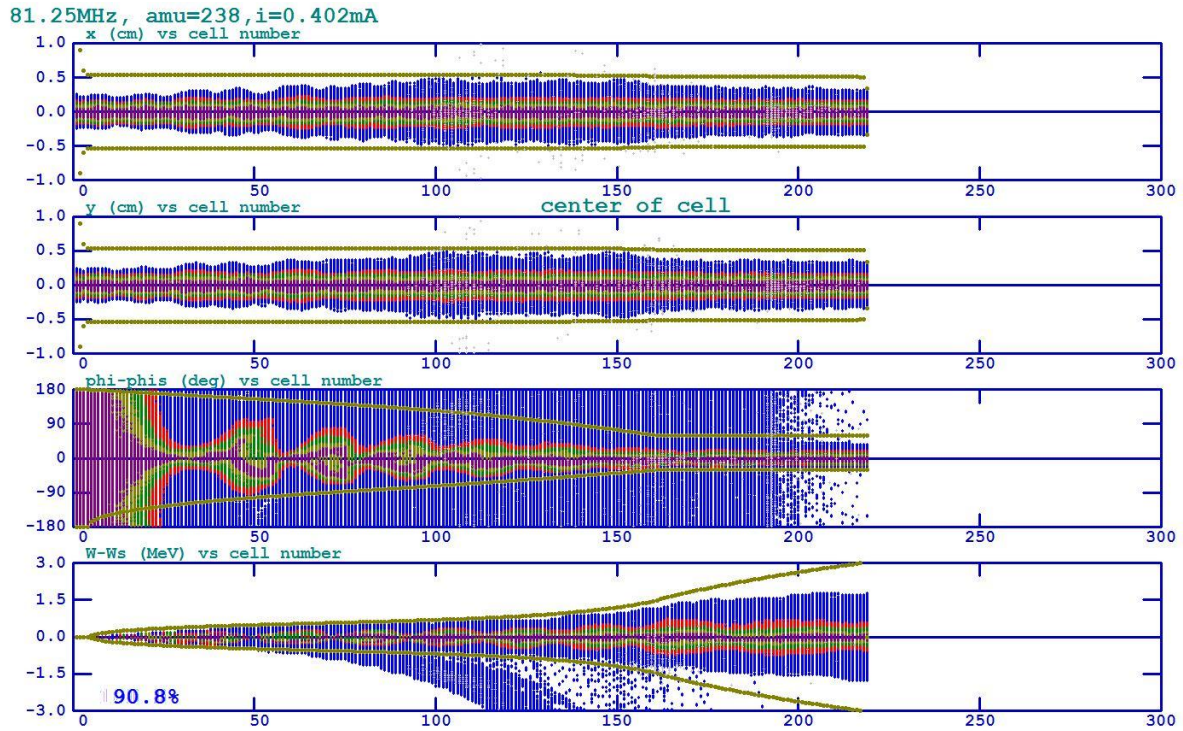


Figure III.1.3.2 Beam distributions at the entrance (top) and exit (bottom) of RFQ



**Figure III.1.3.3 Transverse and longitudinal envelopes**

The normalized rms transverse emittances of output beam are  $\epsilon_x = 0.12 \pi$  mm-mrad and  $\epsilon_y = 0.12 \pi$  mm-mrad. The longitudinal emittance is  $\epsilon_z = 6.6$  MeV-deg. Each single-charge state of +33 and +34 U beam with 12 puA was also tracked at the same design. Table III.1.3.2 shows the simulation result for each charge state.

**Table III.1.3.2: Beam parameters for charge-state of 33 and 34 of U beam**

charge	Transmission rate(%)	$\epsilon_x$ [ $\pi$ mm-mrad]	$\epsilon_y$ [ $\pi$ mm-mrad]	$\epsilon_z$ [MeV-deg]
33	90.7	0.12	0.12	13.53
34	91.1	0.12	0.12	6.0

TRACK simulation code is also used for the two-charge state beam simulation. Field information from PARI and PARMTEQM is used for input beam parameters. In the TRACK code, the aperture radius is fixed to be 5.32 mm. Twiss parameters and

emittance of input beam are the same as the PARMTEQ program. 10000 particles are generated to simulate the beam current of 12pμA. Figure III.1.3.4 shows the result of TRACK code for the two-charge state beam ( $^{238}\text{U}^{33+}$  in blue and  $^{238}\text{U}^{34+}$  in green). The beam transmission rate is 93% and the normalized rms transverse emittances of output beam are  $\epsilon_x = 0.103 \pi$  mm-mrad,  $\epsilon_y = 0.103 \pi$  mm-mrad in horizontal and vertical direction, respectively. A longitudinal emittance is 1.3 keV/u ns.

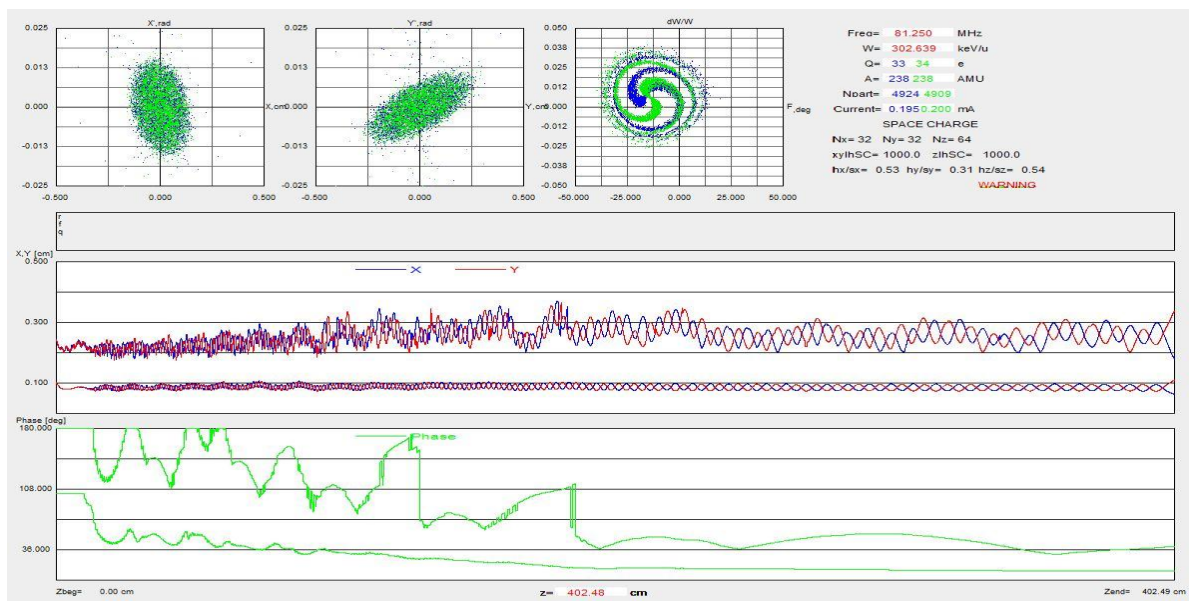


**Figure III.1.3.4: Beam distributions at the exit of RFQ by code TRACK**

Figure III.1.3.5 shows the results for the two-charge state ( $^{238}\text{U}^{33+}$  in blue and  $^{238}\text{U}^{34+}$  in green) beam from the LEBT. The beam transmission rate is 80% and normalized rms transverse emittances of output beam are  $\epsilon_x = 0.14\pi$  mm-mrad and  $\epsilon_y = 0.14 \pi$  mm-mrad in the horizontal and vertical directions, respectively, and longitudinal emittance is 1.08 keV/u ns.

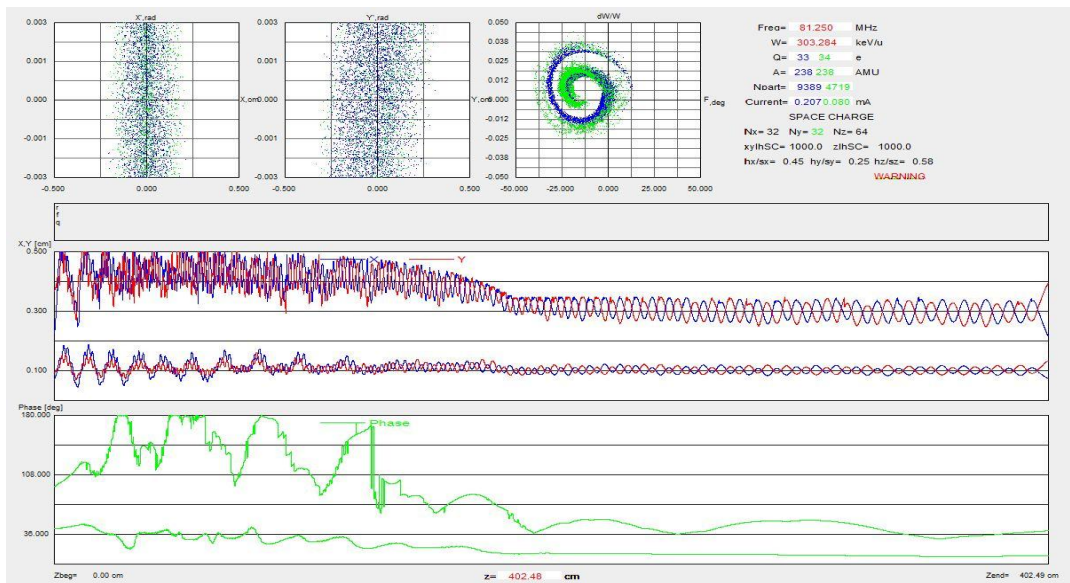


**Figure III.1.3.5 Beam distributions at the exit of RFQ by code TRACK when the beam from the LEBT is used**

## II.1.4 Medium Energy Beam Transport (MEBT)

The Medium Energy Beam Transport (MEBT) system located between the RFQ and superconducting linac (SCL), requires to match the optical parameters in transverse plane and to remove the unaccelerated ion beams from the RFQ. It also includes beam diagnostic devices to measure the beam quality.

### III.1.4.1 MEBT Beam Optics Design

The optics design of the MEBT system was performed by using TRACE3D code and particle tracking was performed using IMPACT-Z code. Basically the optics function was matched to the betatron function at the entrance of the SCL. The MEBT design is to transfer the two-charge state beams of the  $U^{33+}$  and  $U^{34+}$ . The schematic layout of the MEBT is shown in Figure III.1.4.1.1. The MEBT system is designed to have enough spaces

for beam diagnostic devices such as Beam Profile Monitor, Beam Position Monitor, Wire Scanner. The transverse beam size can be controlled by the knobs installed in the upstream of beam diagnostic devices to measure the beam information in MEBT system.



**Figure III.1.4.1.1 Scheme of MEBT system**

Six room temperature quadrupole magnets are used to minimize the transverse emittance growth of two-charge-state beams and to provide the transverse focusing at the entrance of the SCL. Two rebunchers are used to provide flexible longitudinal matching from the exit of the RFQ to the entrance of the SCL. The output of TRACE 3D simulation in MEBT with quadrupole magnets is shown in Figure III.1.4.1.2.

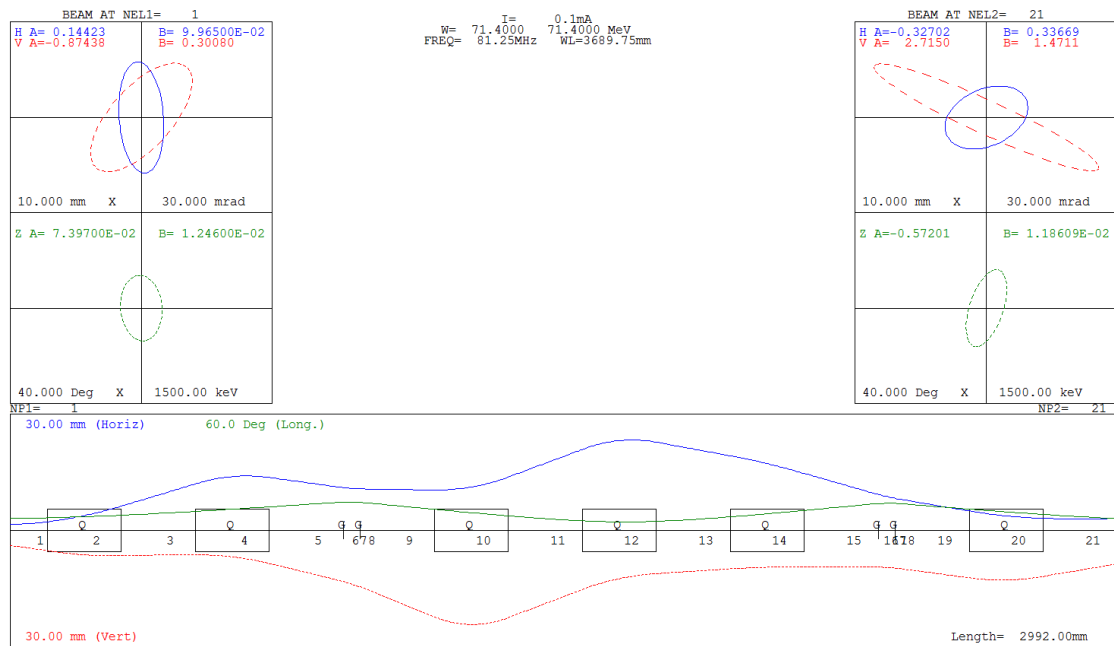


**Figure III.1.4.1.2 Beam envelope and phase space distribution in longitudinal and transverse plane calculated by using TRACE3D of designed MEBT system**

IMPACT-Z code is used to estimate the space charge effects in the MEBT system and its simulation results are shown in Figure III.1.4.1.3. The quadrupole magnets have a field of less than 0.5 T at the pole-tip. The rebuncher will be an 81.25 MHz  $\beta_{opt} = 0.025 \lambda/4$  room temperature resonator. The total length of the MEBT is about 3 meters.

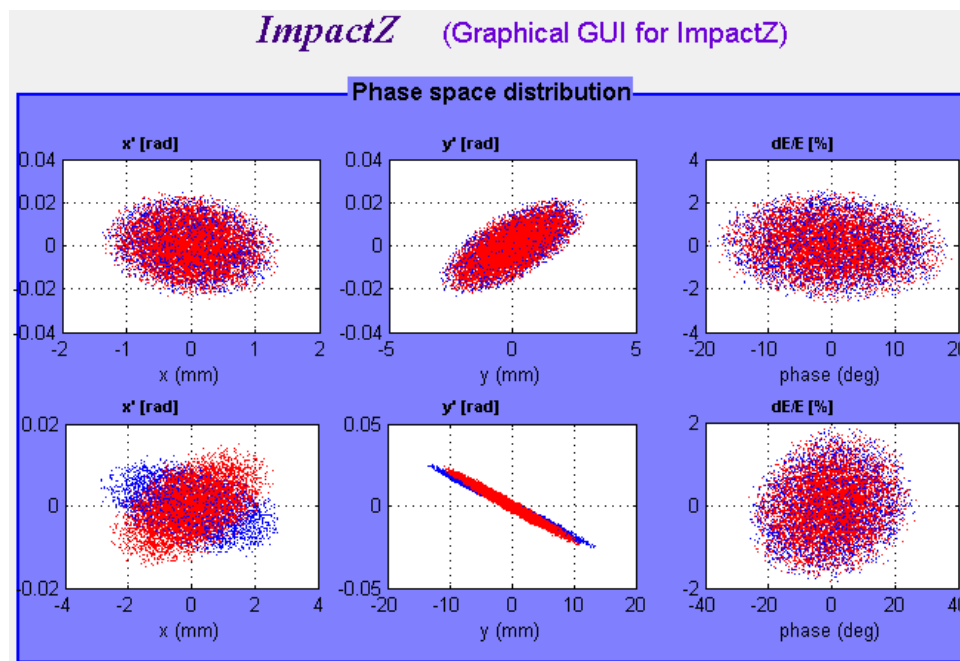


**Figure III.1.4.1.3 Beam envelope and phase space distribution in longitudinal and transverse plane calculated by using IMPACT-Z of designed MEBT system**

### III.1.4.2 Front-end beam simulation

Figure III.1.4.2.1 shows beam envelope and phase space distribution in longitudinal and transverse planes at the MEBT when the front-end beam simulations including the LEBT and RFQ are performed. Table III.1.4.2.3 shows the summary of the beam parameters and particle transmission that are obtained by front-end beam simulations.

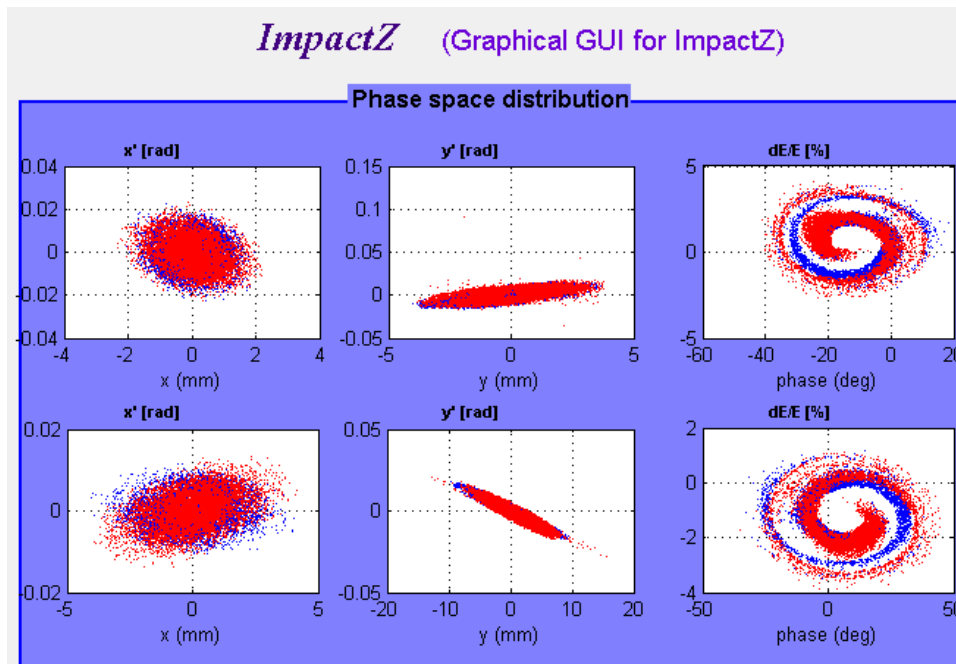


**Figure III.1.4.2.1 Beam envelope and phase space distribution in longitudinal and transverse planes in the MEBT by the front-end beam simulations**

**Table 1.4.2.3 Summary of the beam parameters from Front-End simulations**

With Bunchers	Number of Particle	Transm. Efficiency(%)	Current[mA] 33+, 34+	Nor.rms_x [mmmrad]	Nor. rms _y [mmmrad]	Nor. rms _z [deg-MeV]
Initial	20000	100	0.22, 0.17	0.100	0.100	3.66
LEBT	19253	96.27	0.22, 0.16	0.109	0.174	3.15
RFQ	16093	80.47	0.19, 0.13	0.122	0.183	8.27
MEBT	15790	78.95	0.19, 0.12	0.123	0.181	8.22

### **III.1.5 Super Conducting Linac (SCL)**

#### **III.1.5.1 Frequency Choice**

Study has been conducted for the choice of the base frequency of the Superconducting Linac (SCL). A case is studied with the base frequency higher than 70 MHz, because higher frequency means higher efficiency in general. The following factors are considered:

- Do broad base of world class labs exist that use the frequency, which means that there are subsystems available and that the project can save R&D cost?
- Mechanical rigidity of a cavity increases for higher frequency.
- Many labs have chosen their frequency based on their history and boundary conditions.
- Choice of frequency needs to be backed by beam dynamics.

An investigation shows that there are two major camps of frequency choice. One camp prefers 81.25 MHz (and multiples of this frequency) including ANL, FNAL, TRIUMF, IMP etc, and the other prefers 88 MHz (and multiples of this frequency) including SPIRAL2, CERN, ESS, SARAF etc. Feasibility studies based on beam physics of the SCL are conducted with 81.25 MHz as the base frequency and no show-stopper has been found. A choice between 81.25 MHz and 88 MHz is recommended considering collaboration aspects and the availability of subsystem components. And a decision is made to choose 81.25 MHz as the base frequency of the facility.

#### **III.1.5.2 Driver Superconducting Linac (SCL) Lattice**

It is known that the position of each component in a cryomodule changes by no less than a millimeter in a random fashion during the cool-down of a cryomodule and it is extremely difficult to predict accurately enough alignment of superconducting solenoids

in a cryomodule after the cool-down. Accurate alignment of focusing elements such as superconducting (SC) solenoids is very crucial for maintaining the beam quality of high intensity beams which is envisioned for the heavy ion accelerator. For high intensity operations, the foreseen uncertainty of no less than a millimeter displacement can induce intolerable level of beam loss, leading to activation of accelerator components and potential quench of superconductors inside cryomodules.

The previous SCL design with SC solenoids presents the following challenges and issues:

- Alignment of SC solenoids is not trivial to control. It is known that components in a cryomodule can move no less than a millimeter during cool-down.
- Small misalignment of SC solenoids by  $\pm 0.5$  mm generates significant emittance growth (simulations indicate factor 2.5 emittance growth by the end of the short beta=0.047 SCL11).
- Heat deposit by beam loss in the SC solenoids can be an issue such as quench.
- Operation of the SCL is not trivial for example due to the magnetization of surrounding elements in the cryomodule.
- It is found that the matching between different segments of the SCL is challenging. And the design is not optimized.
- The solenoids in the beta=0.041 segment are very short (12 cm long) and the required field can go as high as 11 Tesla.
- The SCL1 employs long cryomodules that contain 8 cavities and 3 or 8 solenoids. This design imposes significant restriction on the beam diagnostics access and this leads to difficulties in the accelerator tuning for a high intensity operation.

These points raised concerns and studies have been initiated to come up with a better SCL lattice design that can enable high intensity beam operations by improving the beam quality and straightening complexities. These are crucial design considerations in designing the SCL, for the intensity heavy ion beams has increased steadily. The SPIRAL2 project also adopted quadrupole doublet focusing lattice for the high intensity ion beam acceleration (for instance 1 mA of heavy ion beams and 5 mA deuteron beam) [III.1.5.2.1].

Studies have identified that the SCL lattice with normal conducting (NC) quadrupole doublets has the following advantages:

- High intensity beam acceleration and operation are easy – by adopting quadrupole magnets outside the cryomodule. Quadrupole doublets can be aligned better than  $\pm 150 \mu\text{m}$ .
- Through beam dynamics simulations with machine imperfections, we get a very small beam emittance growth in transverse planes, demonstrating that the proposed design is more suitable for high intensity ion beam acceleration.
- Beam boxes between the doublets are regularly placed along the SCL and are reserved for beam diagnostics and collimators. This configuration provides complete beam diagnostics coverage. This is very crucial for tuning for high intensity operation.
- Quadrupoles are integrated with a dipole steering element due to their compact design. Orbit corrections are done using the dipole correctors coupled with BPMs (Beam position Monitors).
- The linac has the same quadrupole lattice with the charge stripping section and the following beam lines.
- Cost estimation shows little difference from the cost of the previous design.

Multi-particle beam tracking using the TRACK code shows that the emittance growth is well controlled and the matching between different beta segments is easy for the proposed linac with NC doublets. Study also shows that the SCL lattice with NC quadrupoles is pretty tolerant against machine imperfections. In-depth multi-particle tracking studies are to be done in the Technical Design Report stage.

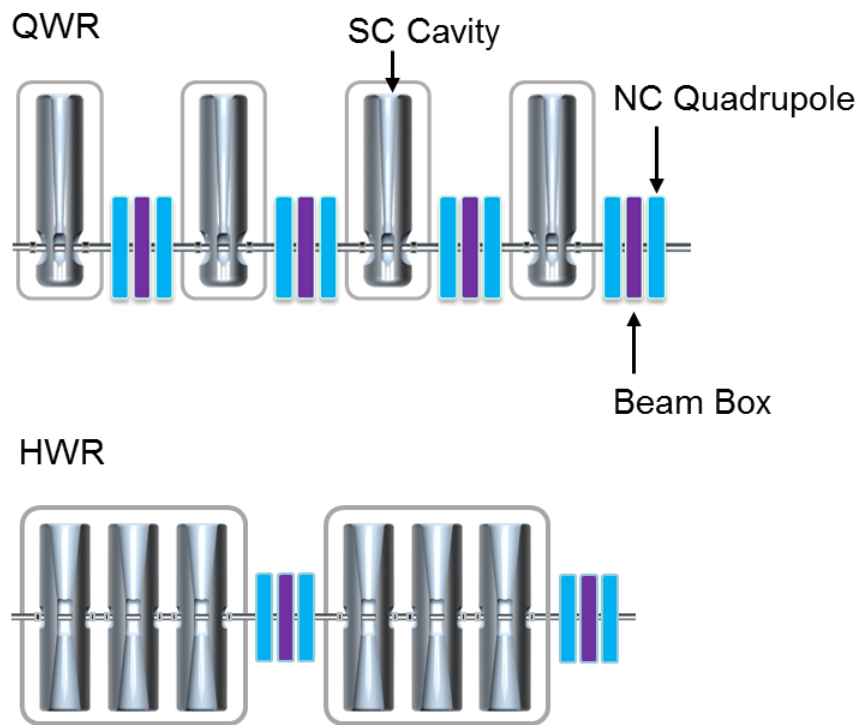


**Figure III.1.5.2.1: Schematic plots showing the baseline SCL1 lattice with normal conducting quadrupoles. Beam boxes are for beam diagnostics.**

**[Reference III.1.5.2]**

[III.1.5.2.1] R. Ferdinand et al., Proc. of LINAC Conference 2010, p. 16, Tsukuba, Japan

### III.1.5.3 Geometric Betas, Types and Parameters of Superconducting Cavities

Over all the design choice of cavities is optimized for high intensity operations anticipating that the performance ion sources will improve ever in the future. Compared with the previous design, the Quarter Wave Resonator (QWR) segment is minimized by eliminating the second family of the  $\beta_g = 0.085$  QWR because of the dipole kick and the asymmetric field of QWR. The second QWR segment is replaced with  $\beta_g = 0.12$  Half Wave Resonator (HWR) segment. Unlike QWR, HWR does not have the  $\beta$ -dependent dipole kick due to their symmetric nature of electro-magnetic fields of the cavity. By adopting HWR, beam quality control becomes easier especially for high intensity beam operation.

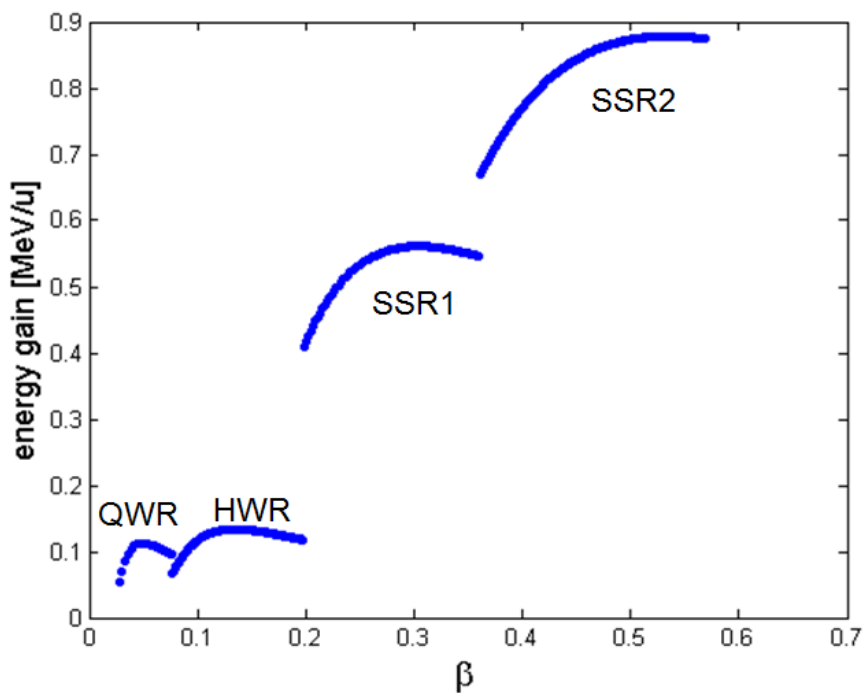


Figure III.1.5.3.1: Plots of energy gain for the Uranium beam with the optimized set of  $\beta_g=[0.047, 0.12, 0.30, 0.53]$ . For QWR and HWR,  $U^{+33}$  beam is used and for SSR1 and SSR2,  $U^{+79}$  beam is used.

The  $\beta_g = 0.285$  and  $\beta_g = 0.53$  HWR segments of the previous design are also replaced with Single Spoke Resonators (SSR) because of the advantage that SSR can have a larger bore radius. This is quite an advantage in reducing the uncontrolled beam loss in the high energy segment of the SC linac for high intensity operations.

Optimization of the geometric betas of SC cavities is done and an optimum set of  $\beta_g = [0.047, 0.12, 0.30, 0.53]$  is obtained. And for each type of SC cavities, optimization of the cavity geometry is being conducted with respect to  $R/Q$ ,  $E_{\text{peak}}/E_{\text{acc}}$  and  $B_{\text{peak}}/E_{\text{acc}}$  etc. Acceleration efficiency is relatively low because of the choice of bigger bore radius of 20 mm for the QWRs and HWRs compared with the 15 mm bore radius of the corresponding cavity families of the FRIB for instance. However, due to the larger bore radius beam loss can be lowered as an advantage.

For the cryogenic requirement, parameters in Table III.1.5.1 are used. The BCS resistance  $R_{BCS}$  is defined by

$$R_{BCS} = 2 \times 10^{-4} \frac{C_{RRR}}{T} \left( \frac{f}{1.5} \right)^2 \exp\left( -\frac{17.67}{T} \right) [\Omega], \quad (1.5.3)$$

where  $T$  is the surface temperature in K,  $f$  is the RF frequency in GHz.  $C_{RRR}$  is the correction factor, assumed to be 1.5 for high-purity niobium whose RRR is about 250. Dynamic load of each cavity type is calculated and a safety factor of 1.5 is multiplied for the wall loss of each cavity  $P_0$  in Table III.1.5.2. The total dynamic load of the driver SCL is estimated to be 1.73 kW at 2K and that of the ISOL post-accelerator is 0.24 kW at 2K. Table III.1.5.2 lists the cavity parameters including dynamic load of each cavity and RF power requirement for uranium beam and proton beam. Beam power is calculated by  $P_{\text{beam}} = I_{\text{beam}} V_{\text{acc}} \cos\phi_{\text{RF}}$  where  $\phi_{\text{RF}} = -30^\circ$ . This is a nominal RF phase.

**Table III.1.5.1 Surface Resistance for the SC Cavities.**

<b>Parameters</b>	<b>Unit</b>	<b>QWR</b>	<b>HWR</b>	<b>SSR</b>
<b>Resonant frequency</b>	MHz	81.25	162.5	325
<b>Operating temperature</b>	K	2	2	2
$C_{RRR}$	-	1.5	1.5	1.5
$R_{BCS}$	nΩ	0.06	0.26	1.02
$R_{res}$	nΩ	10	10	10
$R_s$	nΩ	10.06	10.26	11.02

**Table III.1.5.2 Cavity Parameters.**

<b>Parameters</b>	<b>Unit</b>	<b>QWR</b>	<b>HWR</b>	<b>SSR 1</b>	<b>SSR 2</b>
$\beta_g$	-	0.047	0.12	0.30	0.53
<b>Resonant frequency</b>	MHz	81.25	162.5	325	325
<b>No of cavities</b>	-	24	138	88	136
<b>Aperture diameter</b>	mm	40	40	50	50
$QR_s$	Ohm	37	47	86	108
<b>R/Q</b>	Ohm	480	319	242	304
$V_{acc}$	MV	1.02	1.07	2.04	3.53
$E_{peak}$	MV/m	30	30	30	30
$B_{peak}$	mT	48	41	54	57
$E_{peak}/E_{acc}$		5.08	6.2	4.06	4.15
$B_{peak}/E_{acc}$		9.16	8.4	7.07	8.6
$Q_{calc}/10^9$	-	3.6	4.6	8.1	10
<b>Operating temperature</b>	K	2	2	2	2
$P_0$	W	1.3	1.5	4.7	7.9
<b><math>P_{beam}</math> / emA (proton)</b>	W	854	925	1440	2770
<b><math>P_{beam}</math> / emA (Uranium)</b>	W	113	134	524	926
<b>Beam current (Uranium)</b>	$\mu A$	9.5	9.5	8	8
<b>Average charge state (U)</b>	-	33.5	33.5	79	79

Here  $E_{acc} = V_{acc} / \beta\lambda$ .

### **III.1.5.4 Cost**

Cost estimation is conducted including the cost for cavity, tuner, coupler, internal cryogenics, vacuum system, cryomodule and processing & cryomodule assembly cost. Cost comparison between the two driver SCL options shows that the cost difference between the two options is in the error range of cost estimation, which is less than 1 % of the driver SCL cost. And cost estimation is made for both the driver SCL and the ISOL SCL assuming that we keep the same lattice choice for the ISOL SCL as well. The cost estimation shows that the overall combined cost difference is less than 2 % of the total cost when switching to the SCL lattice with NC quadrupoles. This difference is in the error range of cost estimation and it is concluded that cost is not an issue in adopting the proposed SCL lattice.

### **III.1.5.5 Superconducting Linac 1 (SCL1)**

The SCL1 consists of the SCL11 and the SCL12, each consisting of beta = 0.047, f = 81.25 MHz Quarter Wave Resonators (QWR) and beta = 0.12, f = 162.5 MHz Half Wave Resonators (HWR). The SCL1 accelerates  $U^{+33}$  beam from 0.3 MeV/u to 18.5 MeV/u.

#### **III.1.5.5.1 Superconducting Linac 11 (SCL11)**

The geometry of the QWR, which has beta = 0.047 and f = 81.25 MHz, is optimized with the 20 mm bore radius used to minimize the uncontrolled beam loss at the expense of reduced acceleration RF efficiency. Parameters of this cavity can be found in Table III.1.5.2. This segment accelerates  $U^{+33}$  beam from 0.3 MeV/u to 2.5 MeV/u and the cryomodule contains one beta = 0.047, f = 81.25 MHz QWR and there are twenty four cryomodules of this type.

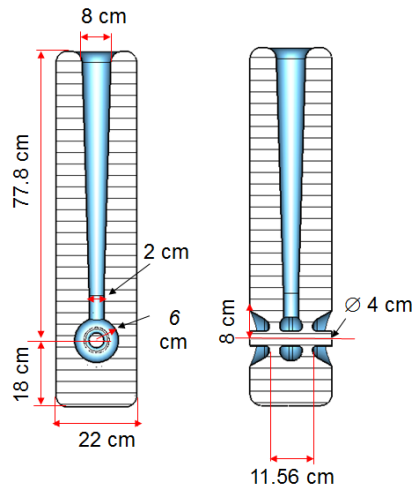


**Figure III.1.5.5.1 Plot showing the geometry of  $\beta=0.047$ ,  $f=81.25$  MHz Quarter Wave Resonator.**

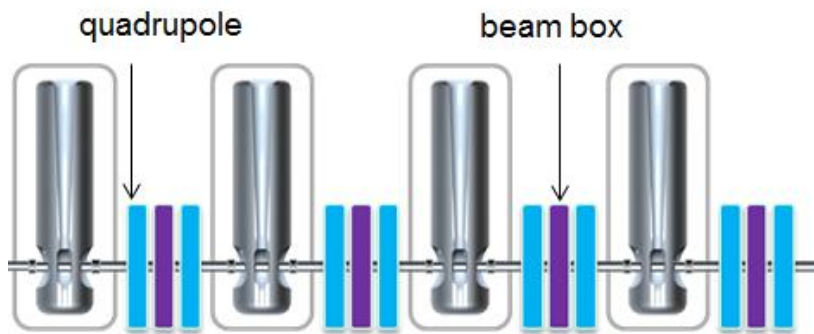


**Figure III.1.5.5.2 Schematic plot of the  $\beta=0.047$ ,  $f=81.25$  MHz segment with normal conducting quadrupoles in blue and diagnostics beam boxes in purple.**

### III.1.5.5.2 Superconducting Linac 12 (SCL12)

The geometry of the  $f=162.5$  MHz  $\beta=0.12$  Half Wave Resonator is optimized with the bore radius 20 mm. Parameters of this cavity can be found in Table III.1.5.2. This segment accelerates  $U^{+33}$  beam from 2.5 MeV/u to 18.5 MeV/u and there are two types of cryomodules, one type containing 3  $\beta=0.12$ ,  $f=162.5$  MHz Half Wave Resonators and the other containing 6  $\beta=0.12$ ,  $f=162.5$  MHz Half Wave Resonators.

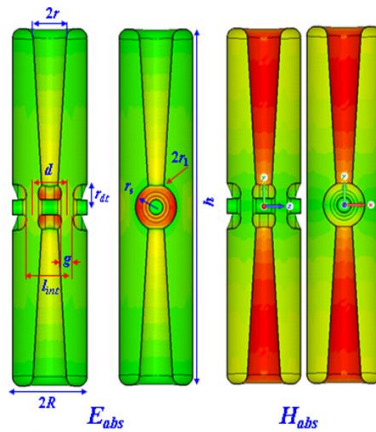


Figure III.1.5.5.3 Plot showing the geometry of  $\beta=0.12$ ,  $f=162.5$  MHz Half Wave Resonator.

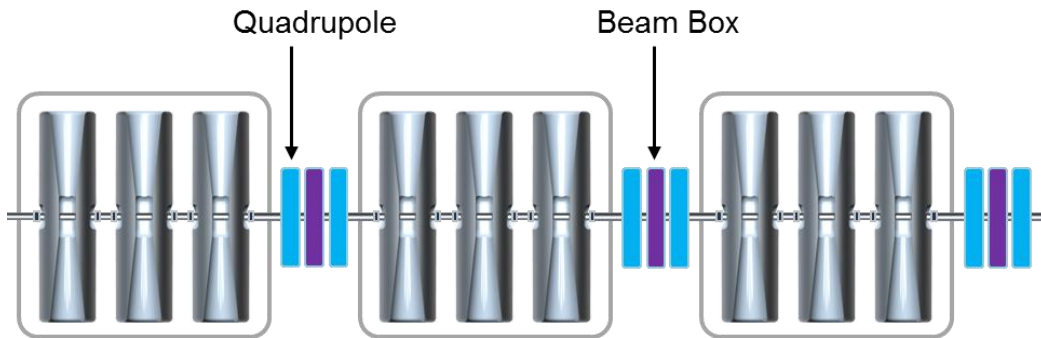
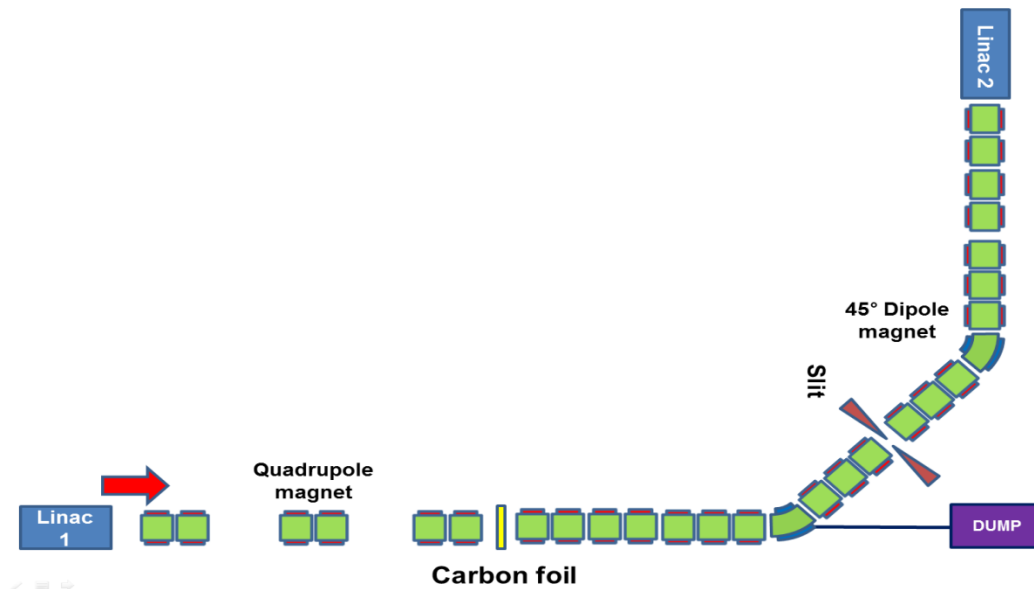


Figure III.1.5.5.4 Schematic plot of the  $\beta=0.12$ ,  $f=162.5$  MHz segment with normal conducting quadrupoles in blue and diagnostics beam boxes in purple.

### III.1.5.6 Charge Stripper Section

One of the critical components of the superconducting Linac (SCL) is the charge stripper because of high power deposited in the stripping material in a small area. Charge stripper strips electrons from heavy ion beams to enhance the acceleration efficiency in the following SCL2.



**Figure III.1.5.6.1 Layout of the Charge stripper section**

Figure III.1.5.6.1 shows the layout of charge stripper section. This section consists of the rooms for installation of solid, liquid and gas type charge stripper. It also consists of matching section to prevent the beam divergence due to the large angle and charge selection section. The charge stripper is reserved to accommodate the liquid Li and thin carbon foil at the down-stream of the SCL1. Five charge state ion beams, which are selected in charge selection section, are matched to transfer to SCL2 by using matching section.

Recent studies done by FRIB indicate that carbon foils show fast decay of performance, which makes this type of stripper is very unlikely to satisfy the FRIB requirements [III.1.5.6.1]. The FRIB looks at other options of the charge stripper which include liquid lithium stripper developed at the ANL, gas stripper, gas stripper with plasma windows, and plasma stripper [III.1.5.6.2]. The charge stripper section is designed to include enough space for the options being considered. Collaboration and intense R&D efforts are in need. Even though carbon foils may have defects in full beam power, it is still

useful for low beam power operation. It is also planned to use the carbon foil during the testing, commissioning, and possibly early low power operation stages. Preliminary study is conducted about the carbon foils using the LISE++ code.

### III.1.5.6.1 Charge Stripping Foil

To optimize the energy at the exit of the SCL1, the dependency of the efficiency of the charge stripping as a function of the incident energy is investigated. It is performed by using LISE++ code which can calculate the charge stripping of Uranium ions in carbon foil and liquid Li. First, the efficiency of the charge stripping of Uranium 33+ ions with 300  $\mu\text{g}/\text{cm}^2$  carbon foils is calculated as a function of the energy of incident beam. It is shown in Figure III.1.5.6.1.1

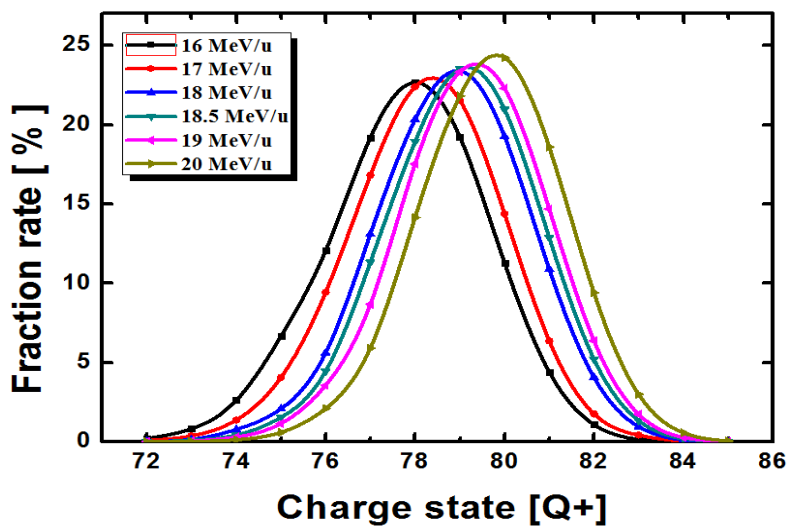


Figure III.1.5.6.1.1 Charge distribution as a function of the incident ion beam energy with 300  $\mu\text{g}/\text{cm}^2$  carbon foil

Table III.1.5.6.1 Charge state and population

Incident energy [MeV/u]	Center charge state	Population within five charge states [%]
17	78	81.48
18	79	87.01
18.5	79	87.63
19	79	86.51
20	80	84.70

Based on this calculation, the ion beam energy at the exit of the SCL1 is optimized around 18.5 MeV/u to get the more efficient acceleration in the SCL2.

### III.1.5.6.2 Optics design for installation of charge stripper

Enough straight section is reserved to accommodate the liquid Li and carbon foil charge strippers at the down-stream of the SCL1 illustrated in Figure III.1.5.6.2.1. A small beam size and a short bunch length are also necessary. A small transverse beam size, however, leads to high beam power density on the stripper. Therefore, the optics design is performed to get the acceptable beam size and bunch length on the stripper. To control the beam size of beam on the stripper, two room-temperature quadrupole magnets are installed at the up-stream of each stripper. The total length of this beam line is 17.4 meters.



Figure III.1.5.6.2.1 Layout of the stripper installation section

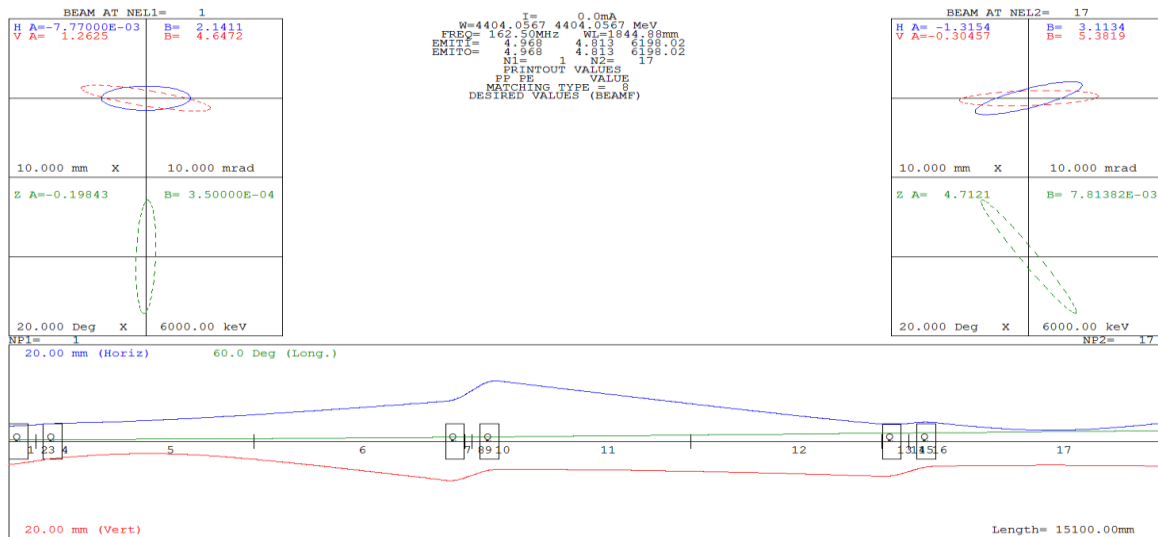


**Figure III.1.5.6.2.1 Optics design for stripper installation section**

### III.1.5.6.3 Optics design for charge selection section

The charge stripping section consists of four room-temperature quadrupole triplets and two room-temperature 45° bending magnets. The quadrupole magnets provide adequate transverse focusing and beam matching to the SCL2 and bending magnet provides the momentum dispersion for the charge selection. Figure III.1.5.6.3.1 shows the schematic plot of the 90° charge stripping after the charge stripper. The charge selection section is designed based on the mirror symmetry. The mirror symmetry optics provides the smaller high order aberration. It has the momentum dispersion of 1.8 m at the first focal plane to separate the ions and the total length of the charge selection section is about 9.8 meters.

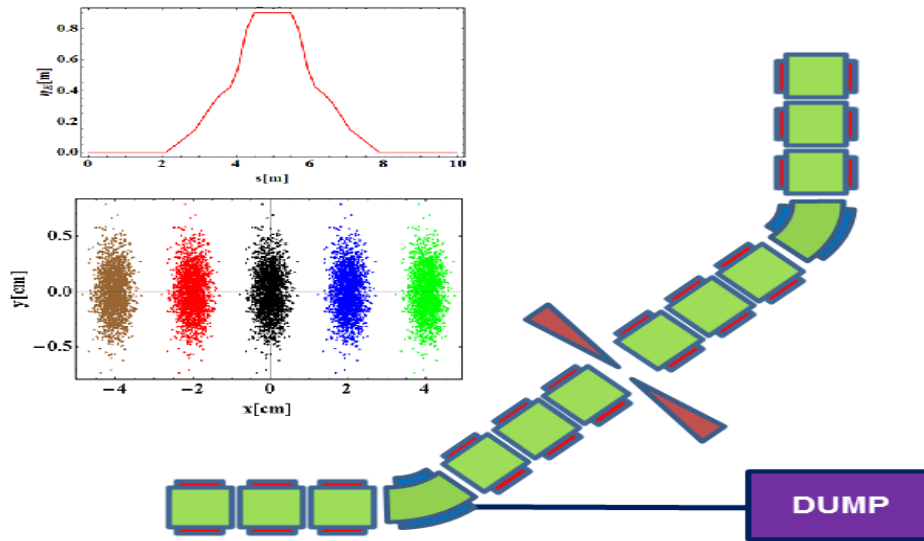


Figure III.1.5.6.3.1 Scheme of charge stripping section

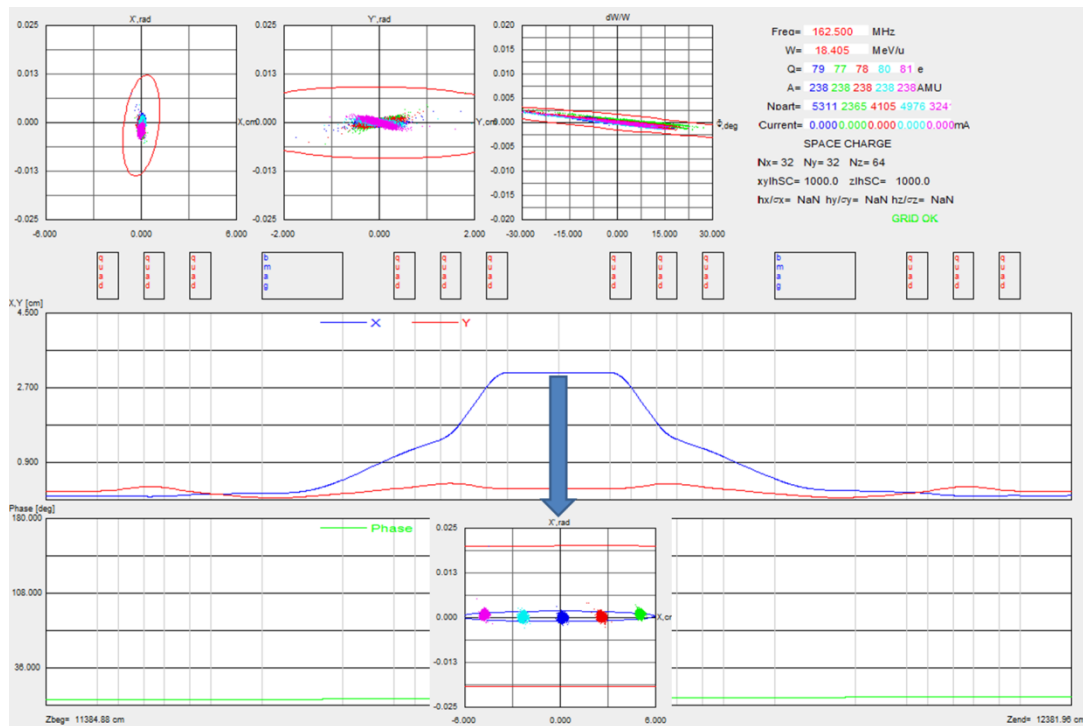
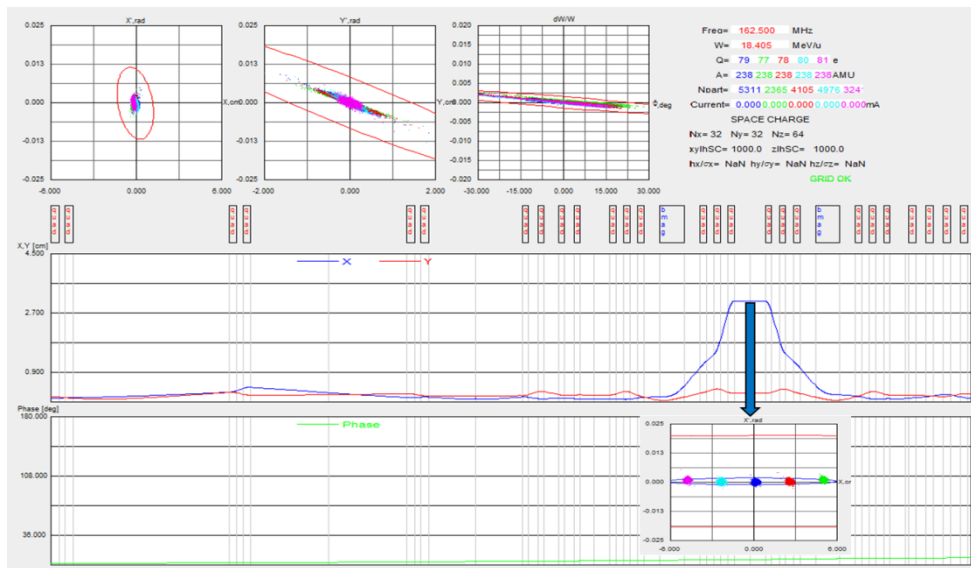


Figure III.1.5.6.3.2 Result of the tracking simulation using TRACK code

The multi-particle tracking simulation is performed using TRACK code. As shown by Figure III.1.5.6.3.2, the multi-charge-state ion beam is well separated in horizontal plane at the dispersive section. Hence, we can select the charge state of the ion using the slit which is installed in the dispersive section.

#### **III.1.5.6.4 Optics design for matching section**

Since the effect of the scattering inside of charge stripper, the angle of the ion beam is increased. Hence the matching section at the down-stream of the charge stripper is required to compensate the effect of the large angle in charge selection section. After passing the charge selection section, the matching for SCL2 is required in transverse and longitudinal direction. Hence the matching section, which consists of the four room-temperature quadrupole magnets, is installed in a down-stream of the charge selection section. And the buncher will also be installed between the charge selection section and matching section to protect the divergence in longitudinal direction. The whole layout with the sections for charge stripper, charge selection and matching section is shown in Figure III.1.5.6.1. The multi-particle tracking simulation was performed by using TRACK code with the solid carbon foil charge stripper.



**Figure III.1.5.6.4.1 Result of the tracking simulation using TRACK code**

**[Reference III.1.5.6]**

[III.1.5.6.1] F. Marti et al., Proc. of LINAC Conference 2010, p. 659, Tsukuba, Japan

[III.1.5.6.2] F. Marti et al., Proc. of LINAC Conference 2010, p. 662, Tsukuba, Japan

**III.1.5.7 Superconducting Linac 2 (SCL2)**

The SCL2 consists of the SCL21 and the SCL22, each consisting of beta = 0.30, f = 325 MHz Single Spoke Resonators (SSR) and beta = 0.53, f = 325 MHz SSR. The SCL2 accelerates U<sup>+79</sup> beam from 18.5 MeV/u to 200 MeV/u. Single Spoke Resonator type is chosen mainly because it can have a larger bore radius compared with the Half Wave Resonator type, which is very essential to reduce the uncontrolled beam loss in the high energy segments of the SCL.

### III.1.5.7.1 Superconducting Linac 21 (SCL21)

This SCL21 accelerates for example  $U^{+79}$  beam from 18.5 MeV/u to 70.9 MeV/u and there are 22 cryomodules each of which contains 4 beta=0.30, f=325 MHz Single Spoke Resonators. Parameters of this cavity can be found in Table III.1.6.2.

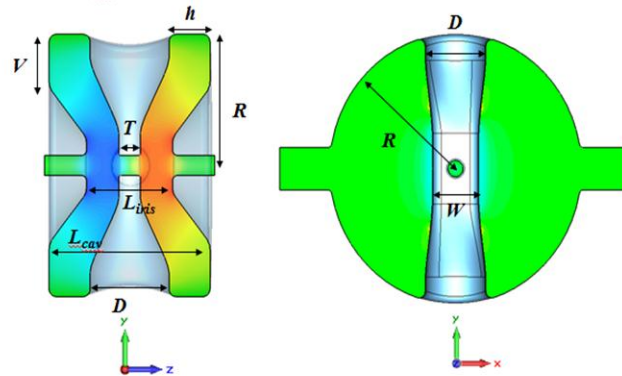


Figure III.1.5.7.1 Schematic plot of the beta=0.30, f=325 MHz cavity with its EM fields.

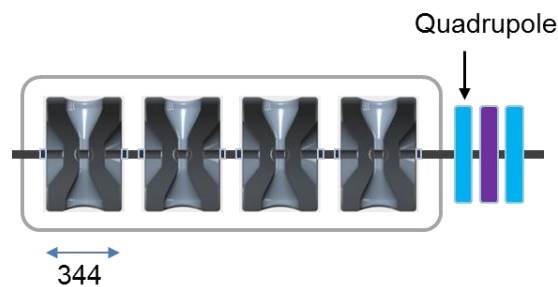


Figure III.1.5.7.2 Schematic plot of the beta=0.30, f=325 MHz segment cryomodule with normal conducting quadrupoles in blue and diagnostics beam boxes in purple.

### III.1.5.7.2 Superconducting Linac 22 (SCL22)

This SCL22 accelerates for example  $U^{+79}$  beam from 70.9 MeV/u to 200 MeV/u and there are 17 cryomodules each of which contains 8 beta=0.53, f=325 MHz Single Spoke Resonators. Parameters of this cavity can be found in Table III.1.5.2.

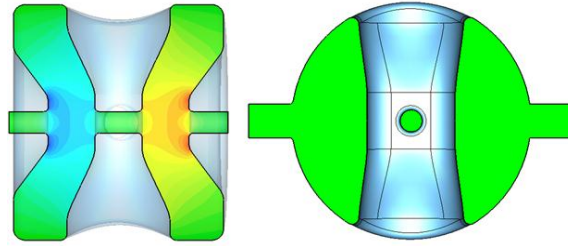


Figure III.1.5.7.3 Schematic plot of the  $\beta=0.53$ ,  $f=325$  MHz cavity with its EM fields.

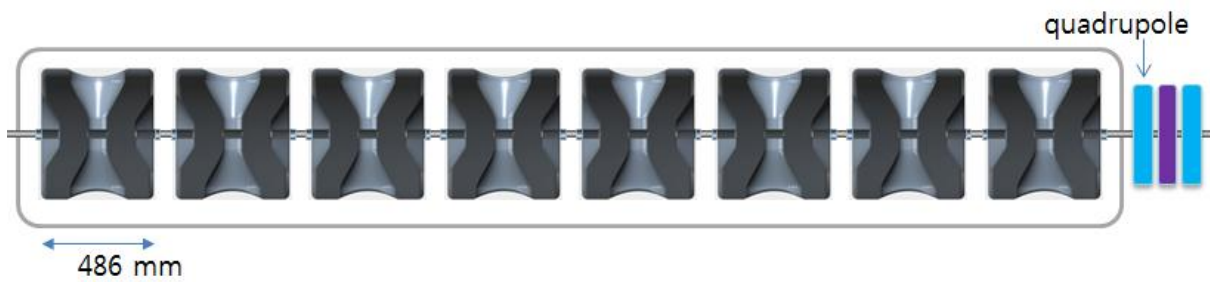


Figure III.1.5.7.4 Schematic plot of the  $\beta=0.53$ ,  $f=325$  MHz SCL22 cryomodule with normal conducting quadrupoles in blue and diagnostics beam boxes in purple.

Table III.1.5.3 Parameters of SCL

Parameters	SCL1		SCL2	
	SCL11	SCL12	SCL21	SCL22
$\beta_g$	0.047	0.12	0.30	0.53
Energy at exit [MeV/u]	2.5	18.5	70.9	200
Length [m]	25.5	71.0	66.0	101.8
# of cryomodule	24	14   16	22	17
# of cavity / cryomodule	1	3   6	4	8
# of quadrupole	48	60	44	34

### III.1.6 Beam Dynamics of the SCL

We have proposed a new Rare Isotope Accelerator driver linac which consists of warm quadrupole magnets for focusing heavy ion beams. Figure III.1.6.1 shows the layout of the SCL1 of the proposed driver linac which accelerates the beam, for an example, Uranium ions from 0.3 MeV/u to 18.5 MeV/u. Fig. III.1.6.2 shows the beam envelope and rms emittance in horizontal plane. The SCL1 uses the two different families of superconducting resonators, i.e., quarter wave resonator (QWR) and half wave resonator (HWR). The SCL11 consists of 24 QWR's whose optimum  $\beta$  is 0.047 and 24 doublets. The cryomodule of the SCL11 hosts one superconducting cavity. The SCL12 consists of 138 HWR's whose optimum  $\beta$  is 0.12 and 36 doublets. This segment has the two families of cryomodules: one type of cryomodule hosts three superconducting cavities and the other hosts six superconducting cavities. The transverse sizes of the beam are controlled by quadrupole doublets. It is essential that the fields in these quadrupoles can be adjusted independently one from another to allow an adequate control of beam parameters.

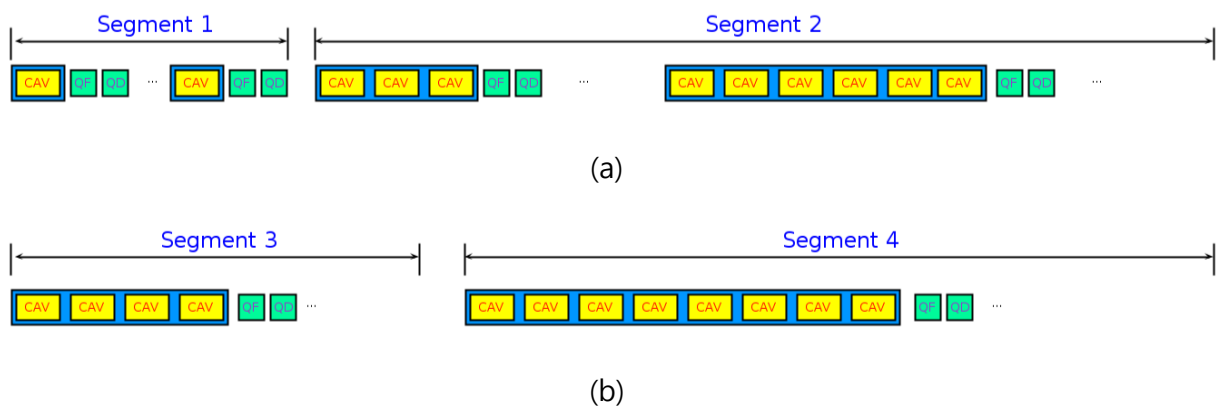
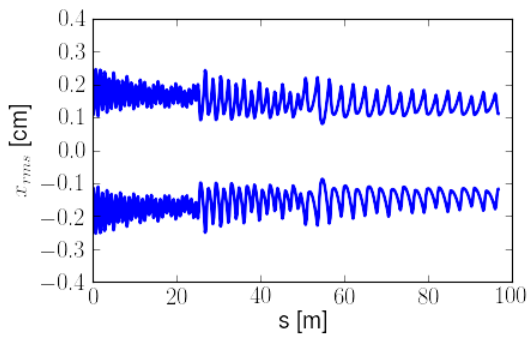
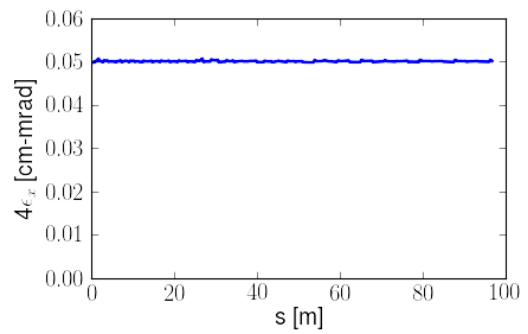


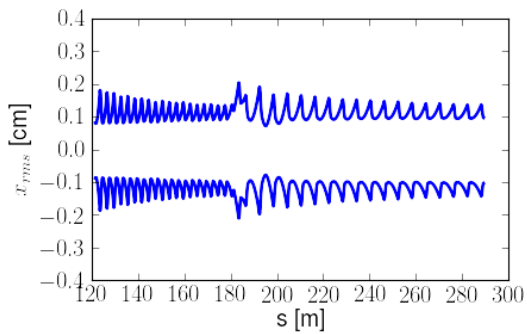
Figure III.1.6.1 Layout of the SCL: (a) SCL1 and (b) SCL2.



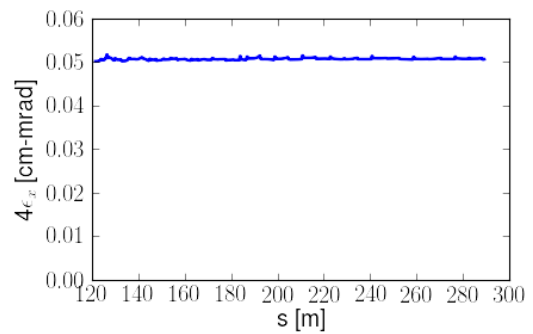
(a)



(b)

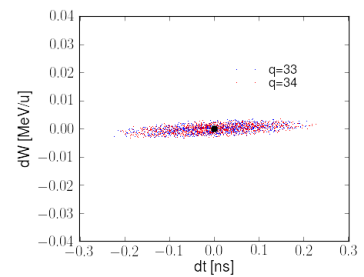
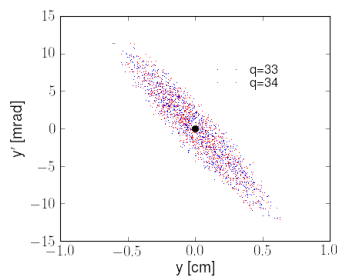
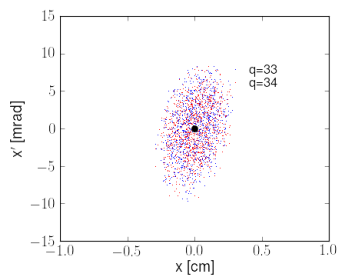


(c)



(d)

Figure III.1.6.2 Plot of (a) horizontal rms beam envelope and (b) horizontal rms emittance for SCL1, and (c) horizontal rms beam envelope and (d) horizontal rms emittance for SCL2 for doublet-based lattice. Misalignment and field error are not included in the lattice.



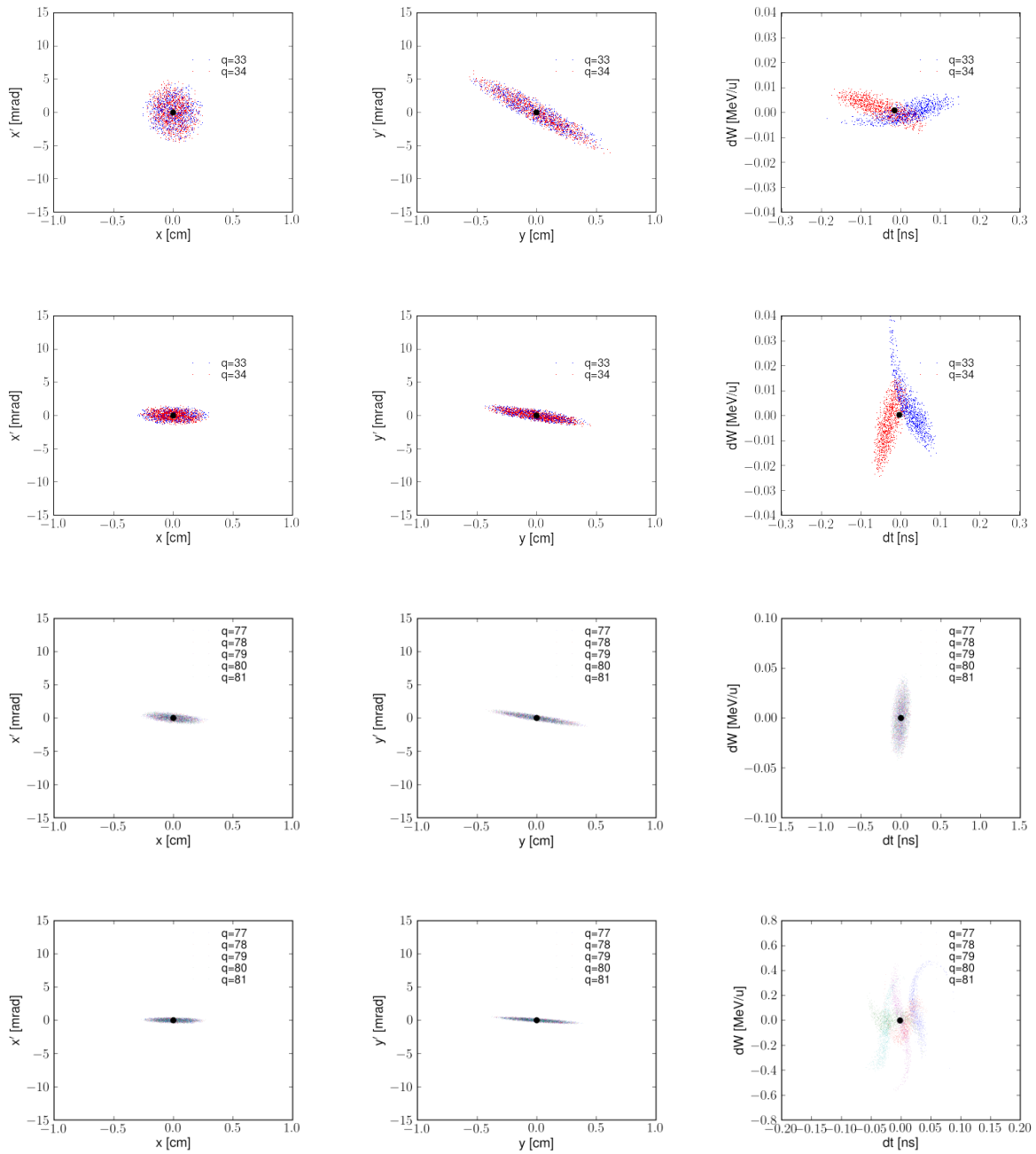


Figure III.1.6.3 Plot of phase space for multi-charge-state Uranium beam: (top) entrance of  $\beta_1$  section, (1<sup>st</sup> row) exit of  $\beta_1$  section, (2<sup>nd</sup> row) exit of  $\beta_2$  section, (3<sup>rd</sup> row) exit of  $\beta_3$  section, and (bottom) exit of  $\beta_4$  section.

For the actual SCL, machine imperfections cannot be avoided. The error comes from the misalignment of the linac elements and the limitation of manufacturing accuracy and various control errors. For instance, steering magnets are used to correct beam orbit displacements. In the doublet configuration, steering magnets are placed where NC quadrupoles are.

In order to examine the quality of the present quadrupole-based driver linac lattice, effects of machine imperfections on the beam parameters are investigated, compared with the previous linac design based on superconducting solenoids. To summarize the layout of the previous SCL design of briefly, the SCL11 consists of three cryomodules where each cryomodule hosts eight superconducting cavities and eight SC solenoids. The solenoid is used to focus the beam. The SCL12 consists of twelve cryomodules where each cryomodule hosts eight cavities and three solenoids.

Table III.1.6.1 summaries the parameters of quadrupole-based lattice compared to solenoid-based lattice. Diagnostic devices and steering magnets can be placed in the drift spaces between cavity and quadrupole or between quadrupoles in the doublet lattice while they should be placed between cryomodules in the solenoid lattice. The length of quadrupole-based linac is commensurate with solenoid-based linac. The particle tracking with machine errors is performed with the TRACK code which has been developed in ANL. The misalignment analysis includes all superconducting cavities and focusing elements assuming a uniform distribution. Table III.1.6.2 summarizes tolerances for the lattice consisting of superconducting solenoids. The maximum transverse displacement of solenoid is set to 0.5 mm. This displacement is half of the offset of SCRF cavities, but the effect of solenoid displacement is expected to be detrimental to beam dynamics in the linac. Table III.1.6.3 summarizes tolerances for the lattice consisting of NC quadrupoles. It has been well known that the NC quadrupole can be aligned in an

accuracy of  $\pm 150 \mu\text{m}$  [III.1.6-1]. The rotation angle about the z-axis is set to 5 mrad. The rotation angle is important due to the skew quad term while it is independent of the solenoid due to symmetry of solenoid field.

In the misalignment and RF error analysis, charge states of 33+ and 34+ of Uranium beams are used. Only the SCL11 is used for comparison of beam performance. For multi-charge state beam acceleration, a strong focusing is required. The misalignment of SC solenoids is, from the error simulations, found to affect the beam properties more than that of NC quadrupole. As shown in Figure III.1.6.4, the misalignment of SC solenoid increases the maximum beam envelope by 3.5 times while the NC quadrupole error increases the envelope only by 0.8 times. The aperture radius of quadrupole and solenoid is 20 mm. The envelope due to solenoid misplacement goes high up to 1.7 cm just after the SCL11. Figure III.1.6.6 shows plot of horizontal rms emittance due to misalignment errors for both doublet lattice and SC solenoid lattice. The maximum increase of rms emittance is 10% for doublet lattice, while it is 140% for solenoid lattice. The effects of cavity misalignment and RF error on longitudinal emittance are less sensitive than focusing elements, as shown in Fig. III.1.6.7.

**Table III.1.6.1 Parameters of the SCL1 with doublet and SC solenoid lattice**

<b>Parameters</b>	<b>Doublet lattice</b>	<b>Solenoid lattice</b>
<b>Length (m)</b>	96.5	97
<b>Input energy (MeV/u)</b>	0.3	0.3
<b>Output energy (MeV/u)</b>	18.5	18.5
<b># of cryomodules</b>	54	15
<b># of quadrupoles</b>	108	-
<b># of solenoids</b>	-	60

**Table III.1.6.2 Machine imperfection for the SC solenoid lattice**

Parameters	SC Cavities	SC Solenoids	Comment
Displacement (mm)	±1.0	±0.5	Uniform
Phase (deg)	±1	-	3σ Gaussian
Amplitude (%)	±1	-	3σ Gaussian
Rotation (mrad)	-	±5.0	Uniform

**Table III.1.6.3 Machine imperfection for the NC quadrupole lattice**

Parameters	SC Cavities	Warm Quadrupoles	Comment
Displacement (mm)	±1.0	±0.15	Uniform
Phase (deg)	±1	-	3σ Gaussian
Amplitude (%)	±1	-	3σ Gaussian
Rotation (mrad)	-	±5.0	Uniform

**Table III.1.6.4 Variation of beam parameters due to machine imperfections**

Parameters		Initial value	Doublet lattice	Solenoid lattice
<b>Max. envelope</b>	x (cm)	0.3	0.7	1.7
	y (cm)	0.6	1.0	1.5
	Φ (deg)	26.8	10.2	75.6
<b>4*rms emittance</b>	x (cm-mrad)	0.05	0.08	0.13
	y (cm-mrad)	0.05	0.08	0.12
	z (keV/u-ns)	5.0	13.7	6.63
<b>Centroid</b>	x (cm)	0.0	0.32	1.20
	y (cm)	0.0	0.50	0.97
	Φ (deg)	0.3	3.25	5.60

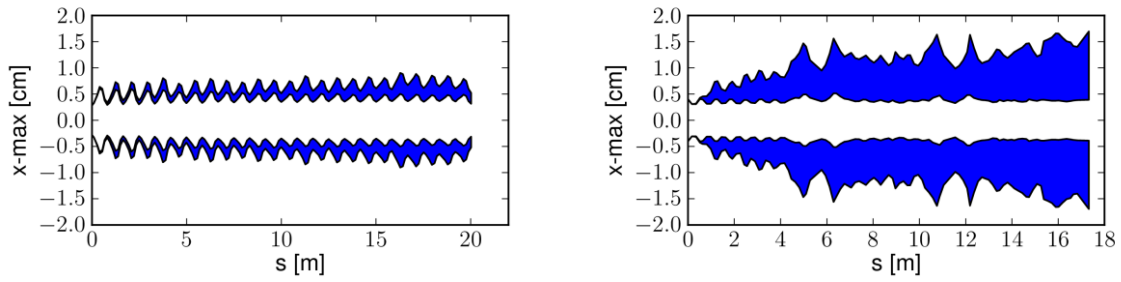


Figure III.1.6.4 Plot of maximum horizontal beam envelope: (a) doublet lattice (left) and (b) SC solenoid lattice (right). The shade region represents the bounds of envelope variation. The aperture of quadrupole and solenoid is 4 cm. The maximum variation of beam envelope is 76% and 350% for doublet and solenoid lattices respectively.

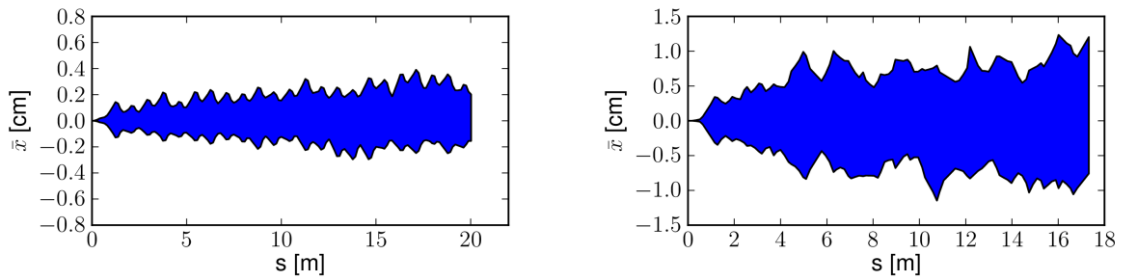
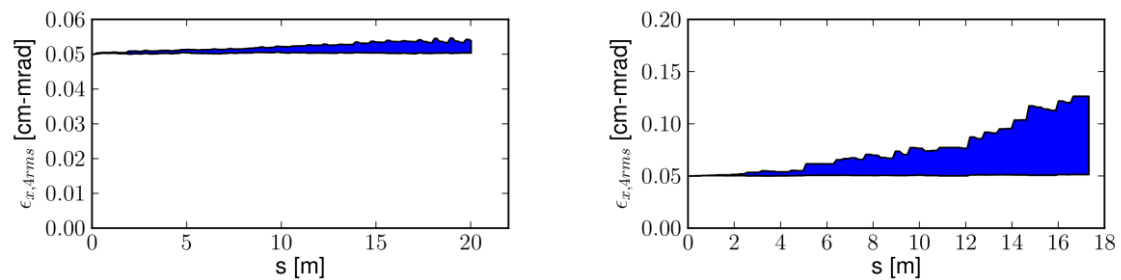
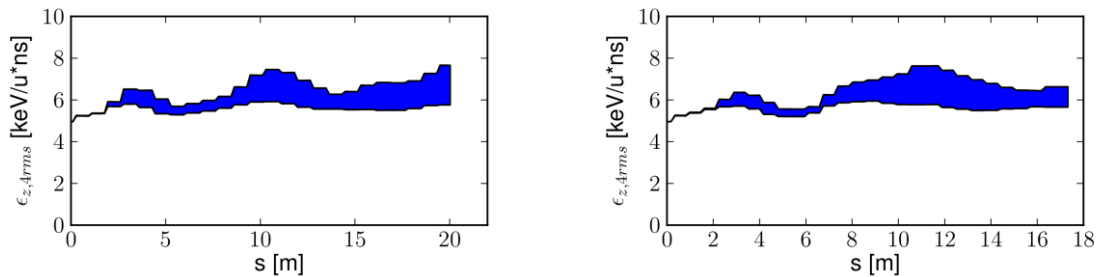


Figure III.1.6.5 Plot of horizontal beam centroid: (a) doublet lattice (left) and (b) SC solenoid lattice (right). The aperture of quadrupole and solenoid is 4 cm.



**Figure III.1.6.6 Plot of horizontal rms emittance: a) doublet lattice (left) and (b) SC solenoid lattice (right). The maximum increases of rms emittance are 10% and 140% for doublet and solenoid lattices respectively.**



**Figure III.1.6.7 Plot of longitudinal rms emittance: a) doublet lattice (left) and (b) SC solenoid lattice (right). The maximum increases of rms emittance are 40% and 50% for doublet and solenoid lattices respectively.**

### [References-III.1.6]

[III.1.6-1] S. Nath et al., ASAC Review presentation, October 2001, SNS/ORNL, Tennessee., USA

### III.1.7 Beam Diagnostics and Collimation

For the previous design, beam diagnostics can be installed only at the limited places, namely the joints between long cryomodules. This is a very serious limitation in light of beam operation such as establishing matching between different segments of the SCL for the high intensity beam operation.

On the contrary, the beam box located at every doublet is reserved for various diagnostics devices such as beam profile monitors, beam current monitors (BCM), Faraday cups, emittance scanners, bunch shape monitors (BSM), etc. Beam position

monitors (BPM) will be installed with quadrupoles, providing beam position and phase data. This feature is a very strong merit in light of beam diagnostics for beam operation and commissioning. Compared with the previous design, there are beam boxes regularly placed for necessary beam diagnostics and this is critical for operation and accurate machine tuning. For instance four profile monitors installed in series can easily establish matching [III.1.7-1]. Because the beam box is in the warm section, maintenance and alignment are straightforward.

One of the challenges of the driver SCL beam diagnostics systems is to detect and measure beam parameters for a wide range of beam intensities. This can be accommodated through proper design of beam boxes and beam diagnostics. Necessary beam diagnostics for high intensity beam tuning are beam profile monitors, BPMs, beam loss monitors, emittance scanners, BCMs, Faraday Cup etc. Figure III.1.7.1 shows a preliminary beam diagnostics configuration of the driver SCL. For the charge stripping station, required beam diagnostics are BPMs, beam profile monitors, BCMs, and beam loss monitors, etc.

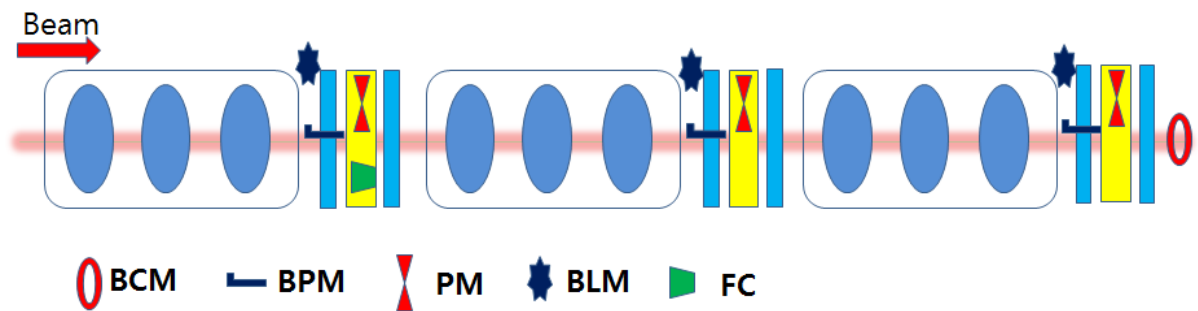


**Figure III.1.7.1 Schematic plot of beam diagnostics configuration of the driver SCL. Here are included BCM (Beam Current Monitor), BPM (Beam Position Monitor), PM (Profile Monitor), BLM (Beam Loss Monitor), FC (Faraday Cup) etc.**

Another advantage is that collimators can be installed at the beam boxes to improve beam quality as needed as shown in Fig. III.1.7.2. These collimators can minimize the uncontrolled beam loss to the superconducting cavities.

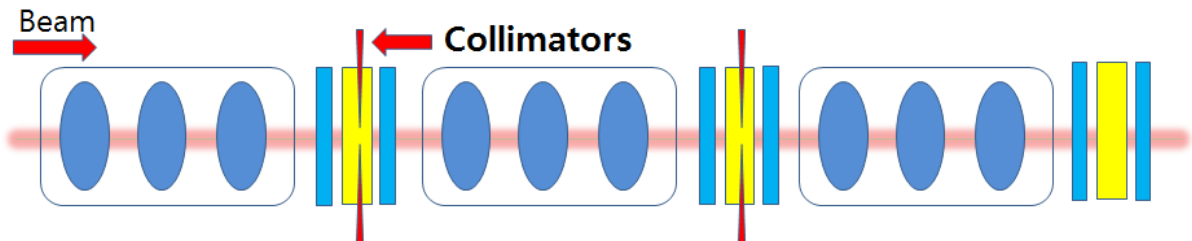


**Figure III.1.7.2 Schematic plot of beam collimation configuration of the driver SCL and the ISOL post SCL. Here are shown collimators installed at the beam boxes.**

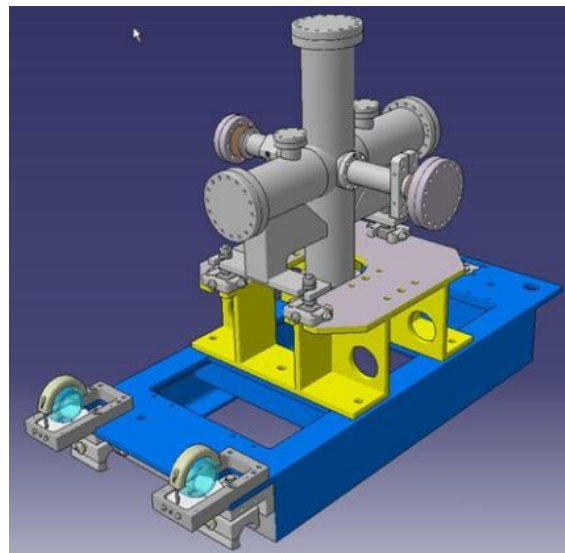


**Figure III.1.7.3 Plot of a sample beam box (courtesy of SPIRAL2). Similar type of beam box will be used.**

**[References-III.1.7]**

[III.1.7-1] D. Jeon, C.M. Chu, J. Stovall, S. Assadi, *Practical Transverse Matching of the High Intensity SNS Linac*, Nucl. Instr. and Meth. A **607** (2009) 517.

### III.1.8 Superconducting RF and Magnet Test Facility

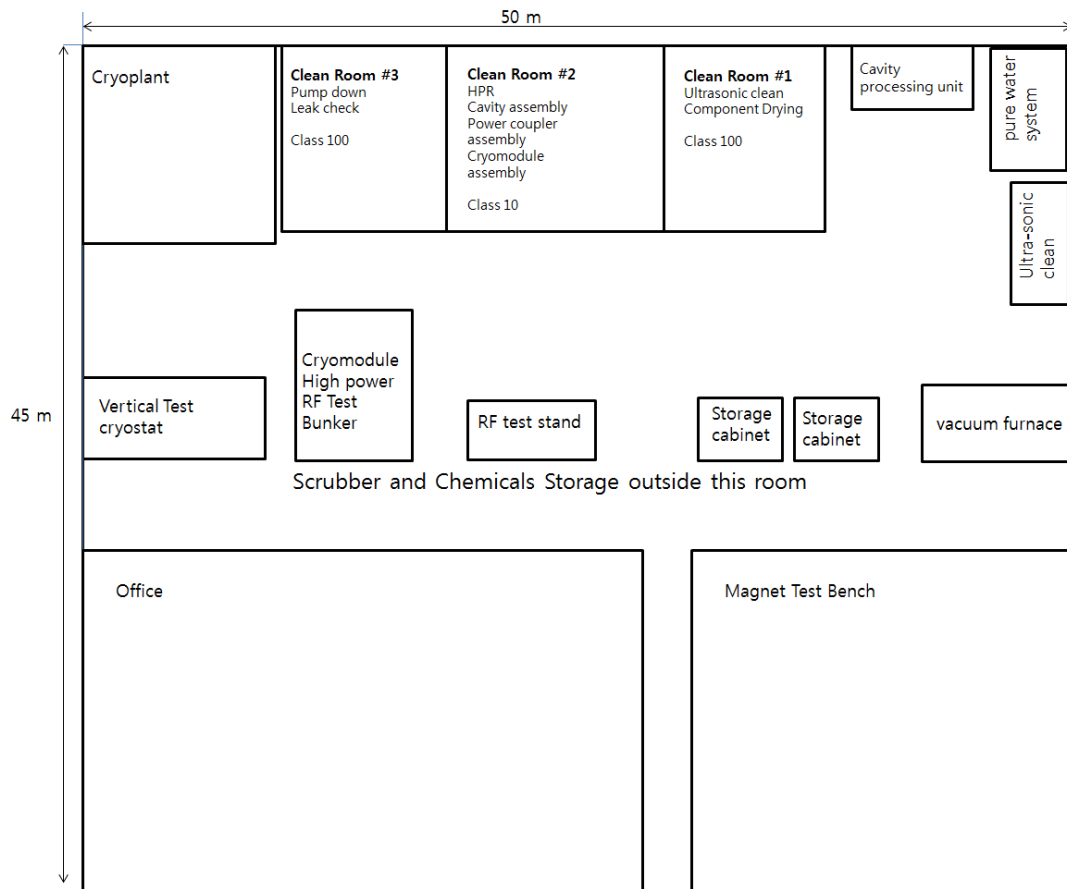


**Figure III.1.8.1: Layout of the temporary Superconducting RF Test Facility.**

Considering the possible delay in procuring the site, a contingency plan for the temporary Superconducting RF and Magnet Test Facility is being developed. Cost of the superconducting RF Test Facility is estimated to be ₹2856 M (excluding cryogenic system). And the facility includes cavity chemical process unit for EP processing and BCP processing, RF test stand, RF systems, class 10 and class 100 clean rooms, two vertical test cryostats, vacuum furnace, etc. Scrubbers and chemical storage space are not included in the layout drawing of Figure III.1.8.1. A space required for the temporary Superconducting RF Facility is about 50 m x 25 m. The plan for the Magnet Test Facility is

developed and its cost is estimated to be ₩1200 M with required space 20 m x 20 m. The Cryomodule Test Bunker can be added as needed depending on the construction schedule of test facilities on site and its cost is not included in the cost estimation given above. Also we are developing a plan for the permanent Superconducting RF Facility to be built on site and cost estimation is developed.

### III.1.9 Engineering Design and Fabrication of Superconducting Cavities

Pure Nb with about 3 mm thickness and RRR > 300 will be used for the construction of the superconducting cavities. Mechanical design aspects, multipacting analysis, and thermal analysis will be conducted for the prototyping of superconducting cavities. As the engineering design is completed, superconducting cavities will be prototyped and mass produced. Figure III.1.9.1 shows the flow chart of the SC cavity fabrication and processing and Fig. III.1.9.2. the flow chart of SC cavity and cryomodule design, fabrication and test procedures

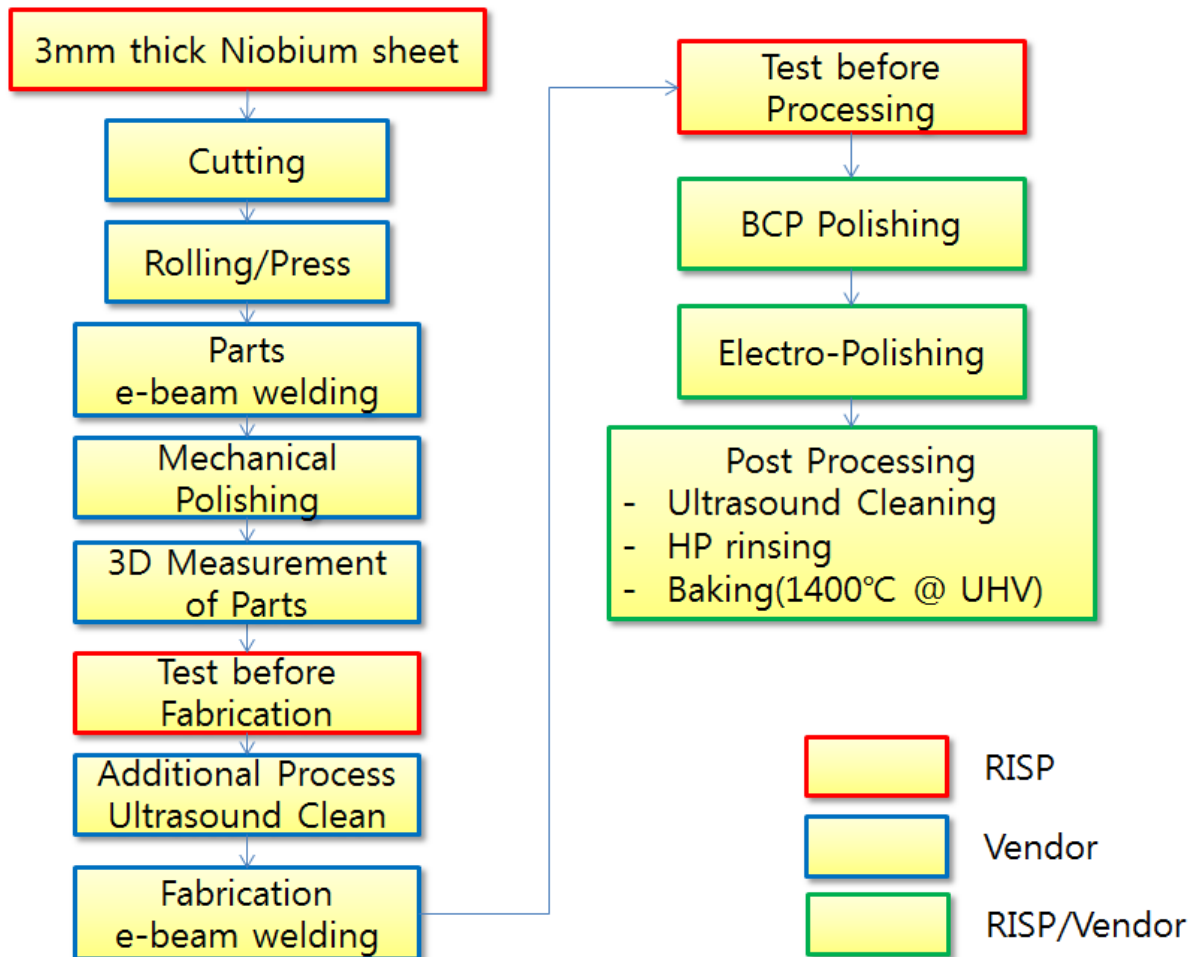


Figure III.1.9.1. Flow chart of SC cavity fabrication and Processing

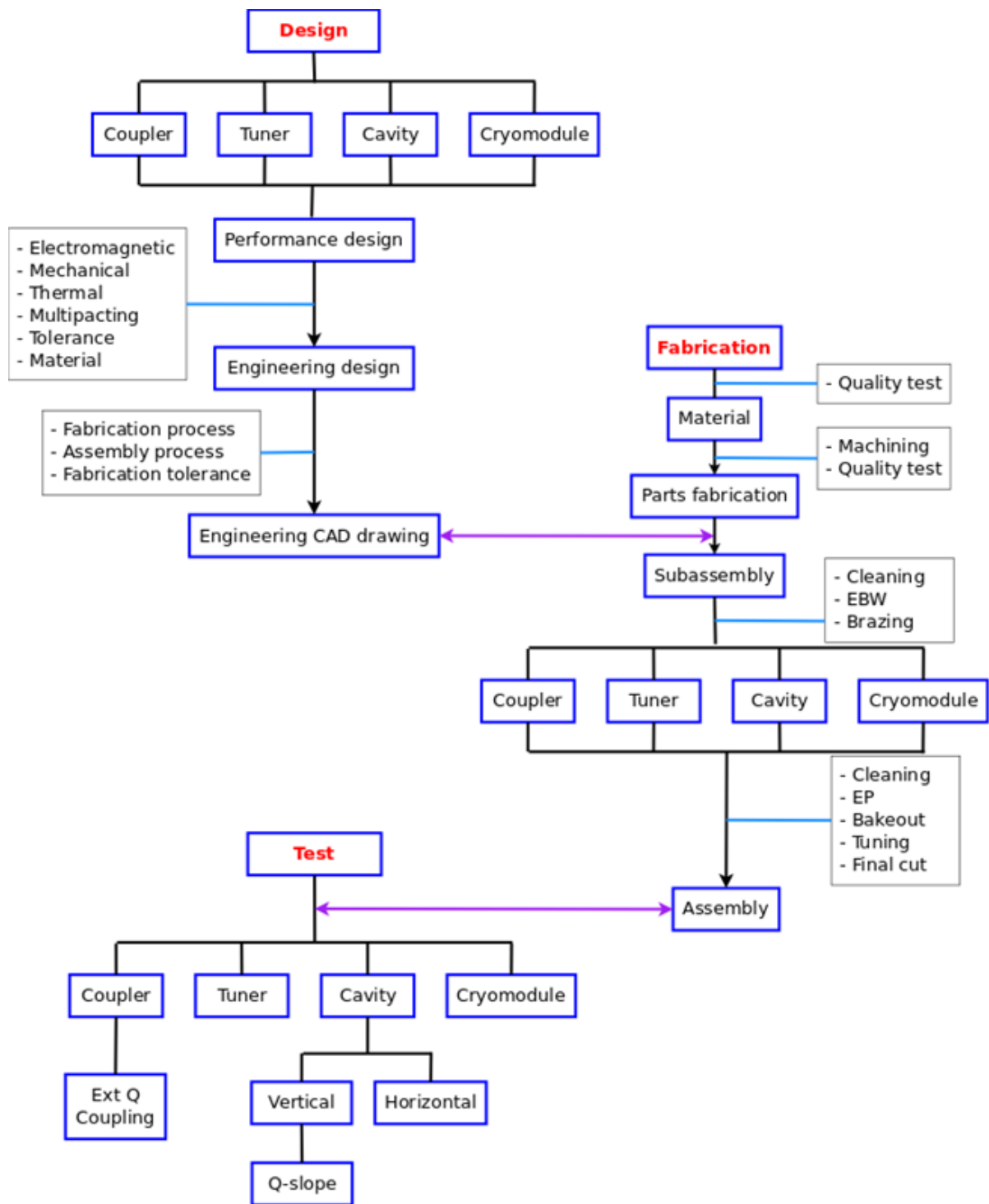


Figure III.1.9.2. Flow Chart of SC cavity and cryomodule design, fabrication and test procedures.

A property of niobium sheet has been carefully chosen in order to achieve the cavity parameters as shown in Table III.1.5.2. The RRR (Residual Resistance Ratio) should be larger than 300. The grain size is about 64 of ASTM E5. The property of niobium sheet is listed in Table III.1.9.1. Thickness of niobium sheet is chosen as 3 mm to keep mechanical stability and to facilitate fabrication process.

**Table. III.1.9.1 Properties of niobium sheet**

<b>RRR</b>	<b>Tensor Strength (MPa)</b>	<b>Yield Strength (MPa)</b>	<b>Elongation (%)</b>	<b>Vickers Hardness (HV)</b>	<b>Grain Size</b>
> 300	> 96.4	48.2 < R <sub>p</sub>	> 40 LD > 35 TD	< 50 (Hv10)	< 64 (ASTM5) < 90 (ASTM4)

### III.1.9.1 Tolerance Analysis

Tolerance analysis related with the fabrication is to be done for the superconducting cavities. Its impact on the parameters of the cavities will be analyzed.

The tolerance on superconducting cavity fabrication shall be minimized, for an example, a minimum tolerance 0.02 mm is considered. Since the cavity fabrication consists of a variety of fabrication process, a fabrication tolerance should be minimized at each fabrication step. The fabrication process should be standardized in order to estimate the tolerance as well. The bandwidth of superconducting cavity is around 40 Hz after applying slow and fast tuners during normal operation. Table III.1.9.2 shows the change of resonant frequency of superconducting cavity which is induced by cavity fabrication and processing, for example, of quarter waver resonator.

**Table. III.1.9.2 Effect of cavity fabrication and processing on resonant frequency for QWR [Ref III.1.9.1].**

Process	Value	Comment
Cavity length(upper)	-132 kHz/mm	Frequency shift by length of center conductor and upper end
Cavity length(lower)	+30 kHz/mm	Frequency shift by length of lower end
Welding	+59 kHz	0.58mm shrink/weld
EP	+238 kHz	125um base, 187um @ DT & Nose
Vacuum	+23 kHz	1 ATM $\rightarrow$ $10^{-7}$ torr
Cool down	+156 kHz	293K $\rightarrow$ 4K
L-He pressure	10s Hz/torr	Fluctuation of L-He
Lorentz Detuning	$\sim 0.1$ Hz/(MV/m) <sup>2</sup>	Deforming of cavity by Lorentz force (MSU, $\beta=0.041$ )

**[Reference III.1.9]**

[III.1.9.1] G. P. Zinkann et. al., Proceedings of HIAT09, p.156, 2009

### III.1.9.2 Mechanical Design

Mechanical characteristics of the superconducting cavities will be analyzed using the CST and ANSYS codes to study and to ensure that the cavity design meets the requirement of Lorentz force detuning, detuning due to helium pressure fluctuation ( $df/dP$ ), microphonics detuning etc. EM design has been conducted to reduce  $B_{\text{peak}}$  and  $E_{\text{peak}}$  which in turn reduces the Lorentz force detuning. Stiffening the cavity endwalls and shell reduces the Lorentz force detuning and detuning due to helium pressure fluctuation. Endwalls of spoke resonators are reinforced with two types of ribs: donut ribs and daisy ribs. The design of the helium jacket is to be studied in light of the  $df/dP$  characteristics.

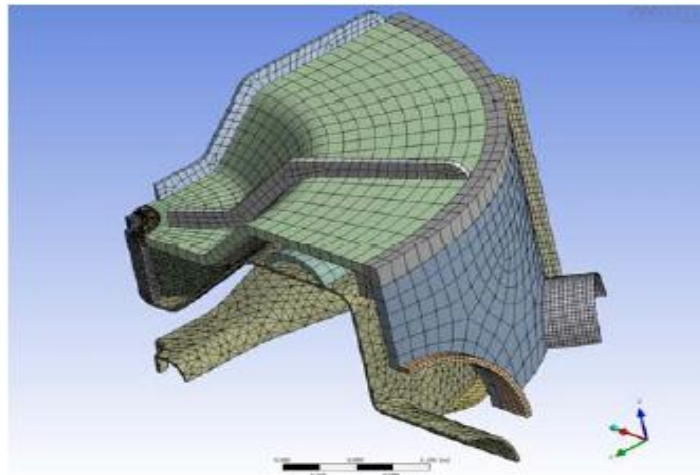


Figure III.1.9.1 Plot of reinforcing ribs (Courtesy of FNAL)

### III.1.9.3 Multipacting Analysis

It is important to avoid multipacting barriers as much as possible and the design should be optimized by using the CST electron tracking code. Multipacting analysis will be conducted for the combined structure of the cavity and power coupler.

### III.1.9.4 Thermal Analysis

Thermal analysis is to be done for the superconducting cavities and special attention will be paid to high magnetic field region, around the coupler port, and beam tubes etc.

### III.1.10 Plan for Cryomodules, Couplers and Tuners

The project can profit from the existing knowledge base, accelerating the learning process and minimizing the R&D workload so that they can concentrate on developing core design and technologies. Existing designs and products of cryomodules, couplers and tuners will be utilized as much as possible for the SCL design. It is planned to carry out R&D for couplers. Through this, the project can concentrate its manpower and resources to the selected areas.

For the couplers and tuners, there are a few existing prototypes and products such as the SPIRAL2 project, the Project-X, and the FRIB etc. These are natural candidates for the frequencies are quite close or identical to the frequency of the RISP cavities.



**Figure III.1.10.1 Photograph of the SPIRAL2 low-beta cryomodule that contains one cavity (the left plot) and the coupler (the right plot). This type of cryomodule and power coupler can be adopted for the RISP SCL1. (Courtesy of the SPIRAL2)**

For cryomodules, the SCL1 section cryomodule design will benchmark/adopt the SPIRAL2 design and the SCL2 section cryomodule design can adopt the FNAL Project-X cryomodule design or ILC cryomodule design.

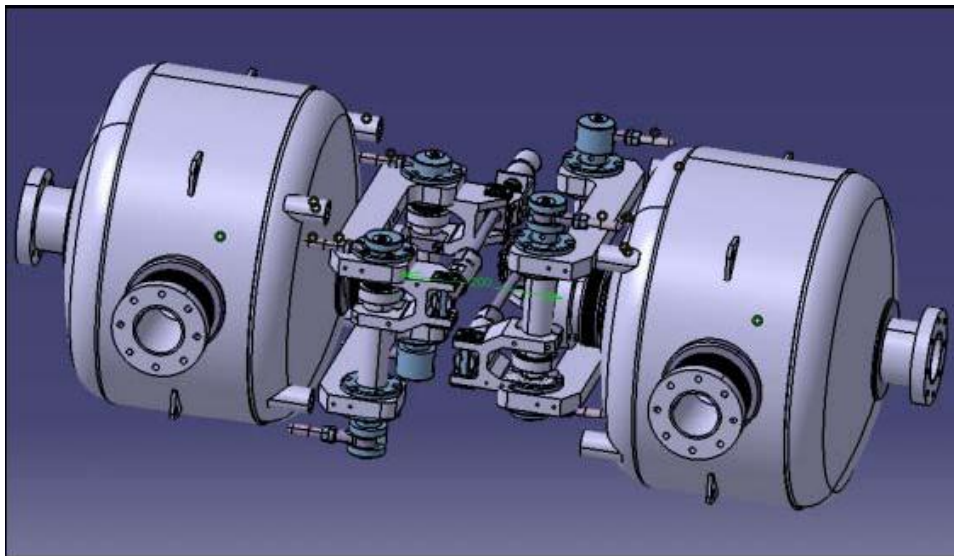


**Figure III.1.10.2. Plot of the tuner with the cavity (Courtesy of the EURISOL).**

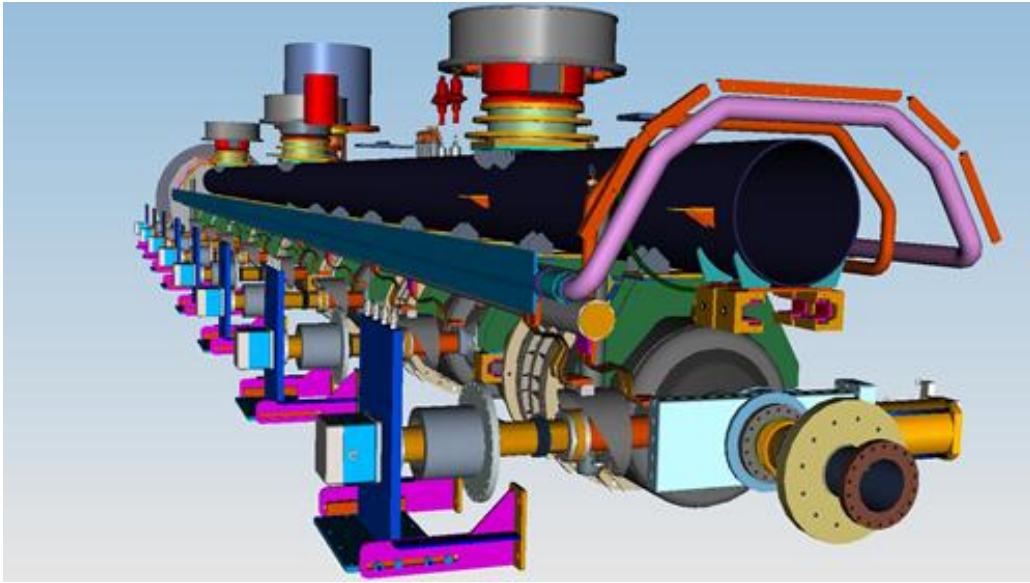


**Figure III.1.10.3. Plot of the FNAL cryomodule (Courtesy of the FNAL). This type of cryomodule can be adopted for the SCL2 cryomodules.**

### **III.1.11 RF System**

The accelerator facility is composed of some accelerator devices such as superconducting cavities for linear accelerator. All these devices accelerate the RI beam by the RF field in the cavity provided by the RF amplifiers. The RF field in the cavity might be fluctuated by the various reasons such as resonance frequency change, temperature variation, helium pressure change, beam current etc. RF systems not only supply RF power for superconducting cavities but also control SC Linac system in order to acquire the good beam stability. Figure III.1.11.1 shows schematic diagram the RF system about RISP. The operating base RF frequency is 81.25 MHz for the QWR, 162.5 MHz for HWR and 325 MHz for the SSR1 and SSR2. The stability of the RF field should be within  $\pm 1\%$  in amplitude and  $\pm 1^\circ$  in phase, and the resonant frequency control is required. The

required RF power is 1 kW and 5 kW including the margin of 50% for the four types of superconducting cavities respectively.

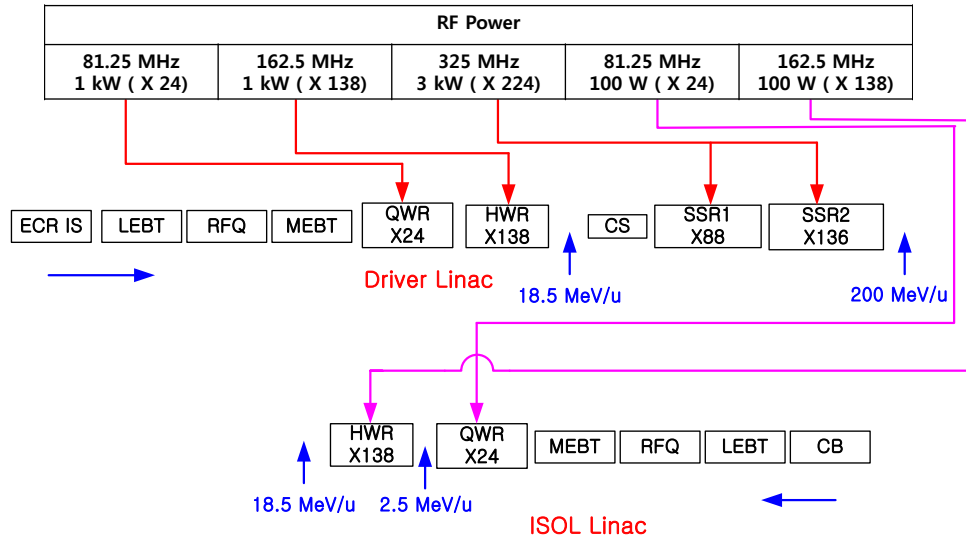


**Figure III.1.11.1 RISP RF System**

The RF system consists of the High power RF (HPRF) system and Low-level RF (LLRF) system. The major works of LLRF system controls amplitude and phase of accelerating RF field in cavity, resonant frequency of RF cavities. The LLRF system performs the RF signal generation and distribution, the feedback control of the RF amplitude and phase for the stability of an accelerating field in the accelerator, the error detection for the resonant frequency control, and the interlock for the HPRF system protection. The digital feedback control board is chosen for the flexibility and accuracy of the LLRF control system, which includes the analog to digital converter (ADC), the field programmable gate array (FPGA), and the digital to analog converter (DAC). Recently, the fast ADCs enable to choose the direct RF sampling method and the high conversion rate of the DACs enable to generate the RF or IF signal directly from the digital board. Because of these fast ADCs and DACs, the LLRF analog part is simpler and it is more economy in the accelerator using a few hundreds of the RF control system. It is necessary to select the

ADCs with the small aperture jitter for the low phase noise in the direct RF sampling using the high sampling clock. The FPGA is chosen to process quickly the digital signal of the in-phase (I) and the quadrature-phase (Q) from the ADCs. The IQ signal of the RF amplitude and phase from the cavity is controlled by the control logic programmed with the PI algorithm in the FPGA.

The HPRF system transmits the high-power RF signal to the cavity and must be protected from the arc and high reflected RF power. The HPRF system includes the high power amplifier, the isolator, the RF transmission line and the high power components. The high power amplifier and high power components are designed according to the RF power level and the operating frequency.

Figure III.1.11.2 shows the conceptual block diagram for the LLRF control system. The operating RF frequency is 81.25 MHz for the QWR, 162.5 MHz for the HWR and 325 MHz for the SSR1 and SSR2. According to the current technologies of the ADCs and DACs, the direct RF sampling and the direct RF generation in the digital FPGA module can be chosen for the digital feedback control. For the direct RF sampling, the sampling clock frequency is determined to 56 MHz clock for the 81.25 MHz RF signal and 224 MHz clock for the 325 MHz RF signal by using the IQ sampling method of every 450 degree phase. It is necessary to select the ADCs with the small aperture jitter for the low phase noise in the high 224MHz sampling clock. The sampling clock signal of 224MHz is distributed from the RF reference line. The RF signal of 81.25 MHz and 325 MHz is also generated directly from the digital module and is transmitted to the cavity through the HPRF system. In this LLRF control system, the LO signal and IF signal used for the heterodyne system are not needed to use for the feedback control. Because of the direct RF sampling and the direct RF generation in the digital module, the analog part of the LLRF control system is simpler and it is more economy in this accelerator using a few hundreds of the RF control system. The forward (FWD) RF signal, the backward(BWD) RF

signal, and the cavity signal is converted directly to the digital signal of the IQ signal in the FPGA module, and the cavity signal is controlled by the control logic with the PI algorithm for the feedback control of the RF amplitude and phase. The error of resonant frequency is also calculated in the digital module and is transmitted to the water cooling control system for the tuner control system for the SC-Linac.

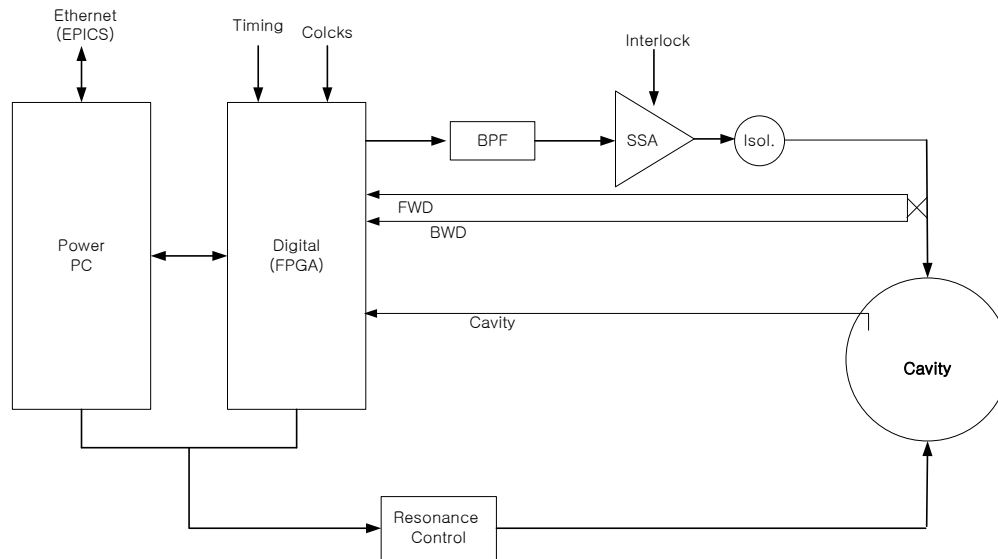


**Figure III.1.11.2. Conceptual block diagram for the proposed LLRF control system**

High power RF system, using RF amplifier, produces several kW level of RF power. This high level RF power is transmitted to 4 kinds of superconducting. It is usually used solid state amplifiers (SSA) which could produce several kW. Because coupling condition of cavities is over coupling, it is required to circulators with RF load or isolator between cavities and RF amplifiers. When RF power is transmitted to 4 kinds of superconducting cavities, it is satisfied required condition. All of cavities have to be satisfied condition that is the stability of the RF field should be within  $\pm 1\%$  in amplitude and  $\pm 1^\circ$  in phase, and the resonant frequency control. It is required the operating RF frequency 81.25 MHz, 1 kW for QWR and 162.5 MHz, 1 kW for HWR and for 325 MHz, 3 kW for SSR1 and SSR2. It has to consider higher power level than operating power level because of high Q value.

The HPRF system is designed with the operating RF frequency and the RF power rating. The HPRF system supply RF power for cavities of superconducting CW Linac. Figure III.1.11.3 shows the conceptual block diagram for the SC-Linac HPRF system. A solid-state RF amplifier drive a SC-Linac, and a circulator and a RF dummy load are installed to absorb the reflected RF power from the SC-Linac in order to protect SSA.

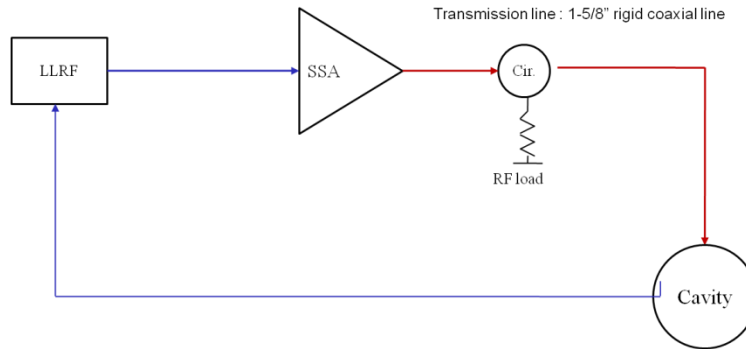


**Figure III.1.11.3. Conceptual block diagram for the SC-Linac HPRF system**

In order to transmit RF to the SC cavities, we usually used rigid coaxial line considering handling power and attenuation per unit length. Figure III.1.11.4 shows rigid coaxial line which is fabricated by MEGA cooperation. It is obtained by utilizing high conductivity copper inner conductors that are supported by Teflon insulators. The outer conductors are precision drawn heavy wall copper tubing.



**Figure III.1.11.4. Picture of rigid coaxial line (MEGA Company).**

Figure III.1.11.5 and III.1.11.6 shows the RF handing power and attenuation of rigid coaxial line, respectively. 1-5/8" rigid coaxial line are available the transmission line between SSA and SC cavities Attenuation of coaxial line per 100 ft is maximum 0.3 dB.

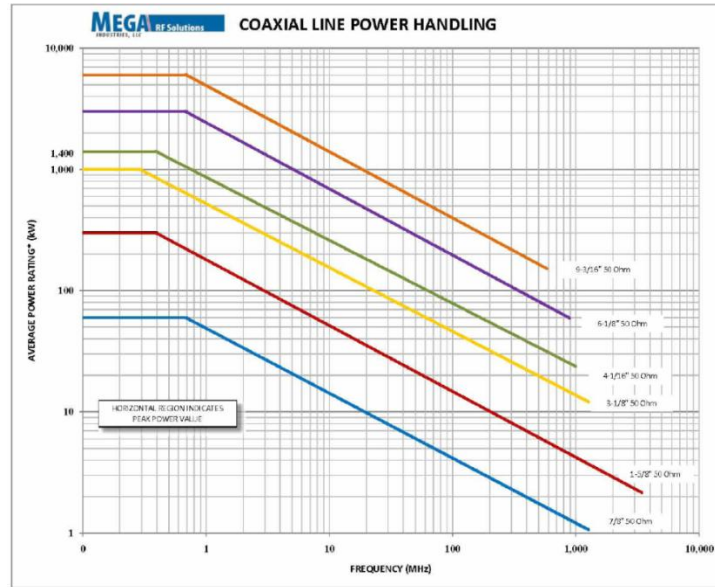


Figure III.1.11.5. Graph of coaxial line power handling.

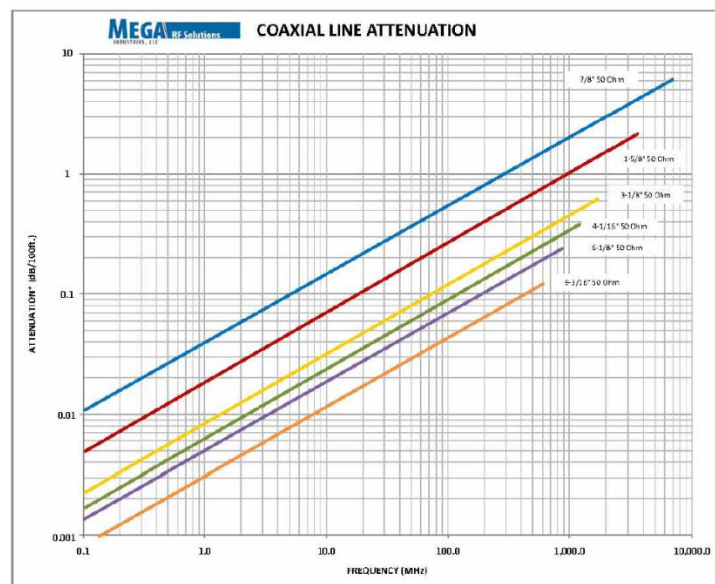
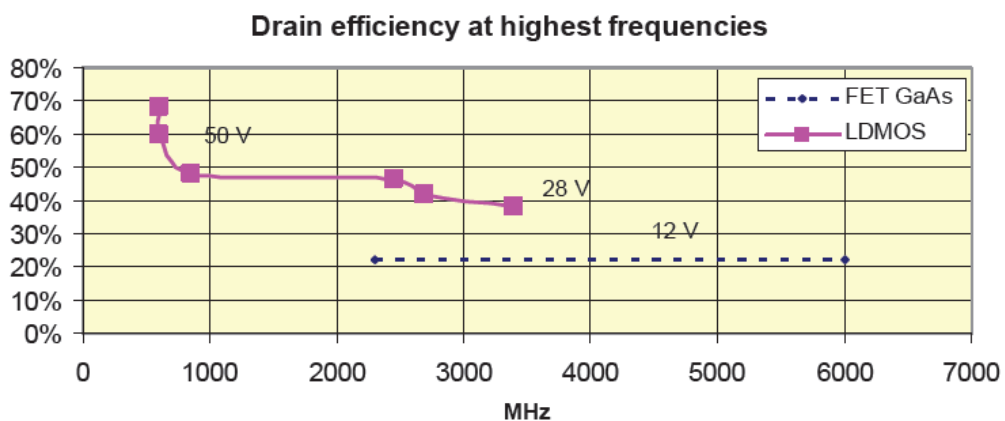


Figure III.1.11.6. Graph of coaxial line attenuation.

Solid state amplifiers (SSA) are based on transistors instead of vacuum electron tubes as active device. Vacuum electron tubes were preferred for medium and high power applications and recent advances in transistor technology are making SSA an increasingly viable alternative to tube system in accelerator applications. Performances have been improved by integrating electrostatic discharge protections, increasing gain, efficiency, breakdown voltages and thermal stability. Nowadays, several transistors cover the bandwidth from few MHz to several GHz, handling average power around hundreds of watts in CW mode. The latest generation of LDMOS RF transistors potentially enables the construction of very high power RF amplifiers with excellent reliability and ruggedness, and a capital cost that competes favorably with vacuum tube technology. Device working at drain bias around 100 V available below 150 MHz.



**Figure III.1.11.7. The graph of Drain efficiency vs. frequency [III.1.11.1].**

SSA is composed of the elementary RF bricks so called 'pallet'. Pallet is based on 1 or 2 transistors and mounted on a highly conducting metallic ground plane and equipped with their biasing network and with input and output matching stage as shown in Fig. III.1.11.8.

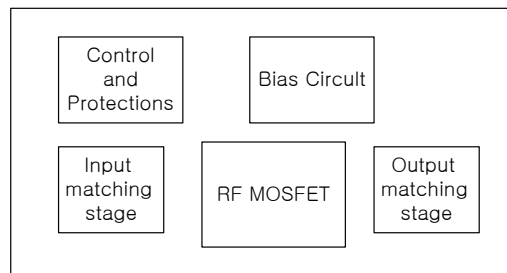


**Figure III.1.11.8. Typical pallet block diagram.**

Figure III.1.11.12 shows 800 W pallet, is based on 2 transistors, having 88 to 108 MHz frequency (©DB ELETTRONICA).

Several of pallets are then combined together to obtain higher output power. Isolated dividers and coupler can be used to avoid oscillations or other phenomena which could bring to the transistor destruction. Circulator or isolators can also be used to decouple each amplifier, making it unconditionally stable, and in this case non isolated splitter/combiners can be used. Splitters, combiners and circulators are therefore extremely important elements of solid state RF amplifier. At very low frequencies, circulators can't be used and transistors are operated at around 50% of their possibilities. In case of failure of a few transistors, the solid state architecture grants significant amount of power being still possible to replace the broken module without interrupting the amplifier operation.



**Figure III.1.11.9. The picture of 800 MW pallet frequency (©DB ELETTRONICA)**

Figure III.1.11.10 shows schematic of which several of pallets (800 W) are then combined together to obtain 5 kW output power. Isolated dividers and coupler can be used to avoid oscillations or other phenomena which could bring to the transistor destruction. Circulator or isolators can also be used to decouple each amplifier, making it unconditionally stable, and in this case non isolated splitter/combiners can be used. Splitters, combiners and circulators are therefore extremely important elements of solid state RF amplifier. In principle power combiners become splitters when used backward. Isolated splitter is usually used Gysel type rather than Wilkinson type at high power. The Gysel scheme is largely used for N-way splitters or combiners in 80 to 200 MHz range of frequency. Circulators or isolators are used when the signal coming back is deviated on a dummy load. This is the configuration used in solid state amplifiers to protect the transistor or all the amplifier devices against reflected power. Isolators have to be disposed between pallets and combiner, because it can be required more high level RF power for SCL cavities to have high Q value.

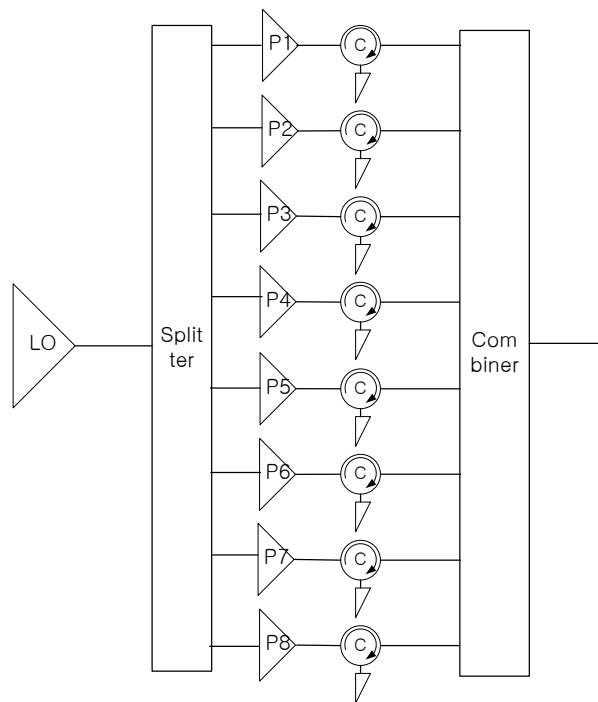


**Figure III.1.11.10. Possible combining schematic for 5 kW SSA**

**[Reference III.1.11]**

[III.1.11.1] Marco Di Giacomo Solid state RF amplifiers for accelerator applications, PAC09, Canada (2009)

### III.1.12 Control System

The RISP Accelerator Control System (RiCS), shown in Figure III.1.12.1, has the omnipotent policy of standardization. The strict standardization is absolutely essential to mitigate the integration risk. If we do not follow this policy, the risk will ask the RISP for prohibitively expensive efforts with respect to money, time, and man-power, because of the complexity of the RISP accelerator. And this term of the standardization gives a guarantee so that we can extend and upgrade existent all software and hardware equipment later. Thus, to pursuit the strict standardization is indispensable for the scalability of RiCS.

Moreover, we would like to build the maximum security control system for the RISP, because much more control equipment are going to be online within private, public networks, and both and many users and operators use their online devices in order to access valuable information from whole control system network. The security system will be the challenges of the next few years, especially, when the RISP accelerator will be being operated, because we cannot predict how complicated network environment will be due to its evolution speed.

For the cost-effective integration and scalability, a modular block system will be designed based on an abstract object-oriented device with standardized interfaces. Therefore a modular block can communicate with other blocks, can be integrated into others blocks as a sub-block, and can be extended into new blocks easily.

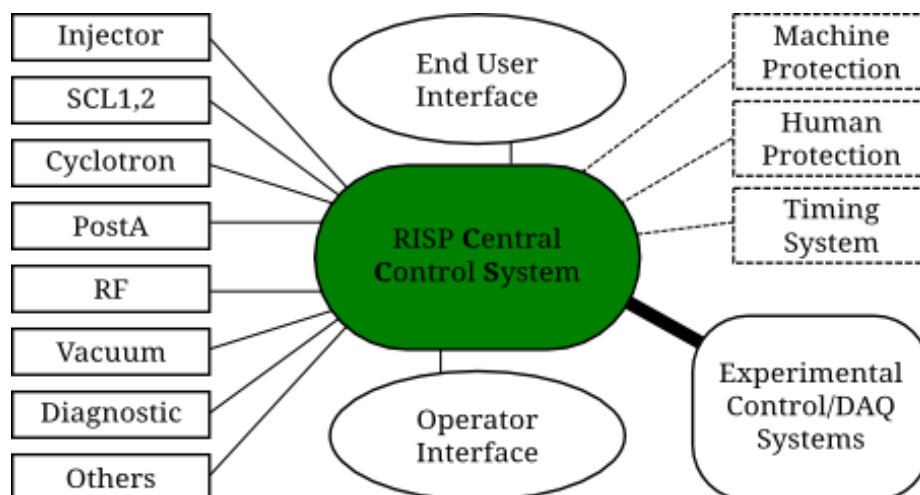


**Figure III.1.12.1. Conceptual Architecture of the RISP Control System (RiCS).** In the drawing, SCL stands for Superconducting Linac, PostA does Post-Accelerator, RF does Radio Frequency system, and so on. End user represents who wants to check or monitor the RISP control system passively and Operator does the system actively. DAQ represents Data Acquisition. The experimental control/DAQ systems can communicate with RiCS.

### **III.1.12.1 Requirements**

The RISP control system (RiCS) should be reliable, scalable, maintainable, and low-cost system that could be used easily and fun by end-users and operators. Therefore the Experimental Physics and Industrial Control System (EPICS) is selected as an infrastructure for RiCS, because it is reliable, scalable, maintainable, low-cost system, and standard. EPICS is an open-source, i.e. the source code is accessible, software that has various tools, libraries, and predefined applications developed by a world-wide user community and is used in large and small experimental physics projects such as particles accelerators, telescopes, and light sources since 1994. In addition, EPICS supports several hundred different modules with almost all bus types that produced by more than hundred manufacturers. Especially, in South Korea, EPICS is the crucial infrastructure at the Pohang Accelerator Laboratory (PAL) and Korea Superconducting Tokamak Advanced Research (KSTAR). As a result, RISP will benefit from PAL and KSTAR that have already done a huge contribution to EPICS community in South Korea.

The main operating system (OS) is selected as Linux, because it also fulfills the control system design goal, i.e. reliable, scalable, maintainable, and low-cost. In addition, Linux is open-source software and has almost no malicious softwares to compare with other OSs, especially Windows series. Two Linux systems are considering now; Debian and Red Hat Enterprise Linux (RHEL). Debian system is a complete free OS and RHEL is also a free OS,

but has commercial supports. Debian is a better choice than RHEL according to the cost of OS itself in the long term, but Debian Linux experts must be recruited at the early stage in order to maintain OS itself. For RHEL, Linux OS experts are not mandatory, because of Red Hat customer supports.

Here some important requirements which RiCS must fulfill are itemized as follows:

- RiCS could read, change, and record all raw signals from all equipment of the accelerator and all logic signals generated by some raw signals.
- RiCS could provide an effective user interface, e.g. graphical users interface (GUI), so that users can access any recorded signal easily.
- RiCS could record standard procedure for running up the accelerator and related configuration for all equipment.
- RiCS could provide automatic procedure for running up the accelerator according to preset conditions.
- RiCS could provide the continuous optimization of all equipment during the accelerator running.
- RiCS could oversee all equipment, alert operators, end-users, or both to fault conditions, and could provide tools in order to analyze any fault quickly.
- A control system of a device could be a member of other integrated control system and could be one component of RiCS.

### **III.1.12.2 Abstract Concept of a Basis**

Figure III.1.12.2 shows an abstract concept of a basis for RiCS, within the EPICS framework, which could be divided into three modular blocks as follows: Application Block, Service Block, and Resource Block. Three modular blocks are divided according to each key role. In reality, however, each block has similar components that exist in other block.

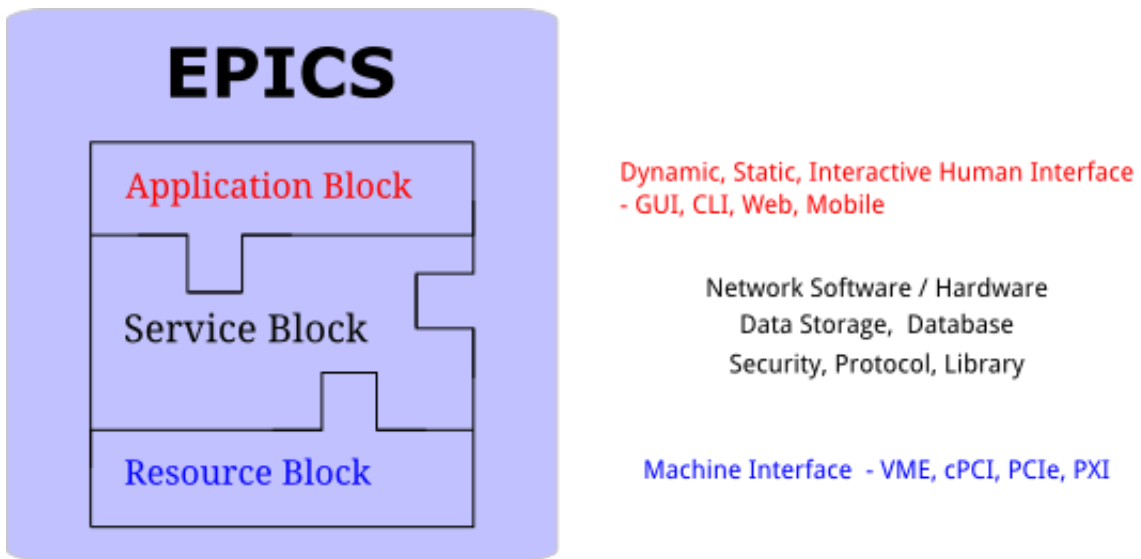


**Figure III.1.12.2 An Abstract Concept of a Basis for the RISP Control System.** Within the Experimental Physics and Industrial Control System (EPICS) framework, all blocks are integrated in order to provide end users and operators with comfortable and rock-solid interfaces.

**Application Block** In short, the application block represents many different types of software which will be designed for all human beings. It could be dynamic, static, or interactive human interfaces. Technically, they are GUIs, command-line interfaces (CLIs), PC-based web pages, Mobile web pages, or Televisions. Since the application block communicates with many different human beings, it is crucial to do careful block design, especially interactive GUIs, so that the block could predict any kind of human responses, controls, or both and must protect the control system from any mistakes. Script languages, e.g. Python and BASH, compiled languages, e.g. C/C++ and FORTRAN, and technical computing languages, e.g. Matlab and Mathematica, could be provided for monitoring, operations, and accelerator studies.

**Resource Block** The resource block represents many different types of hardware designed for all machine interfaces and most interesting information which we want to monitor, control, or both. Technically, it also contains software in order to send and receive all information between the service block and the resource block. International standards such as VME, cPCI, PCIE, and PXI as the interfaces must be selected in order to upgrade and maintain them later without any difficulty.

**Service Block** The service block covers a broad range of hardware devices, for example, computers for simulation and analysis, operators consoles, databases, network switches, gateways, and backbones, displays, e.g. TVs and monitors, data storage, uninterruptible power supplies, port-servers, remote-access power distribution units, and so on. In addition, all configuration files, libraries, and software for all hardware devices are included in the service block. This block must be designed to share any kind of a basis information with other systems, e.g. Machine Protection System, Human Protection System, Timing System, and Experimental Control / DAQ systems, because it is one basis of RiCS.

### **III.1.12.3 Operation Designs**

From the operation point of view, the control system is divided into three separated, but integrated, designs: Stand alone, Operation, and Debug. Each design shares its functionality with others or itself and can be easily integrated into others or itself according to a place where it is used.

**Stand-alone Design** A compact and modularized system, that has three basis blocks, i.e. Application, Resource, and Service blocks, could be used as stand-alone system especially during testing on a prototype of any equipment of the accelerator. Simple,

intuitive, and self-descriptive interfaces should be considered for developing GUIs and CLIs. By using these interfaces, low level hardware accesses could be possible. This design is a basic single component of the RiCS, and could be integrated into the other components, the central control system, or both. Figure III.1.12.3 shows the stand alone design in the first row. Four elements, i.e. hardware, a database manager, an operator or end-user interface, and an expert interface, connect with each other via Ethernet, and should have a standard interface in order to connect to Ethernet and others, e.g. RS-232 connection, according to their purposes. The GUI and CLI should read, set, and monitor any signals

**Operation Design** A simple and easy-to-use system, that has three basis blocks, could be used for accelerator operators and for various end-users. The accelerator operators actually operate the accelerator and monitor or change its configuration while running up. So this system should provide a collection of tools for monitoring, alarm handling, and logging. Moreover, standard procedure for running up the accelerator and related configuration for all equipment could be saved into database systems automatically. These saved entries in the databases could be used in the restoration of the preset accelerator configuration and in the further investigation of the accelerator equipment. End-users want to see, save, monitor, and re-use any kind of information form the accelerator on the basis of time with their interest. Figure III.1.12.3 shows the operation design in the second row. This design excludes end-users and operators from expert interfaces. However, these excluded expert interfaces could be accessible via an expert mode when it is necessary. And it includes feedback systems that might be needed to optimize devices into desired accelerator operation.

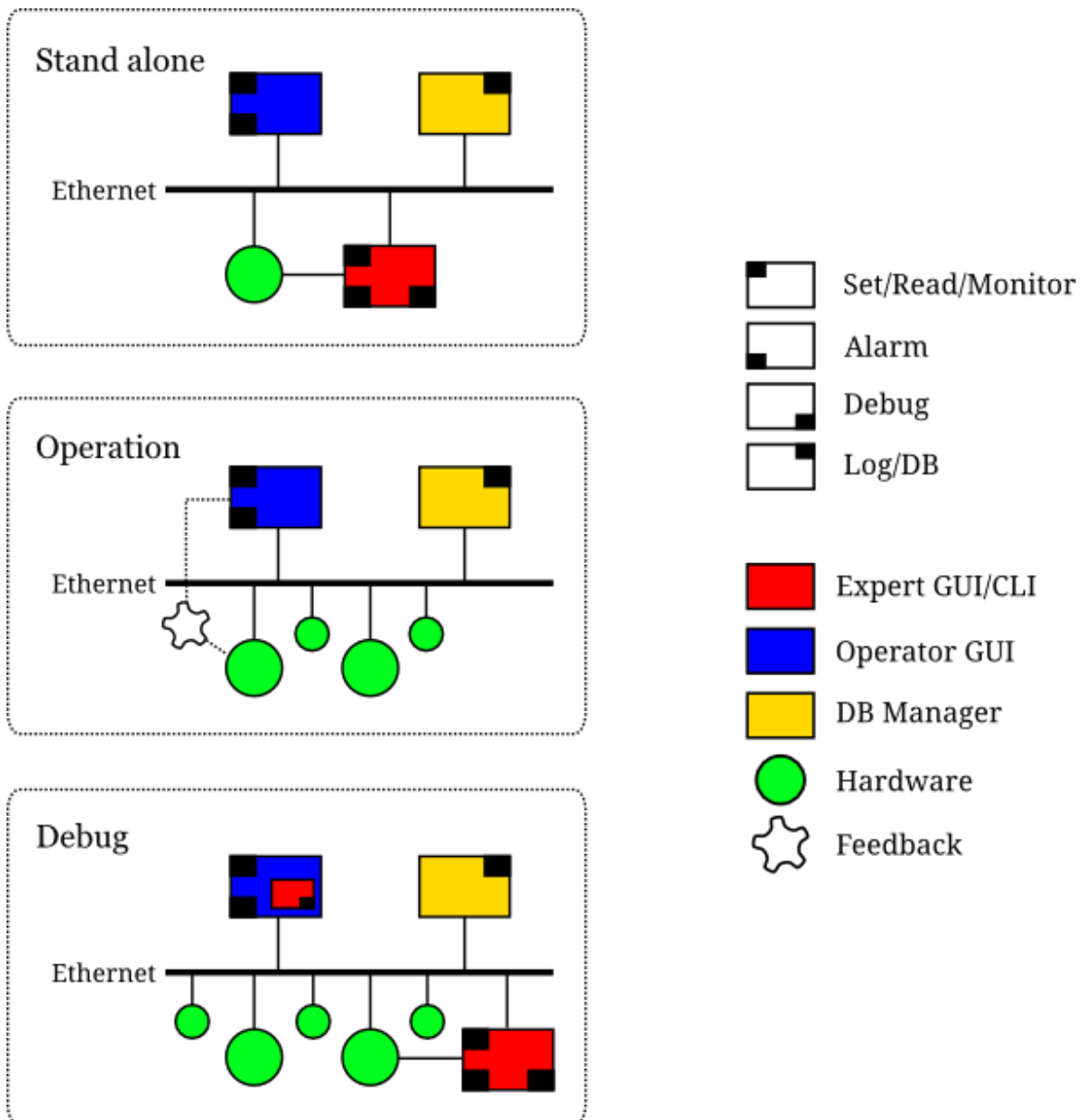


**Figure III.1.12.3** Left dot-lined boxes show the three Operation designs. Set/Read/Monitor is an operational functionality that operators or end-users could set, read, and monitor any signal from a system. Alarm is an integrated tool within GUI and CLI and could alert operators or users. Log/DB represents database related software and hardware that are under DB manager. Hardware does any kind of hardware device which could accept raw signals.

**Debug Design** A modularized and portable system, which has three basis blocks, could be used for experts who are interested in understanding, debugging, and troubleshooting any device that is identified as a bad or malfunctioning one. It should provide a cost-effective way to experts in order to find reasons for any malfunction and to do a quick recovery. It might be one subsystem of an operator interface, a stand-alone system, or both. Sometimes, a malfunctioning system or device cannot be accessible remotely, so experts have to recover the non-accessible system via a direct connection. Therefore, portability is essential. Figure III.1.12.3 shows the debug design in the third row.

#### **III.1.12.4 Safety System**

Safety system is an integrated part of the control system and consists of Personnel Protection System (PPS) and Machine Protection System (MPS).

##### **III.1.12.4.1 Personnel Protection System (PPS)**

The PPS protects personnel from the radiation and other hazards caused by the operation of the accelerators and its subsystems. As the PPS assures the safety of people, it should be highly reliable and failure-proof. The system makes use of Programmable Logic Controllers (PLCs). Usual computers are not used in the interlock sequence because their limited reliability. They are used only in software development and monitoring of PLCs. The PPS is isolated from other systems, such as the accelerator control system, to prevent it from being disturbed. In order to make the system reliable, PLCs are installed redundantly. The signals of important devices, such as emergency buttons, door switches, etc., are also redundantly read. Metal wires are used to connect these devices to PLCs in a local control room. The central control room and local control rooms are connected with both of optical fibers and metal wires.

#### **III.1.12.4.1.1 Interlocks**

We will have at least two levels of interlock. In case of the level 1 interlock (emergency button, door interlock, etc.):

- the ion source is interlocked off,
- three beam stops in LEBT and MEBT are inserted,
- the safety bending magnets for the interlocked area are turned off,
- high power equipment of the area are turned off.

In case of the level 2 interlock (radiation monitor interlock, etc.):

- one or two beam stops in the LEBT and/or MEBT are inserted into the beam line.

#### **III.1.12.4.2 Machine Protection System (MPS)**

Machine Protection System (MPS) is to protect the accelerator system against equipment failure and excessive beam losses, depending on the operational mode of the accelerator and the beam dump in use. This system is tightly integrated with the timing system. The MPS uses the timing system to assure operation within specified parameters. In addition, information on shut-down causes originating with the MPS is broadcast by the timing system for post mortem analysis. The main functions of the MPS are as follows:

- Protect the beam tubes and insertion devices (slits, Faraday cups, targets, etc) from beam thermal damages,
- Control the operating range of the facility,
- Control the accelerator device activation due to beam losses (beam losses limited to 1W/m),
- Ensure protection of the beam dumps and targets.

### III.1.13 Vacuum System

Vacuum system can be divided into ultra-high vacuum (UHV) system ( $10^{-8}$  -  $10^{-9}$  torr) for the beam line and high vacuum (HV) system ( $\sim 10^{-6}$  torr) for cryogenic insulation and preliminary pumping of the beam line. In the beam line, UHV condition is needed for preventing contaminations on SC cavities which can cause field emission and lower the accelerating voltage. Because cavity which is cooled down to 2K absorbs molecules like a cryopump, cavities must be at UHV condition before cool down and UHV pumping stations have to be installed nearby the cavity to intercept contaminations from the warm section as shown in the schematic drawing. One or two mounted HV pumping station is needed to keep the thermal insulation between the outside and the inside of a cryomodule. Two particle-free UHV gate valves per one cryomodule are installed in both ends for the isolation.

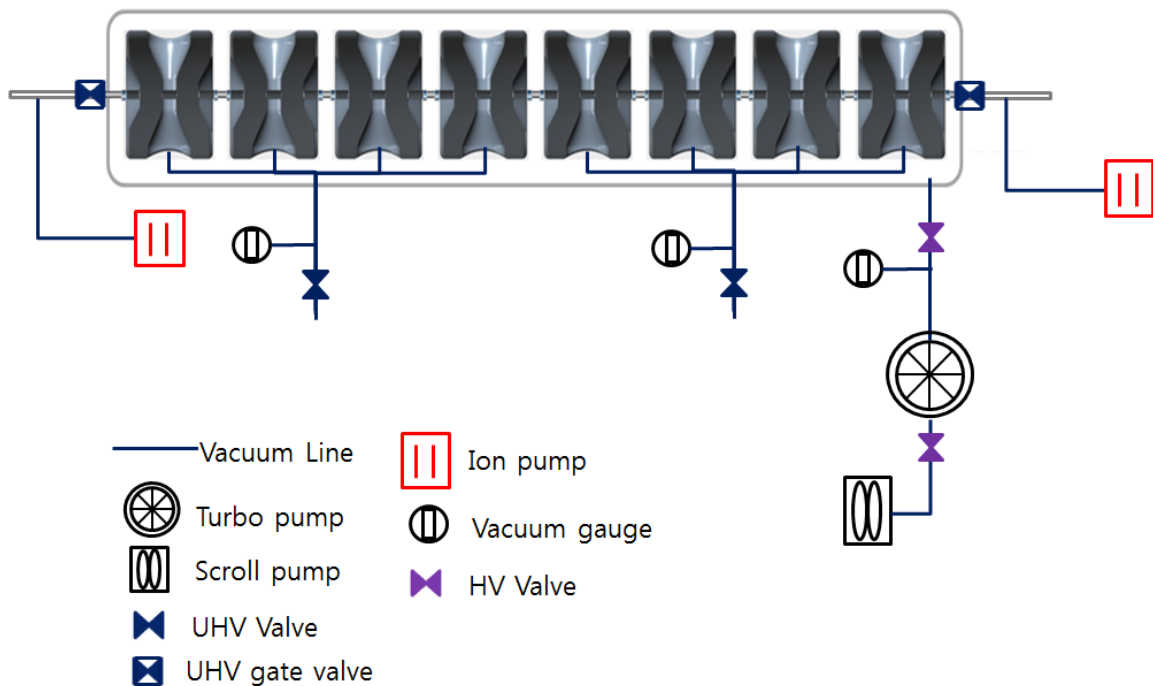


Figure III.1.13.1. Schematics of vacuum system in a cryomodule of SCL

### **III.1.13.1. HV System**

A HV pumping station consists of an oil-free scroll pump for a backing pump, a turbo molecular pump (TMP) for high vacuum generation, a full-range cold cathode type vacuum gauge, and HV valves. In the case of backing pump, the pumping speed is around 500Liters/minute and the ultimate vacuum level is high  $10^{-3}$  torr. After the vacuum level of low  $10^{-2}$  torr is attained using the backing pump, the TMP starts up and generates vacuum until  $10^{-6}$  torr  $\sim 10^{-7}$  torr. The TMP of  $\sim 1,000$  Liters/sec pumping speed is adopted in consideration of the efficient vacuum generation and the cost effectiveness. The full range vacuum gauges which can measure the vacuum until  $5 \times 10^{-10}$  torr are installed in external ports of a cryomodule.

Before cooling the beam line, mobile HV stations are temporally connected preliminary pumping lines of cavities and mount-type HV stations are installed in a cryomodule permanently for the thermal isolation. These HV stations are assembled with a cryomodule in a class 100 clean room. The mobile HV station will be removed from the preliminary pumping line when the vacuum level of the cavity reaches the  $10^{-9}$  torr after cooling. The vacuum level for the thermal insulation is less than  $10^{-5}$  torr.

Vibration dampers and protections of EM field, etc. are considered in the HV system.



**Figure III.1.13.2. Mobile HV system**

### **III.1.13.1. UHV System**

Starcell type ion pumps are adopted in UHV system. The lifetime of these ion pumps is 80,000 hours at  $10^{-6}$  torr. Ion pumps are installed in the warm section of the beam line to eliminate molecules which can contaminate cold cavities. Quantity of pumps and the pumping speed depend on the length and the volumes of the warm section. All vacuum lines, pumps, valves must be proper at the UHV condition and must be baked, cleaned as same as SC cavities to reduce the outgassing rate. The UHV system must be designed in considering the reduction of contaminations from the motions of gate valves, venting systems, bolting, etc.

Cavities can be disassembled in class 100 clean room when the pressure difference is less than 1mbar between the outer air and the inter dry  $N_2$  gas of cavities which is filled using a venting system with mass flow controllers.

### III.1.14 Accelerator System Installation Plan

SAR (Safety Analysis Report) Review and its related permits are required, for the construction of accelerator tunnels, buildings, and target areas. SAR Review is a critical path to the installation of the accelerator systems. As shown in the Fig. III.1.14.1, the SAR Review ends January 31, 2016 and the construction of the accelerator tunnels is scheduled to begin February 1, 2016. After allowing minimum time of five months, the installation of accelerator system is scheduled to start July 1, 2016, including the injector, the low energy part of the driver SCL, ISOL post accelerator, and cyclotron. For more details, please refer to the project schedule. Starting the installation of the accelerator system on July 1, 2016 allows only one and a half years for the installation and the commissioning, to support the 2017 completion. This presents a very aggressive schedule.

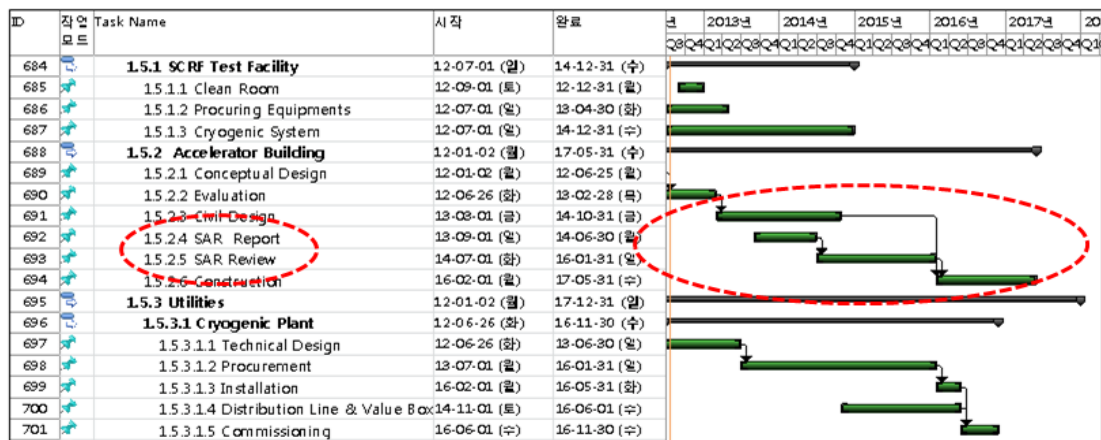


Figure III.1.14.1 Schedule of the SAR (Safety Analysis Report) ending January 31, 2016.

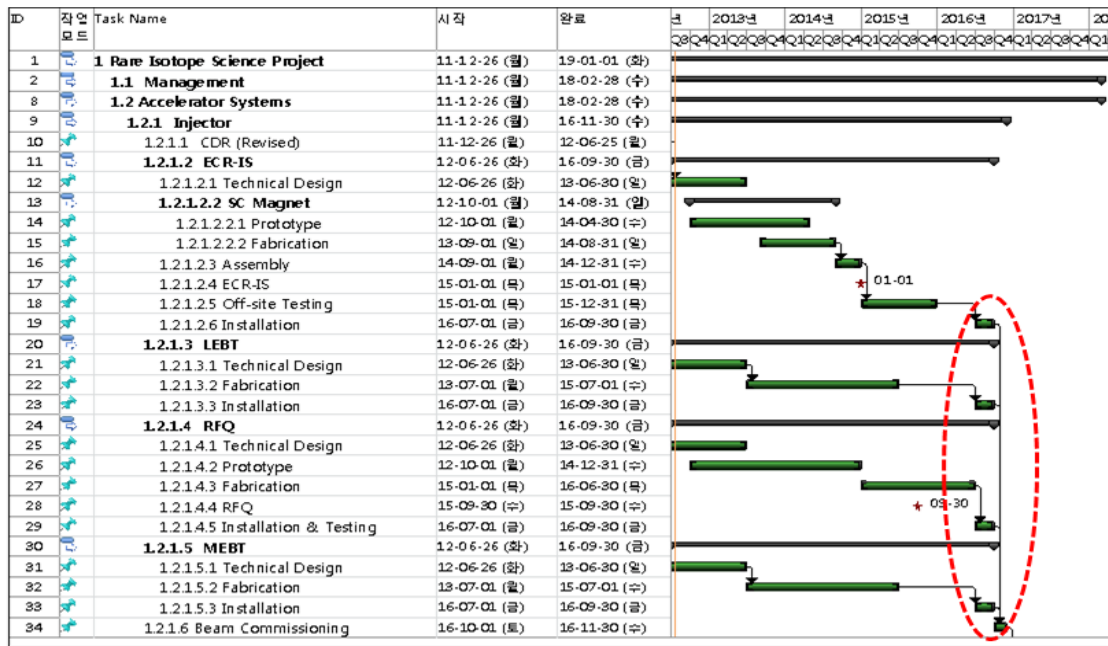


Figure III.1.14.2. Schedule of the Injector installation starting July 1, 2016 and commissioning starting October 1, 2016.

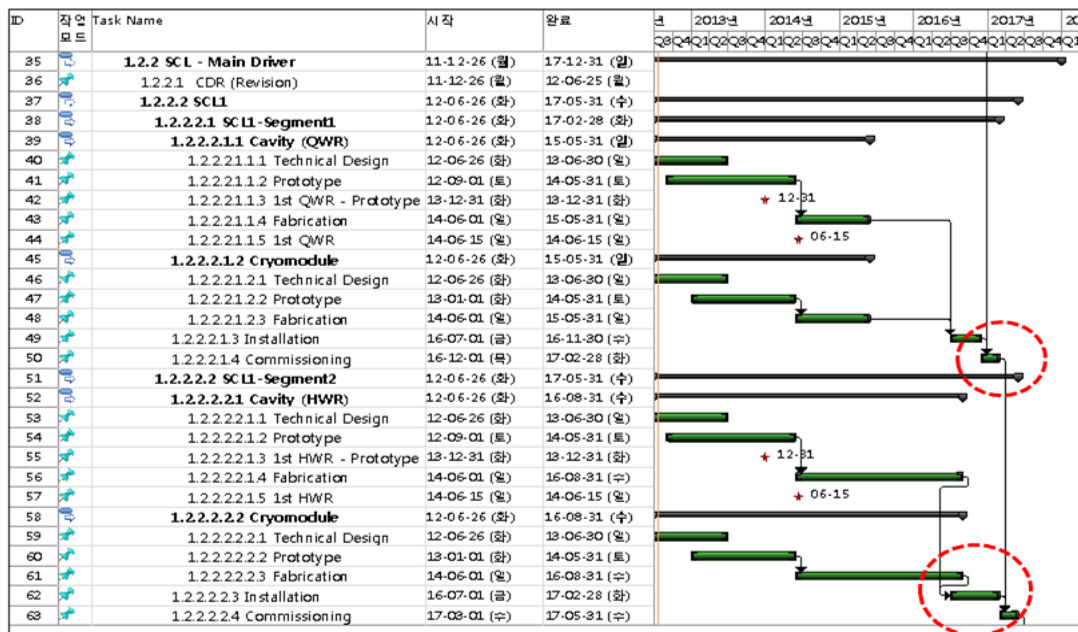


Figure III.1.14.3. Schedule of the SCL1 installation starting July 1, 2016 and commissioning starting December 1, 2016.

### **III.2 In-Flight Fragment System**

The in-flight fragment system consists of pre- and main separators. The pre-separator includes the target system for the production of rare isotope beams by the mechanisms of such as projectile fragmentation and in-flight fission. The isotope beam of interest passes thru the pre-separator, and the remaining beam, which is mostly the primary beam, needs to be dumped in localized areas. This front-end of pre-separator including a target and beam dump should be well shielded from the other regions. All of the parts will be made in detachable modular form so that any malfunctioning can be repaired by taking out the affected module to designated repair area. This remote handling will require careful mechanical design on the joining parts of the modules as they are related to vacuum sealing and alignment. Modern robot system for remote handling often heavily uses semiconductor devices, which are weak to radiation damage. Major parts of the handling system should use metallic components to avoid fast radiation damage. An efficient approach to the system development would be to adopt established technology at the high-current beam facility in operation such as the SNS in the US.

A major item requiring development is superconducting quadrupole magnet downstream of the target in the pre-separator area. This magnet receives the highest level of radiation dose, and still needs to have a large aperture for large acceptance of isotope beams. A high-T<sub>c</sub> superconducting magnet with warm iron yoke has been developed for the FRIB project by the BNL group. We will try to develop a similar magnet, and it will be helpful to collaborate with the BNL group.

We plan to develop superconducting quadrupole magnets for the separator with helps from domestic companies and laboratories. The superconducting magnets will be of superferric type, whose field is dominated by iron pole and yoke. A prototype superconducting cryostat containing a quadrupole magnet triplet with multipole coils wound on the cold bore tube is planned to be constructed. Magnetic field calculations

using OPERA3D have been performed, and will be compared with field mapping results when the prototype is ready, which will assure the precision of field calculations. The dipole magnets are planned to be conventional.

### III.2.1 RI beam production

The production rate of RI-beams on the in-flight separator system has been calculated. Momentum and angular dispersions of the  $^{132}\text{Sn}$  beam produced by projectile fragmentation and abrasion fission are shown in Fig. III.2.1.1 as a function of the primary beam energy.

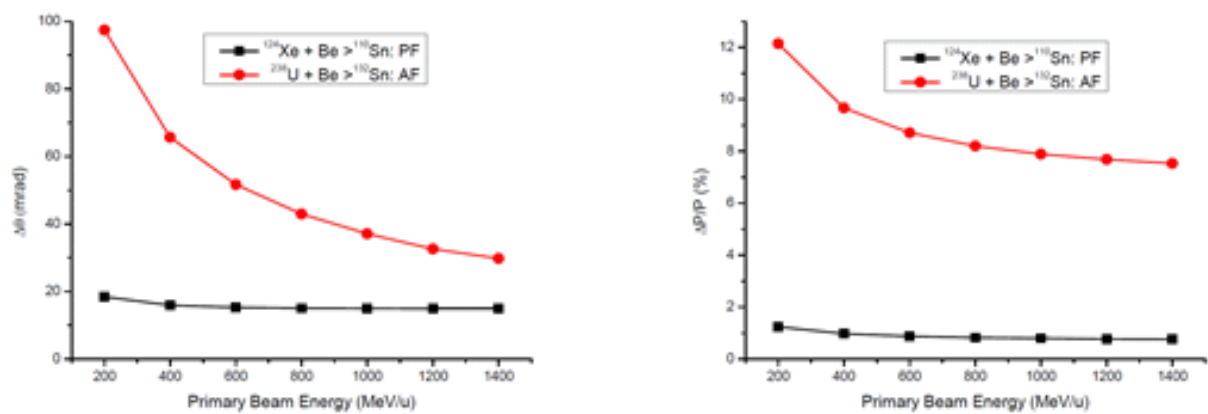


**Figure III.2.1.1 The momentum and angular dispersions of  $^{132}\text{Sn}$  beam produced from projectile fragmentation (PF) and abrasion fission (AF).**

Assuming that angular dispersion of the separator is about 70 mrad in both horizontal and vertical directions and momentum dispersion accepted is 10%, we calculated all of rare isotope beams which can be produced from the projectile fragmentation and the abrasion fission. The results are shown in Fig. III.2.1.2 and Fig. III.2.1.3.

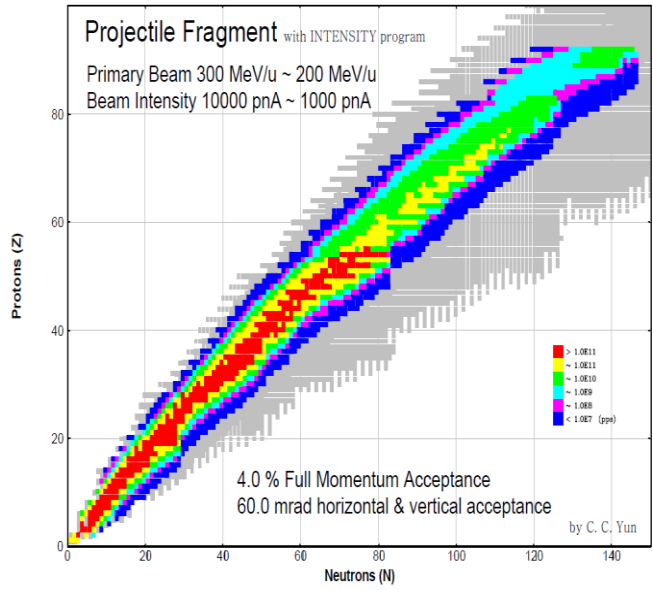


Figure III.2.1.2 The production rates of RI-beams by projectile fragmentation

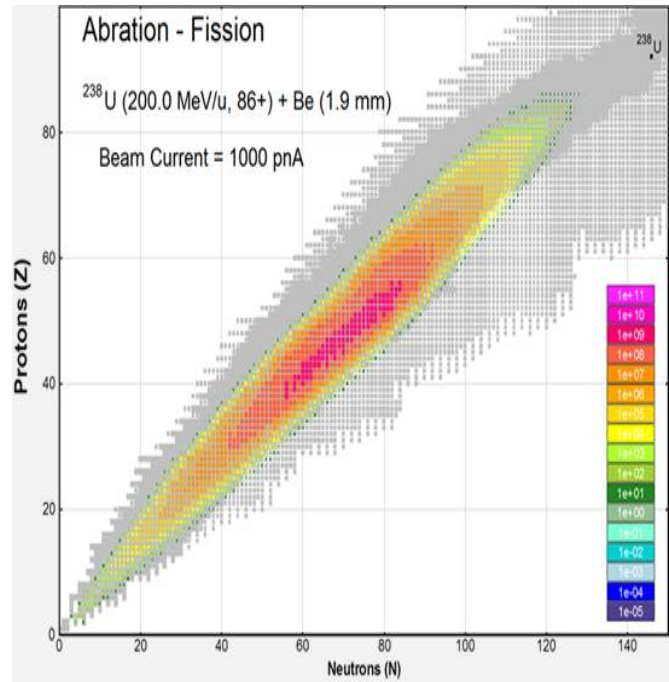


Figure III.2.1.3 The production rates of RI-beams by the abrasion fission.

### III.2.2 Target

The target for in-flight fragmentation absorbs about 30% of the primary beam power in average case. The resultant power density inside the target is very high, and thus cooling is critical. The high-power target for in-flight fragmentation has been numerically studied using PHITS, which is a heavy-ion radiation transport code to evaluate the generation of heat and radiation.

The highest power density is calculated to be around 65 MW/cm<sup>3</sup> for a U beam of 200 MeV/u at 400 kW, and can be reduced to tens of kW/cm<sup>3</sup> by using a rotating target. The maximum allowable temperature for graphite target is around 1900 °C, but temperature inside the target reaches higher for a single-layer target with a thickness of over 1 mm for the U beam. A multi-slice target with a thickness in the order of 0.1 mm can reduce the temperature with enhanced radiation cooling, but then structural problem has been observed at the high rotating speed. To reduce the hot-spot temperature, rotation speed for the target diameter of 30 cm needs to be over 3000 rpm. Recently a new target design, which will be tested using an intense electron beam, has been reported by the FRIB group [III.2.2.1]. If successful, we will consider testing a similar design.

Fig. III.2.2.1 is a diagram of high power target technology in the world's leading heavy ion facilities. Power density inside the target (C, Be and Liquid Lithium) is represented as a function of the beam power deposit. Blue marks show the devices in operation, while green ones show the prototypes and the red ones are for technologies which are to be developed.

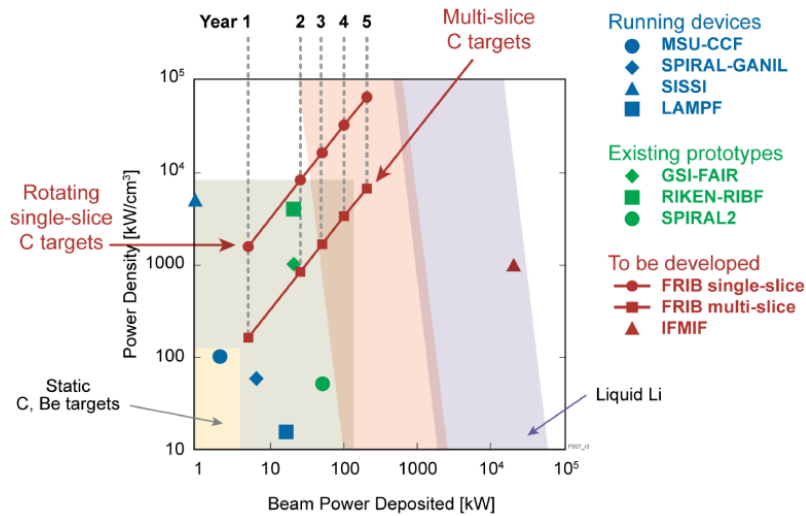


**Figure III.2.2.1 Diagram of high-power target development in the world's leading heavy ion facilities [III.2.2.1].**

Another target to be considered is a liquid lithium jet. The lithium target has been considered as a charge stripper for heavy-ion superconducting accelerators as other kinds of target seem to fail to extend the stripper lifetime and also fail to attain high-charge states. Li target requires special handling, and the ANL, which has specialty in handling hazardous material, is involved in developing Li target as the charge-striper for the FRIB. It may be difficult for us to carry out the development of Li target independently. We are considering possible international collaboration and working with a KAERI group, which has experience in handling liquid Li.

According to a recent report, the ANL group achieved a stable Li film at the thickness of several microns for the diameter of 9 mm [III.2.2.2]. In producing a  $^{132}\text{Sn}$  beam via nuclear reaction of a U beam of 200 MeV/u at the beam power of 400 kW on a Li target, maximum yields can be obtained with the target thickness of about 1 cm. Fig. III.2.2.2

shows calculated stopping power of U beam in Li target. The stability condition for the thick target would be different from the condition for a thin film of charge stripper.

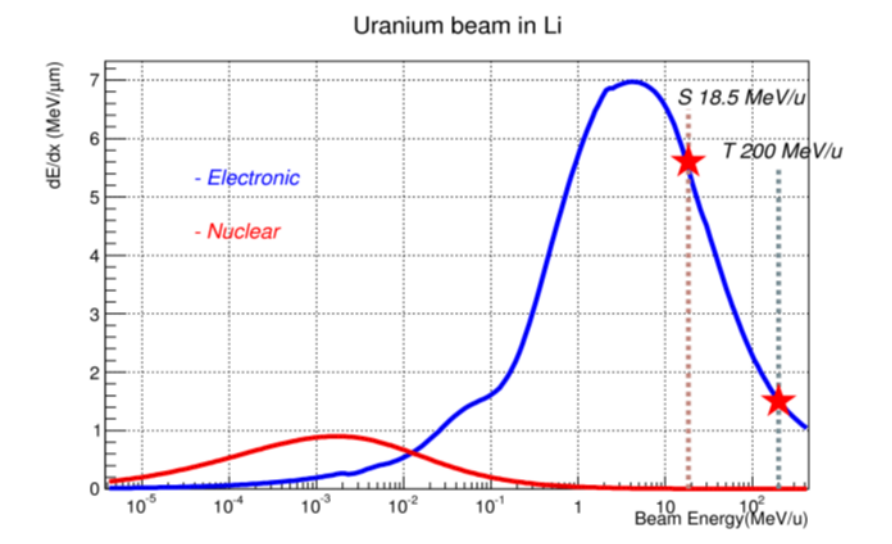


**Figure III.2.2.2 Stopping power of U beam in liquid Li calculated with SRIM.**

To assure the design of the target, it is essential to perform empirical tests. High current heavy ion beams are not available worldwide so that electron beams that can simulate the maximum energy density inside the target have been used instead. Such electron beams are locally available in Daejeon area.

A baseline design of the target relies on rotating graphite disk. In general a larger size disk can sustain a higher beam power, such that usual graphite targets can be used for different kinds of primary beams. To have our own experiences, we plan to test graphite targets using high-current electron and proton beams in different settings of thickness, diameter and manufacturer, measuring temperature distribution and mechanical deformation.

The analysis of mechanical stresses for the target is also important. ANSYS is a code, which can analyze the mechanical stresses along with heat transfer. The code will be extensively used, and the results will be compared with experimental outcomes in search of the optimal design of the target system.

### **[Reference III.2.2]**

[III.2.2.1] W. Mittig, 4<sup>th</sup>High Power Targetry Workshop, Malmö, Sweden, 2011.

[III.2.2.2] Y. Momozaki et al., JINST, Vol. 4, P04005, 2009.

### **III.2.3 Radiation effect**

Computational efforts have been made using PHITS to calculate radiation transport as well as radiation heating for the configuration of the pre-separator in the current design. The radioactivity accumulated by irradiation also considering radiation decay can be calculated using DCHAIN-SP, which directly accepts the outputs of PHITS. It may require extensive computational time to consider different combinations of primary beams and target material.

In further study, radiation damage especially on the materials used in the target and beam dump is an important subject. The codes such as TRIM, PHITS, may not correctly predict the lifetime of material by radiation damage. It is generally known that mechanism of radiation damage by the heavy ion irradiation is different from other kinds of radiation. The dpa (displacement per atom) is thought to be a main indicator of heavy-ion radiation damage. It would be an interesting future study to establish a model to predict radiation damage more correctly. If needed, it will be helpful to co-work with material scientists.

In some cases, annealing restores material properties damaged by radiation. This is also the subject of future study for the target material because the target requires frequent replacement. If annealing works, the amount of activated material can be reduced by recycling the parts.

The remote handling system is needed for the front part of pre-separator. All the components in the front part should be modular and detachable for remote controlling. This will require special connection joints such as pillow seal and self-alignment configuration. PSI, TRIUMF and SNS have extensive experiences in this aspect, and their technology has been transferred for the FRIB. However, it is not clear whether we can directly access to the US technology.

The possibility of radioisotope harvesting will be evaluated as some useful isotopes can be harvested along the separator by installing isotope catchers. Especially, the beam dump including cooling water line will be a source of intense isotope production. The radiochemistry laboratory can be shared with the isotope handling and hot laboratory facilities for the ISOL cyclotron.

### **III.2.4 Beam optical design**

The in-flight fragment separator is a device to separate isotope beam of interest and to purify the chosen isotope beam. The separator is divided into two sections: pre- and main separators as for the separators at the RIKEN, FRIB and FAIR, where the high primary beam power is removed in the front part of the separator.

The optical design of the separator has been performed using COSY Infinity, GICOSY and other optics codes. GICOSY is often used due to its convenient graphic package and COSY Infinity for higher-order calculations. To consider the effects of degrader realistically,

Monte Carlo codes such as MOCADI has been used. Beam tracking capability implemented in LISE++ is also to be utilized as we compare the results by different optical codes.

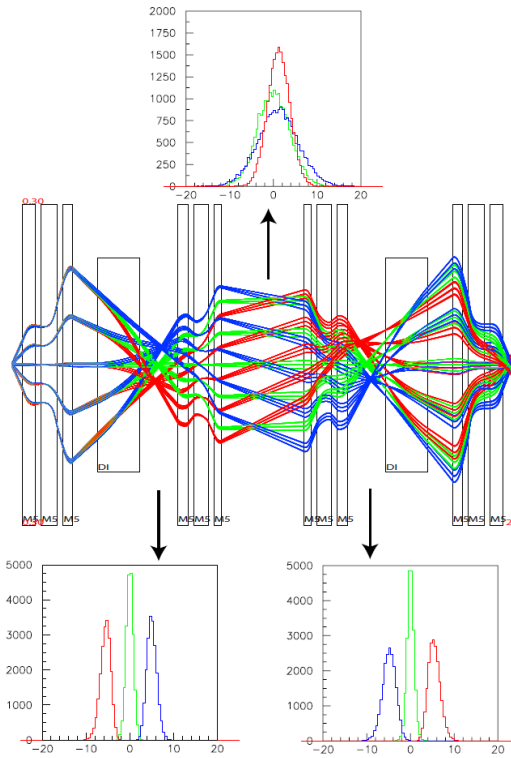


**Figure III.2.4.1 Beam optics calculation for the S-shape pre-separator.**

In the previous conceptual design study, the layout of the separator chosen was namely S-shape for pre-separator, and C-shape for main separator as shown in Fig. III.2.4.2. The entire separator beam line will be located in the same vertical level, which requires a unique design, which is different from the existing and planned designs in other facilities. The C-shape for the main separator was also chosen by the FRIB as it has advantages in accepting higher rigidity beams and in simple configuration compared to different shapes.

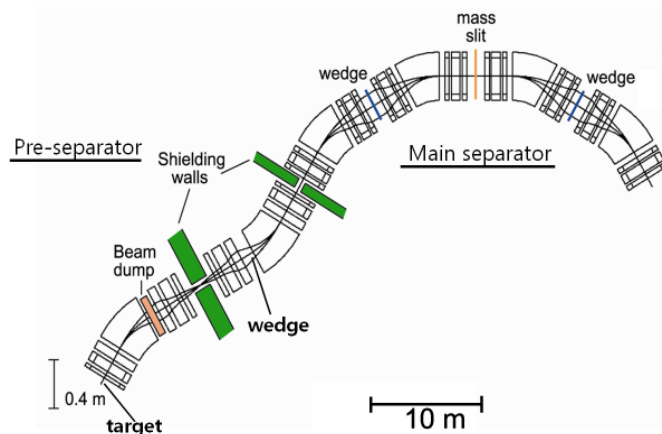


**Figure III.2.4.2 Configuration of the IF separator with S-shape for the pre-separator and C-shape for the main separator.**

The wedge for the S-shape pre-separator is located in the mirror location of the beam dump, which can be used to compress momentum spread. The final selection of separator configuration will be made considering acceptance of rare isotope beam, mechanical convenience and so forth.

The higher order components of the magnetic fields mainly come from the fringe fields of both the quadrupole and dipoles. Especially, a short length with a large aperture for the quadrupole magnets makes the fringe field calculation less accurate. The current calculation by COSY Infinity, which was done for the initial conceptual design, utilized an assumed fringe field description.

The acceptance by the linear optics will be limited mainly by the quadrupole aperture. The momentum and angular acceptances are around  $\pm 4\%$  and  $\pm 50$  mrad, respectively when the largest aperture radius is 15 cm for the S-shape pre-separator.

The multipole magnets to correct high-order field components were initially considered to be independent magnets, by which interference with the main quadrupole fields can

be reduced. However, the beam optics indicated the correction can be more efficiently done by incorporating the multipole coils with quadrupole magnets. These types of the magnet were also chosen for the FRIB. The prototype quadrupole magnet will include superconducting multiple coils wound on the cold bore tube. The field mapping will indicate more precisely the interference field effects for instance depending on the coil excitation.

### **III.2.5 Superconducting quadrupole magnet**

The quadrupole magnets will be superconducting, while dipoles are currently thought to be of conventional type. The maximum magnetic rigidity for the dipole will be over 9 Tm, which can be used even when the primary beam energy of U beam is upgraded to around 400 MeV/u.

The acceptance of beam elements in the IF system should be large to achieve a high current of rare isotope beam. Therefore the quadrupole magnet should have a large aperture and a high field gradient. A superferric quadrupole magnet having a superconducting coil and ferromagnetic yoke can be used. As the magnet aperture becomes larger, the effect of the high-order field components becomes more severe. An extensive magnetic field mapping is needed.

In the target region, the beam line components are under the influence of high radiation heat load. Therefore usual low-temperature superconducting magnet is less practical because heat load to 4 K system amounts to hundreds of watt. An air-core type superconducting quadrupole triplet is used at BigRIPS, which avoids the heat load when cold iron yoke is used. For the FRIB a warm-iron HTS (high temperature superconducting) coil magnet has been developed. The temperature of HTS coil is at 40-60 K. HTS conductor based on BSCCO and YBCO could be used, but winding technique of HTS coil

is to be further established. Prototypes of HTS magnet have been reported to be developed at the BNL for FRIB [III.2.5.1].

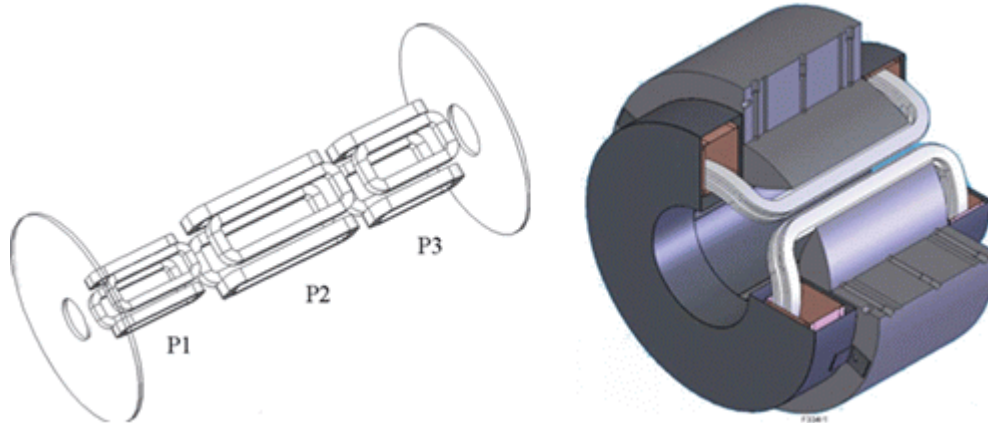


**Figure III.2.5.1 Left: Schematic of an air-core type magnet used for BigRIPS [III.2.5.2], Right: a warm-iron type HTS magnet [III.2.5.3].**

The design of the separator is most critical for the region of the front part. We need to consider different combinations of target and primary beams to efficiently remove unwanted beams in the localized area, which requires extensive isotope beam generation and optics calculations. In the recent FRIB design, the use of second beam dump has been chosen depending on operation mode. As the magnet arrangement in our separator design becomes more concrete, its configuration is to be inserted in LISE++ to perform more realistic rare isotope beam transport calculation. MOCADI developed at the GSI will be also used.

Structural design of the beam dump has not performed yet. The design principle applied to the beam dump of the FRIB can be shared, but its configuration should be redesigned since the direction of beam bending is different. The wedge is a critical element for

precise beam energy degradation and momentum compaction. We plan to be involved in beam experiments at existing foreign facilities to gain experiences in using high-order beam optics and Monte Carlo simulation codes.

#### **[Reference III.2.5]**

[III.2.5.1] R. Gupta et al.,IEEE Trans. Appl. Supercond., vol. 21, no. 3, pp. 1888-1891, 2011

[III.2.5.2] K. Kusaka et al.,IEEE Trans. Appl. Supercond., vol. 18, no. 2, pp. 240-243, 2008

[III.2.5.3] FRIB Conceptual Design Report

#### **III.2.6 Beam measurement devices**

In order to separate and identify the RI-beam, in which different rare isotope beams produced from in-flight fragmentation are mixed, we need to measure the position, time of flight, energy, energy loss and gamma ray of the isotope beam of interest. The position of the beam is measured using PPAC (parallel plate avalanche counter),TOF using plastic scintillator, beam energy using NaI detector, energy loss using Si-detector or TEGIC(tilted electrodes gas ionization chamber), and gamma ray using Ge-detector. RI-beam produced from the target can be separated using TOF- $\Delta$ E-E method. PPAC can measure the position of the beam with a resolution about 0.5 mm, and Ge-detector is used for the measurement of gamma-ray from the isomer. Each detector is shown in Figs. III.2.6.1 and III.2.6.2.

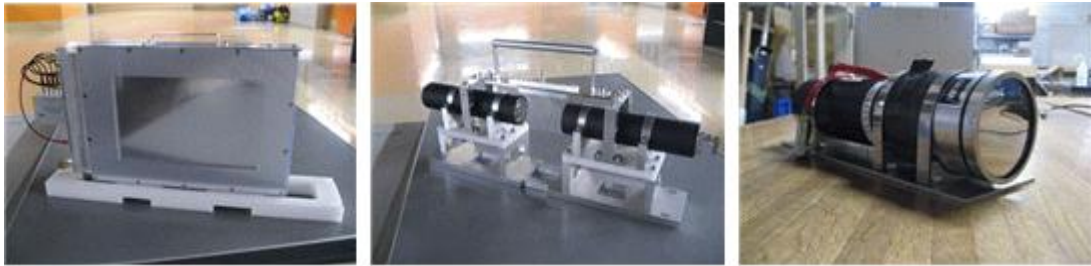


**Figure III.2.6.1 Left: PPAC, Middle: Plastic scintillation detector, Right: NaI detector.**

**(Courtesy of BigRIPS group of RIKEN)**



**Figure III.2.6.2 Left: Si-detector, Middle: TEGIC, Right: Ge-detector.**

**(Courtesy of BigRIPS group of RIKEN)**

The experimental equipments used for the separator is to be identified. LISE++ simulation helps in clarifying the use of some major components to measure the properties of rare isotope beams.

### III.3 Cyclotron

A high-current  $H^-$  cyclotron is to be used as a driver for the ISOL facility. The beam energy is 70 MeV, and the maximum current specified is 1 mA. This beam current has not been achieved yet by  $H^-$  cyclotron. Another request from the user is a pulsed proton beam to produce pulsed neutron beams.

In the previous conceptual study, a combination of compact and separated-sector cyclotron, which is similar to that at the PSI in Switzerland, was proposed. This system should be capable of accelerating the beam current of a few mA and is considered to be more than needed for the ISOL users because a higher power proton beam will be eventually provided by the main superconducting linear accelerator.

Also in the conceptual design, acceleration of deuterons was considered in the beginning. However, the maximum beam current of deuteron beam will be much lower than that of proton beam, and there is a significant advantage in designing a cyclotron, which can accelerate only protons. The option of deuteron beam acceleration was discarded.

#### III.3.1 Specification of the cyclotron

The beam energy of 70 MeV was chosen considering optimal proton energy in producing rare isotope beams, which was carried out by nuclear experimental group. Higher beam energy is somehow limited by the size of cyclotron. A 70 MeV cyclotron weighs around 200 tons, while 100 MeV weighs 400 tons. Much higher cost is expected for the 100 MeV cyclotron.

An important rare isotope beam of interest is  $^{132}\text{Sn}$ , which is a double magic nucleus. The beam energy of 70 MeV is thought to be optimized for the production of the tin isotope as listed in Table III.3.1.1.

**Table III.3.1.1 Fission rate of  $^{132}\text{Sn}$  isotope for 70 kW ISOL system using  $\text{UC}_2$  target**

$p+^{238}\text{U}$	fission rate	Cut-off energy
70 MeV, 1.0mA, 30disk	$1.22 \times 10^{14} /s$	20 MeV

The design and construction of a high-current cyclotron is challenging and takes a long time to develop. A current plan of acquiring the cyclotron is to request commercial vendors to deliver the fully operational cyclotron to the site. If needed, the installation and maintenance can be handled by the RISP staffs upon contractual agreement with cyclotron vendor for necessary technology transfer. A couple of vendors expressed interests in working with us. One of the companies is in fact building a cyclotron for the INFN in Italy with a similar specification for the beam.

Another possibility under consideration is to find a domestic vendor, which has previous experiences in manufacturing cyclotrons preferably related to the 30 MeV cyclotron presently in test operation at Jeong-Up city, Korea (Fig. III.3.1.1). The beam current specified is 300  $\mu\text{A}$ , but is currently below 100  $\mu\text{A}$  when the beam is extracted by a carbon foil. It is expected that the domestic company should possess the manpower capable of designing all aspects of the cyclotron including cyclotron magnet and rf system when it decide to join the bidding with foreign companies having more experiences. Nonetheless, it would be reasonable to consider the involvement of RISP staff to a certain degree.

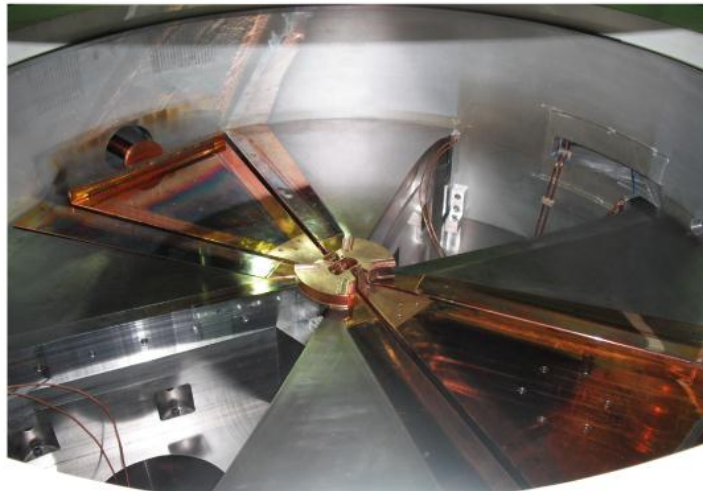


**Figure III.3.1.1 (Left) A 30-MeV cyclotron magnet designed and constructed domestically, (Right) Inner view of the cyclotron vacuum chamber.**

The cost and major cyclotron parameters of the manufacturers that can build a cyclotron of our specification are listed in Table III.3.1.2.

**Table III.3.1.2 Comparison of the cyclotrons of two companies.**

Items	Sumitomo Heavy Industry	Best Cyclotron Systems
Ion species	H <sup>-</sup>	H <sup>-</sup>
Energy	70 MeV fixed	35-70 MeV

Weight	160 tons	195 tons
Max. Beam current	1 mA	0.7-1 mA
RF frequency	75 MHz	58 MHz
Harmonic number	4	4
Power	450 kVA	400 kVA
No. of extraction port	2	2
Delivery	20 months	30-36 months

The beam current of 1 mA may cause a short lifetime on the carbon-foil charge stripper used for beam extraction. This concern has been presented by one of vendors, and will be asked for empirical test results when the vendors submit the specifications of the cyclotron.

### **III.3.2 Injection and distribution beam line**

The injection beam line will be designed to be capable of pulsing the proton beams at certain rates by the combined use of rf buncher and chopper. This requirement can be rather special for commercial vendors as the use of pulsed beam is limited to particular research, which would require R&D efforts to be a deliverable item by the vendor. Thus it could be more suitable to design and construct the pulsed-beam injection line by the RISP staffs.

The cyclotron facility will be mainly used for isotope beam production by the ISOL method. Two target stations are minimally needed considering the alternative use of the target system. Also, there will be a couple of rooms used for beam irradiation study. In addition, a room can be allocated for isotope production for research, and then liquid and gas targets will be needed.

To estimate radiation dose depending on the shielding thickness, MCNPX was used. Dose accumulated for assumed 1 mA·hr was calculated, and the yearly dose rate was used to determine the shielding wall thickness. In addition, dose per hour is to be evaluated to classify radiation areas when the beam is on a target. Some results of MCNPX calculation were compared to the estimation by analytical expression.

### III.4 ISOL system

The Isotope Separation On-Line (ISOL) technique has been used for over 50 years to produce, ionize, mass separate, and study short-lived nuclear isotopes [III.4-1]. The technique refers to a process in which radioactive atoms are produced in a thick target and subsequently extracted from an ion source to form an ion beam. The radioactive atoms are produced via nuclear reactions between an energetic ion beam and the target nuclei. The RIs are extracted from the production target using specific techniques, ionized, pre-accelerated and selected by means of high resolution electromagnetic devices, and then re-accelerated. ISOL-type facilities provide high quality, low energy RI beams.

Figure III.4-1 shows the conceptual design layout of the ISOL system. The basic elements of the ISOL facilities are the driver accelerator, the production target coupled to the ion source, the RF beam cooler, the High Resolution Mass Separator (HRMS), the charge breeder, the beam transport system, and the post-accelerator. According to the experimental requirements, a HRMS is considered as a part of the transport system. Two production target stations are proposed to produce various short-lived rare isotopes; one is for spallation, in which mainly proton-rich isotopes are produced, and the other is a fission target station. Note that a MW target station is planned in a future extension beam line for the production of more intense RIBs. The primary accelerators are a high energy proton (~600 MeV, 660  $\mu$ A) LINAC and a cyclotron proton driver. In the conceptual design, we concentrate on the feasibility study of the 70 kW direct fission target to provide intense, high-quality beams of neutron-rich radioactive nuclei with masses in the range of 80-160 created through uranium fission at a rate of  $10^{14}$  fissions/s. The idea of the high power direct target is an expansion of the facilities at HRIBF-ORNL [III.4.2] and SPES-LNL [III.4.3]. The proposed production mechanism is fission induced by protons in fissile material targets. The fission mechanism has the advantage that neutron-rich radioactive beams can be produced. The rare isotopes produced in the production

target pass through a heated tube to a source, where they are ionized, accelerated off the source high voltage platform, sent through a mass separator to select the ion beam of choice, and injected into a charge breeder. To supply an intense and various RI Beam for users experiments, we proposed three types of ion sources: a surface ionization type ion source for ionization of alkali, alkaline earth, and rare-earth elements, and a FEBIAD type source [III.4.4] for ionization of gaseous and volatile elements. In addition, the possibility to add a laser ionization device is also considered to improve ionization selectivity with the aim of producing high purity exotic beams. For this purpose, an RF-cooler and an HRMS with a resolving power of 45,000 are also planned. To reach the charge state and ion velocity required for injection into the RFQ of the post acceleration system, a charge breeder and high voltage platforms would be required.

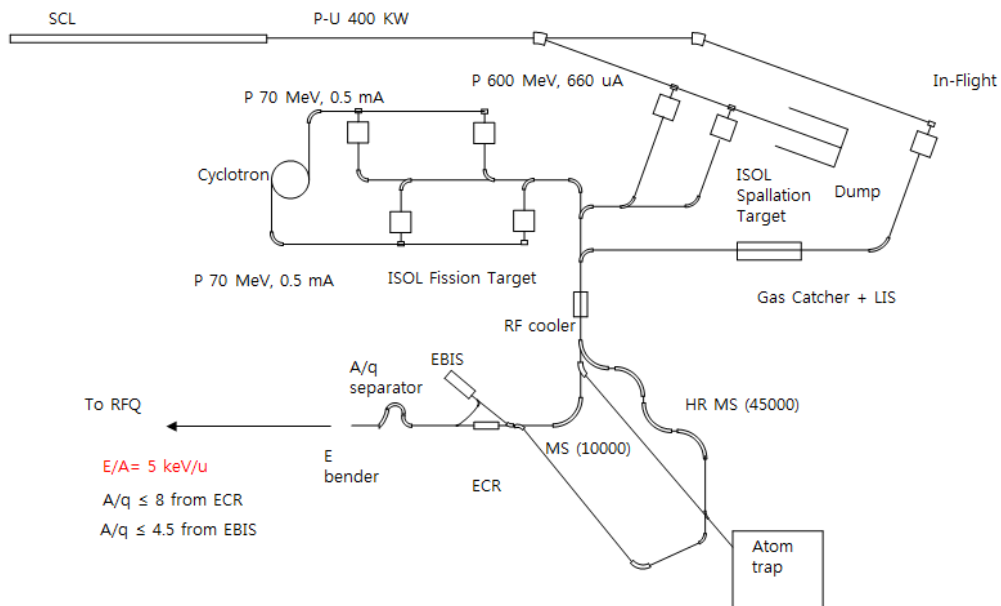


**Fig III.4.1 Conceptual Layout of ISOL Target and RI Beam Transport Line**

**Table III.4.2 Main conceptual design of the RISP ISOL facility**

Fission Target	High power (70 kW) multi-layered fission target		
	Material/ density	UC <sub>x</sub> / 2.5 g/cm <sup>3</sup>	
	Expected fission rate	1.3 x 10 <sup>14</sup> fission/s	
	Expected production rate for <sup>132</sup> Sn	1.9 x 10 <sup>10</sup> /s	
Spallation Target	Target power	400 kW	
	Material (candidate)	BN, C, Al <sub>2</sub> O <sub>3</sub> , HfO <sub>2</sub> , ZrO <sub>2</sub> , LiF, MgO, SiC, CeS, CaO, NiO, Ni, ZnO, GeO <sub>2</sub>	
	Expected RIB	<sup>14</sup> O, <sup>13</sup> N, <sup>10,11</sup> C, <sup>19</sup> Ne, <sup>21</sup> Na, <sup>30</sup> P, <sup>34</sup> Cl, <sup>36,37</sup> K, <sup>58</sup> Cu, <sup>63,64</sup> Ga, <sup>69,70</sup> As	
Ion Source	Automatic attach/detach system of target/IS module		
	Type	SI, FEBIAD, and RILIS	
RF-Cooler	Output emittance	3 π mm mrad	
	Energy spread	< 10 eV	
	Transmission	> 60 %	
HRMS	Resolving power	10,000 and 45,000	
Charge Breeder	ECR	RF frequency	18 GHz
		A/q	Mainly 4-8 up to 8.5
		Transverse output emittance	0.1 π mm mrad (norm)
		E/A	5 keV/u
	EBIS (FRIB EBIT)	Breeding time	~ 50 ms
		Efficiency	~ 40%
		Beam rates	~ 10 <sup>10</sup> /s
		Current density	> 10 <sup>4</sup> A/cm <sup>2</sup>
A/q Charge Separator	Resolving power	3000	
Expected Beam Intensity on Experimental Hall	<sup>132</sup> Sn	~10 <sup>8</sup> /s	
	<sup>142</sup> Xe	~10 <sup>9</sup> /s	

**[Reference III.4]**

[III.4-1] O. Kofoed-Hansen, K.O. Nielsen, Mat. Fys. Medd. Dan.Vid. Selsk. **26**, 1 (1951)

[III.4-2] Annual Science and Technology Review of the Holifield Radioactive Ion Beam Facility (2008)

[III.4-3] F. Gramegna, ACTA PHYSICA POLONICA B, **38**, 4 (2007)

[III.4-4] Akihiko Osa, et al., Nucl. Instrum. Meth. B **266**, 4394 (2008)

### III.4.1 ISOL Target and Ion Source

#### III.4.1.1 Concept of ISOL Target

Utilizing an ISOL system with fission targets has been the most effective way to produce the medium mass neutron-rich RIBs [III.4.1.1.1]. The basic principle of the ISOL method is the use of a light ion beam on a thick target of a high mass material to induce nuclear reactions. Depending on the energy of the primary beam will undergo fission, spallation or fragmentation. The reaction products diffuse out of the target material and are transported via a transfer line into an ion source.

Several institutes are making an effort to produce high intense fission fragments using a uranium target, under uranium carbide ( $UC_x$ ) form. In this report, the proposed target configuration for proton beam energy of 70 MeV and intensity of 1 mA was split into several thin disks in order to increase the total exchange surface for emitting thermal radiation.

The combination of ISOL targets with ion sources is a key element for facilities aiming to produce neutron-rich radioactive ion beams. The highest production of neutron-rich isotopes can be achieved via proton- or neutron-induced fission of  $^{238}\text{U}$  and  $^{232}\text{Th}$ , while proton-rich nuclei are efficiently produced through the spallation process on suitable targets [III.4.1.1-2].

The concept of target configuration has been designed in order to satisfy some main requirements, such as:

- high production of Rare Isotope
- short release times and highly efficient release
- low power deposition for the materials .

The target is maintained at a high temperature (up to 2100 °C), and the RIs diffuse out of the target and are transported to an ion source where the RI beams are formed. A target configuration is chosen, consisting of a proton beam directly impinging on the fission target. The main problem for this configuration concerns the power deposition of the incident beam, due mainly to the electromagnetic interactions. To overcome this problem, only protons with higher  $^{238}\text{U}$  fission cross-sections are exploited. The low energy protons are less efficient production targets because they have lower fission cross-sections and higher stopping power values, as shown in Fig. III.4.1.1.1.

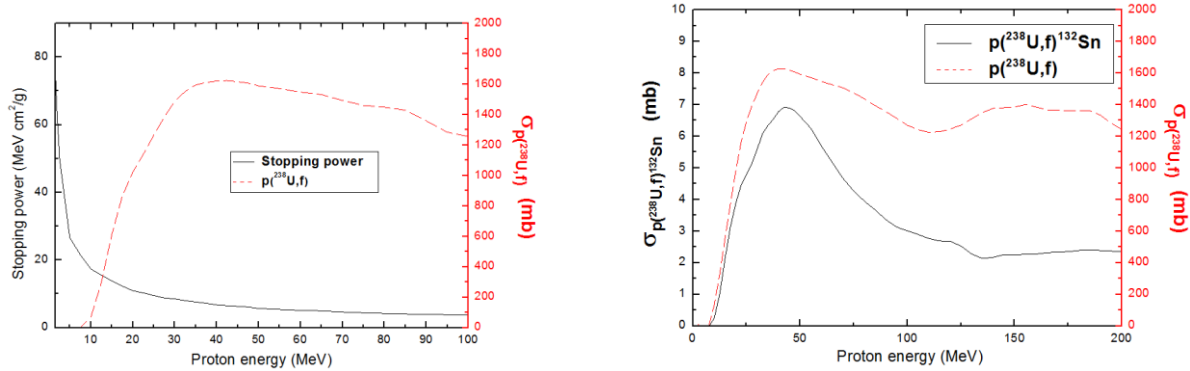


**Fig III.4.1.1.1 (left) Stopping power and fission cross-section for protons on  $\text{UC}_2$ . (right) Proton induced  $^{238}\text{U}$  fission cross section and the  $^{132}\text{Sn}$  production cross section on the proton induced  $^{238}\text{U}$  fission**

Forcing protons with energies lower than about 20 MeV toward a passive dump, the power deposited in the target is lowered considerably, and a large number of fission reactions are maintained. In order to optimize the heat dissipation and release time of the fission products [III.4.1.1.3], a target constituted of porous thin uranium carbide disks is used [III.4.1.1.4]. In this way, the cooling of the target is greatly simplified; in fact, due to the vacuum environment, the heat dissipation is fully entrusted to the thermal radiation, and this mechanism is directly proportional to the body surface. The use of several thin disks increases the total surface and improves cooling.

The requirement of fast release from the target material implies a high operating target temperature. Therefore, the target material must be a high-temperature, low vapor pressure metal or refractory compound in solid, liquid, or powder form. Moreover, the target must exhibit low vapor pressures (below  $10^{-4}$  mbar) at elevated operating temperatures (300 °C – 2500 °C) in order to avoid sublimation or vaporization of the target material at vapor pressures exceeding those required for efficient ionization. Ideally, the radioactive atoms should possess physical and chemical properties almost opposite those of the target; that is, they should be diffused easily from the target material (either in elemental or compound form) and be readily desorbed and vaporized from the target surface. The pressed powder targets using  $UC_x$  grains of 3  $\mu\text{m}$  or smaller size were developed in the Chemical and Material Sciences Facility at ORNL [III.4.1.1-5]. This method can decrease the diffusion times of fission fragments in grains compared with those of  $UC_x$ -coated Reticulated Vitreous Carbon (RVC) fiber targets. This requires that the desired radioactive species are not refractory, and that they do not form refractory compounds within the target material.

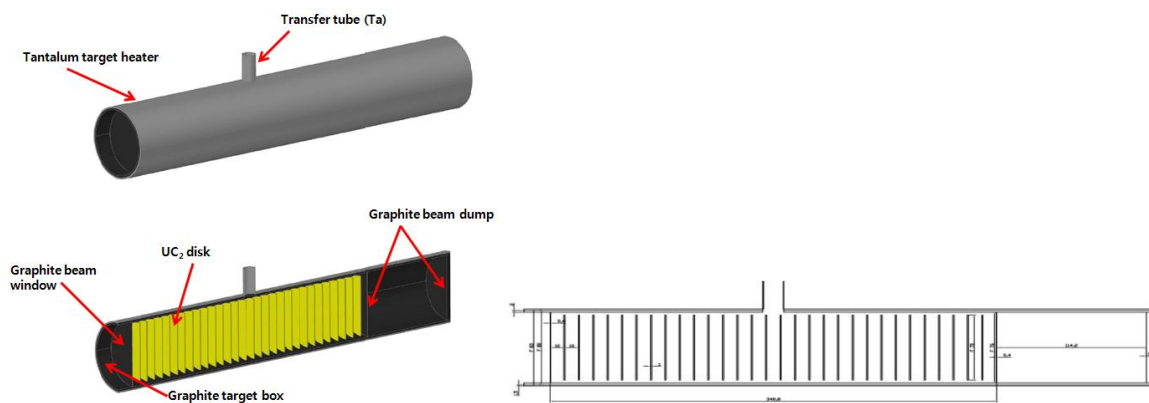


**Fig III.4.1.1.4 Concept of direct target configuration**

All of these considerations lead to the system configuration shown in Fig. III.4.1.1-4 and the following detailed parameters:

- Incident 70 MeV proton beam has a current of 1 mA. The beam profile spans uniformly over a circular distribution with a diameter of 7 cm, matching the disk diameter.
- UC<sub>2</sub> target ( $\rho=2.5$  g/cm<sup>3</sup>), 1-mm-thick 30 disks (289 g of total mass).
- Beam dump and box containing the disks are made of graphite.

The power deposition distribution, the fission rates, and the fission fragment distribution were calculated mainly through a Monte Carlo simulation based on transportation model MCNPX [III.4.1.1.6]. The following results were obtained through several Monte Carlo calculations performed for the target configuration described in the previous section. A power of 0.64 kW was deposited in the window, 36.72 kW in the thirty UC<sub>x</sub> disks, and 34.39 kW into the dump and graphite box (due to proton scattering). Thus, the average power deposition for the UC<sub>2</sub> target disks was about 1.22 kW/disk. With 1 mA, the power deposition per unit volume in the UC<sub>2</sub> target disks was 33.3 W/cm<sup>3</sup>. Figure III.4.1.1.5 shows the radial profile of the power deposition in the disks. As expected, the radial profile was uniform in the window (following the entering uniform beam profile), and it became less and less flattened in the last disks because of the proton scattering.

The fission target/ion source chamber is designed in such a way that it can be removed for servicing or storage. Since the target can be used several times, it will be stored into a container with thick lead walls while not in use. The handling system must be designed to transport such a heavy container into the area where the target will be used, to open the container, and to connect the source chamber to the injector. After the experiment, the source chamber must be first removed from the injector, then stored in the container, and finally sent out of the hot area for further handling and long term storage. One note that the 70 kW high power target are planning to design under the assumption of  $\Phi$  7 cm uniform beam from cyclotron driver. However if the driver cyclotron have 2 beam

port of 0.5 mA, it is difficult to get a 1 mA uniform beam. In this case we have another option that is two 35 kW high power as an alternative of 70 kW target.

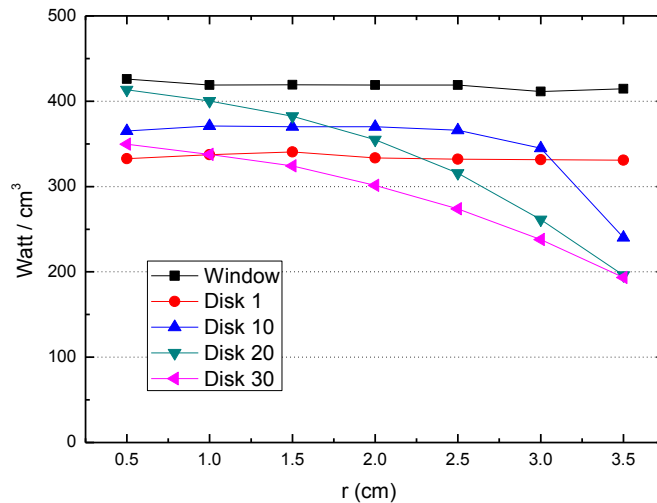


**Fig III.4.1.1.5 Radial distribution of the power deposition in the disks**

**[Reference III.4.1.1]**

[III.4.1.1.1] C. M. Folden III, A. M. Amthor, T. N. Ginter et al, Fission and properties of neutron-rich nuclei: proceedings of the fourth International Conference, Sanibel Island, USA (2007)

[III.4.1.1.2] H.L. Ravn et al., Nucl. Instrum. Meth. B, **88**, 441 (1994)

[III.4.1.1.3] M.Re et al. RNB7 conference proceedings, Cortina, Italy (2006)

[III.4.1.1.4] A. Andrighetto, S. Cevolani, C. Petrovich, Eur. Phys. J. A **25**, 41 (2005)

[III.4.1.1.5] Annual Science and Technology Review of the Holifield Radioactive Ion Beam Facility (2008)

[III.4.1.1.6] D. B. Pelowitz, MCNPXTM User's manual, Version 2.5.0, LA-CP-05-0369 (2005)

### III.4.1.2 Ion Source

The ion source cannot be considered as a stand-alone device but as a part of the complete front end of an ISOL system in which the target is integrated with the source itself. Careful attention must be paid to the selection of the most appropriate ion source for efficient ionization and selection of the species delivered to the ionization chamber of the source. Ion sources dedicated to the production of RI beams have to be highly efficient, selective (to reduce the isobar contamination), and fast (to limit the decay losses of short-lived isotopes). For radioactive beam generation, the source must operate steadily for extended periods of time at elevated temperatures (up to 2000°C). The selection of the most appropriate target/ion source is of paramount importance since its performance determines the intensity, the beam quality, and the number of radioactive beams that can be provided for experimental use. RI beam facilities worldwide utilize a variety of solutions to meet part or all of these requirements, such as surface, plasma, electron cyclotron resonances and laser ion sources [III.4.1.2.1]. Figure III.4.1.2.1 presents a figure of merit of the  $1^+$  ion sources for RIB as a function of the ionization potentials.

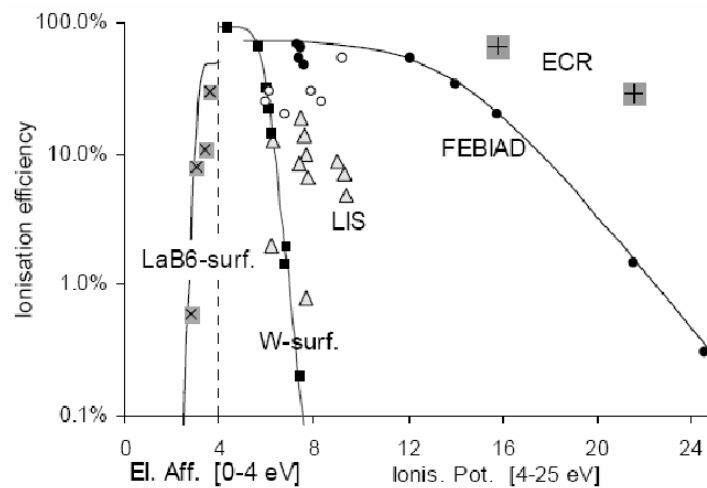


Fig III.4.1.2.1  $1^+$  Ionization efficiencies measured with surface (black squares), plasma-FEBIAD (circles), laser (triangles), and ECR ion sources.

For RI beam generation, the source should ideally exhibit the following properties:

- high ionization efficiency and chemical selectivity
- high temperature operation and flexibility for adaptation to different temperature ranges and modes of operation
- low energy spreads
- stable electrical and mechanical properties

The source should also be designed for safe and practical insertion/removal from the ISOL facility in order to permit changing of the target material and source repairs. We consider three kinds of ion sources for the direct target: the Surface Ion Source, the Forced Electron Beam-Induced Arc Discharge (FEBIAD), and the Resonant Ionization Laser Ion Source (RILIS). All three sources are used at ISOLDE and constitute a good reference point for further RISP goals regarding ion source development.

#### **[Reference III.4.1.2]**

[III.4.1.2.1] J. Lettry, Proceedings of the 1999 Particle Accelerator Conference, New York (1999).

#### **III.4.1.3 Concept of Target Area**

Because the facility will handle radioactive species, special care is devoted to radiation protection safety, and several systems are added to prevent radiation hazards. Highly radioactive areas like the target/IS bunker are ventilated using a nuclear ventilation system. The control system will use a homogeneous architecture to integrate the many subsystems necessary to operate the facility, ranging from the accelerator control to the

radiation and safety survey. Figure III.4.1.3.1 shows the proposed ISOL target area, composed of a two-target room (Operation room, Preparation room) for one primary beam port, a handling zone, and a services zone. The ISOL target room would be located in front of the handling zone and would be surrounded by massive shielding blocks. To simplify the handling and service of target components, the beam extraction lines are aimed in the same direction. The facility will require a target crane and a high-bay crane above the target gallery for assembly and replacement of the large components in the area. An automatic control system is required to minimize downtime during maintenance operations and waste disposal.

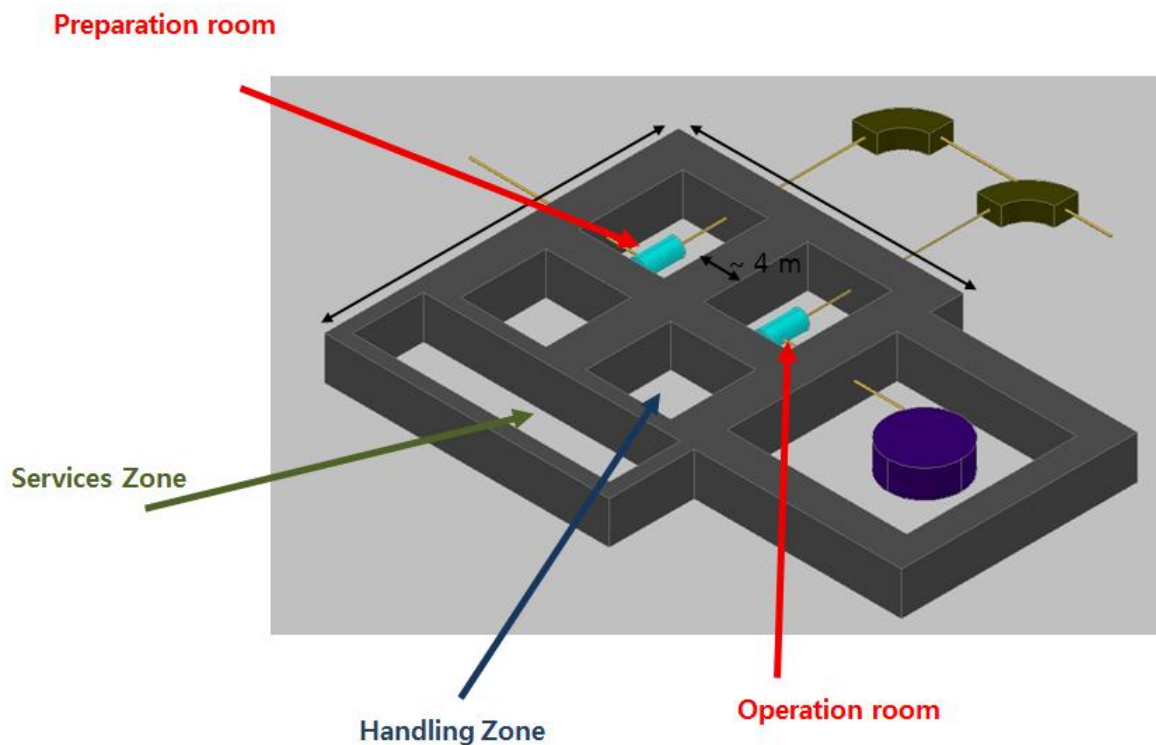


Fig III.4.1.3.1 3-D view of the proposed ISOL target area configuration

### III.4.2 ISOL RI Beam Transport System

The ISOL beam transport system will manage the radioactive beam from the output of the ionization source to the low-energy experimental area and to the post-accelerator complex. At the ion source exit (located on a high voltage platform), the beam has charge state  $1^+$  and energy of 30-40 keV due to the extraction voltage. One of the main problems of operating an ISOL facility is the beam purification, because the extracted species are transported according to their  $A/q$  value. To improve the isotope selection, three mass separators with different mass resolving powers will be implemented along the transport line. The first separation stage is the pre-mass separator with a resolving power of 100. The second and main purification stage is the High Resolution Mass Separator (HRMS), which has a resolving power of about 10,000, 45,000. The last separator will be installed after the charge breeder to avoid contamination of the selected beam by the stable contaminants introduced by the charge breeder itself. Due to the low rigidity of the beam, electrostatic quadrupoles can be used to focus and transport the beam. This guarantees reliable beam handling and a simple procedure to configure the beam transport line. The electrostatic devices scale with the voltage of the source and are independent of the ion beam charge. Thus, the optic of the beam line inside the production platform does not need further adjustment after configuration if the source is operated at a fixed voltage. Also, the beam transport along the beam lines outside of the platform can be achieved by an electrostatic lens. As in other facilities, we plan to install an RF-cooler device as a beam cooler. The details and advantages of this device are described later.

In recent year, A KEK on-line isotope facility of a TRIAC facility, was transferred to KAERI in Korea except for Target and ion source. This ISOL facility was used for production and separation of rare isotope using UCx target and can accelerate the isotopes up to 1.1 A MeV. The facility which is being installed will be used for the developments of ISOL

target/ion source and ISOL RI beam transport system, a performance test of detection system, and so on.

**RF-Cooler** : To improve the performance of the high-resolution mass separator, an RF-cooler will be installed to reduce the incoming beam emittance before separation. An RF-cooler offers reduced transverse emittance, energy spread, and beam-bunching capability for a wide range of masses on a time scale ( $< \text{ms}$ ) appropriate for radioactive ion beams. The RF-cooler depends on the emittance of the target/ion source used; the resulting emittance is typically a factor of 10 or better. In this cooler, the beam emittance is reduced, sending the beam with a low energy ( $E < 100 \text{ eV}$ ) through a gas damping, which removes the transversal component of the velocity. In other words, the beam temperature is cooled by the interactions with a cold gas. This step is necessary to reduce the beam speed and thus increase the time of interaction. This is accomplished by placing the device on an insulated platform with a proper voltaged. This solution allows for energy recovery after the cooling process. The deceleration and mainly the reacceleration optics have to be well designed to preserve the beam emittance. An RF quadrupole filter is used to prevent beam particle diffusion through the gas during the interaction process. The quadrupole filters were developed for an ion trap and consist of a set of four electrodes. Each pair of opposing electrodes is connected and driven by a RF voltage with a polarity opposite that of the other electrode pair. According to the existing device, the space necessary to allocate this RF-cooler is about 1-1.5 m. The beam optics designed to transport the beam from the RF-cooler, through the HV platform and to the HRMS have to be thoroughly studied to avoid deterioration of the beam emittance.

**Table III.4.2.1 Requirement of RF-cooler design**

Input Beam	continuous 30–60 keV beam
Transmission	> 60 %
Output Beam Qualities	3 $\pi$ -mm-mrad at 40 keV extraction energy
Energy spread	< 10 eV

**HRMS (High Resolution Mass separator):** In an ISOL-type facility, the nuclides of interest are produced in conjunction with a whole range of neighboring isotopes in a production target that is bombarded by a proton or light ion beam. The closest ion species are separated in mass according to the difference in binding energy between isobars of the same mass number. Moreover, for any production scheme of radioactive ion beams, the wanted species are produced with rates that are usually many orders of magnitude lower than the unwanted, more stable species. Therefore, an efficient separation method has to be used to deliver an isotopically pure beam to the experimental areas. The mass separator performance specification is determined by the beam quality, the mass range of interest, and the desired transmission. The required performance is noted by the mass difference along isobaric lines and the relative abundances of the various isobars. The mass resolution is the minimum relative mass difference  $\delta m/m$  that can be resolved with a given system, and the mass resolving power is the reciprocal of the resolution.

Three distinct goals of the separator system are:

1. Eliminate most of the radioactivity to avoid activation in the downstream transport or accelerator.

2. Eliminate the stable contaminants produced in the source system (stable isobars, isotopes with the same mass-to-charge ratio, and molecules), which can outnumber the desired radioactive ion beam by several orders of magnitude.
3. Separate all radioactive ion species.

The first goal is achieved by incorporating a low-resolution pre-separator magnet just downstream of the target/source. A resolving power of only  $\sim 100$  is sufficient to remove most of the radioactivity at the image slit of the pre-separator. For light ions, the elimination of most of the contaminants requires a resolving power in the range of 1,000–2,000, although in some particular cases, a resolving power of 20,000 may be needed. The selectivity of the source system could help to suppress these specific elements. Also, the use of experimental techniques to reject some unwanted components may allow for some relaxation in the separation requirements, resulting in better transmission and reduced tuning time. In general, the mass difference between isobars is smaller for heavier ions, and a mass-resolving power of 10,000 or more would be sufficient in many cases. The beam quality is important in determining the resolving power of a certain magnetic system. The resolving power is given by the ratio of the magnet dispersion to the beam width at the focal point ( $R_m = D_m/x$ ). Thus, beam emittance is an important criterion that affects the achievable spot size for a given tune. For example, the use of an RF-cooler to significantly reduce the emittance of the beam entering a mass-separator system can significantly improve the resolving power.

The proposed configuration is shown in Fig. III.4.2.1. Each of two-target source units has a pre-separator with a resolving power of 100. After separation, the beams are directed to the HRMS, which would have a resolution of 45,000 and be equipped with an RF-cooler to reduce the emittance of the beam before separation. Presently, there are a few isobaric separators planned or already constructed in some European and U.S. laboratories. However high technologies are required for development of the 45,000 and

long times are needed. For reduce the risk of 45,000 HRMS we are planning to develop 10,000 HRMS which have a capability of isotope selectivity with a laser ion source.

Figure III.4.2.1 shows the conceptual design of 45,000 HRMS (High Resolution Mass Separator) and it consist of 4 dipole magnets and 12 quadrupole magnets and total length is about 38 m. The dipole magnet has deflection angle of 90 degree and central trajectory radius of 2 m. The quadrupole magnet has effective length of 20.0 cm and half aperture of 4.0 cm.

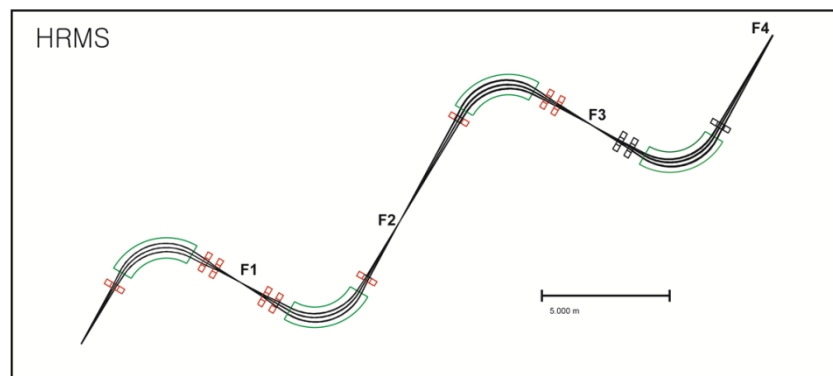


**Fig III.4.2.1 Schematic view of HRMS**

The HRMS have four focus points from F1 to F4. Figure III.4.2.2 shows the result of beam envelope. Upper and lower panel indicate beam envelope in horizontal and vertical, respectively. The absolute value of dispersion at each focus points are 5.6, 19.2, 22.8, 29.4 cm/%. Figure III.4.2-3 shows the result of separation for momentum difference of  $1/80000$  at each focus points. As show in Figure 3, the tail in low momentum side increase with increase in dispersion. In order to collect the tail, the higher component of magnet is under consideration.

The mass resolving power from present calculation is about 55000 at F4. For all calculation and simulation using TRANSPORT and TURTLE program, the initial beam emittance is  $3 \pi$  mm mrad.

The present results indicate possibility of high resolution mass separator with  $R_M > 45000$ . However, the results by COSY infinity or GICOSY disagree with the present results. The reason for the discrepancy is not yet understood. It will take firm steps to clarify the cause. The other hand, the present results indicate the requirement specification of RF-cooler. The beam emittance after RF-cooler has got to be below  $3 \pi$  mm mrad.

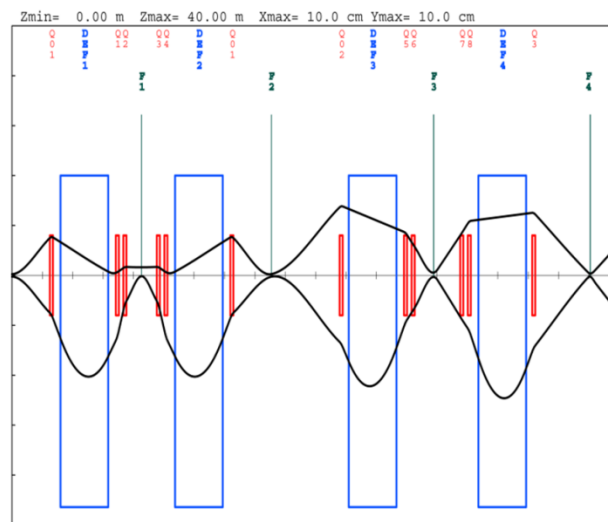


**Fig III.4.2.2 Beam Envelope in horizontal and vertical direction using TRANSPORT program**

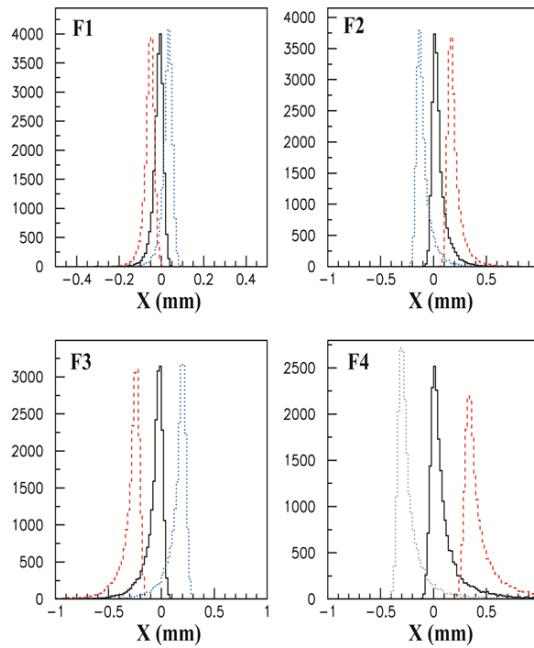


**Fig III.4.2.3 Results of separation at each focus points using TURTLE program. Each peak is with momentum difference of 1/80000**

### III.4.3 Yield estimation

Extensive calculations of radioisotope production rates have been performed using Monte-Carlo code MCNPX. The proton fission cross-section is obtained from the experimental data and the ETFSI fission model calculations [III.4.3.1]. The target is designed to reach a fission rate greater than  $10^{14}$  fission/s, which represents a challenging amount. A crucial point of the final beam current is linked to the short-lived RIs produced in the target: the target ion source system has to be manufactured considering the properties related to the release and efficiency of the system. The important step for creation of a RI beam is the overall efficiency of the target-source system plus the efficiency linked to the post-accelerator configuration; the evaluation of the intensity of some RI beam species is of interest to the nuclear physics community and has been performed and validated through the existing experimental data. The production yields in the present design of the facility are presented with the evaluation

of the final beam current on the target. The intensity  $I$  of an exotic beam available for an experiment is determined by the following factors:

$$I = \Phi \cdot N \cdot \sigma \cdot \epsilon_r \cdot \epsilon_i \cdot \epsilon_c \cdot \epsilon_s \cdot \epsilon_{cb} \cdot \epsilon_t \cdot \epsilon_p$$

$\sigma$ : the cross-section of the production reaction,

$\Phi$ : the primary beam intensity,

$N$ : the thickness of the production target,

$\epsilon_r$ : the efficiencies of release of the target and transfer,

$\epsilon_i$ : the efficiency of the ion source,

$\epsilon_c$ : the efficiency of the RF-cooler,

$\epsilon_s$ : the efficiency of the separator,

$\epsilon_{cb}$ : the efficiency of the charge breeder,

$\epsilon_t$ : the delay transfer efficiency due to radioactive decay losses,

$\epsilon_p$ : the efficiency of the post-accelerator.

The final RI beam current depends on the efficiencies of several chemical physical processes and beam transport elements. For ISOL facilities, the total efficiency is highly case-dependent and lies between  $10^{-2}$  and  $10^{-6}$ . To evaluate the final beam, the exotic species must be followed along their paths. The exotic species are produced inside the target as neutral atoms and are extracted in a gas phase due to the high operating temperature of the target (2000°C). This process is governed by the release efficiency; that is, those of the diffusion processes in the uranium carbide grains, the effusion in the container, and the injection in the ion source. As soon as the atoms are in the ion source, they should be ionized  $1^+$  to be extracted and injected into the transport system. This

process is controlled by the source ionization efficiency. For an efficient reacceleration, it is necessary to increase the charge states of the ions.

This increase is achieved by the charge breeder. Finally, we must consider the overall efficiency of the transport and post-accelerator system. All of these parameters strongly affect the final current, but the target efficiency itself is complicated. The diffusion in the material is a complicated and unknown phenomenon, especially when the material is at high temperature; it strictly depends on the material structure and the temperature at which the material is maintained [III.4.3.2]. The calculated fission rate in all 30 disks approached  $1.3 \times 10^{14}$  fissions/s. The isotope in-target production reached values up to  $\sim 10^{12}$  atoms/s (see Figure III.4.3-1). The  $^{132}\text{Sn}$  isotope is a double-magic nucleus and is thus one of the radioactive nuclei of interest. Its production was here estimated to be  $\sim 10^{10}$  pps on. A more general view of the in-target yields is given in Figure III.4.3-2. The overall efficiency is defined as the product of the efficiency of release from the target, the decay losses, and the efficiency of transport to and ionization in the ion source. This overall efficiency depends critically on the detailed design of the production target, the chemistries of the extracted activities, and the ion source design. The efficiencies of these three processes are more important in determining the resulting secondary beam intensities than they are for determination of the primary intensity and the formation cross-section, which determine only the production rate of the target. The expected beam intensities in a uranium target are evaluated and shown in Table III.4.3.1, taking into account the efficiencies experimentally obtained from other studies [III.4.3.3, III.4.3.4].

Estimates of RI beam intensities also have to consider the transmission associated with the RF-cooler, the mass separation, charge breeding, and the secondary beam acceleration. In cases of high selectivity in the ion source, as for alkalis and noble gases, isobar separation is not required, so the mass separation can be performed with low resolution and high transmission. For cases with minor selectivity in the ion source, the

high resolution isobar separator has to be used, and the transmission may drop down to 50–80% depending on the output emittance of the ion source. In addition, the efficiencies of charge breeding and acceleration have to be considered. No charge breeding is required for  $1^+$  beams delivered to the trap experiments at ion source energy, so these intensities are the highest. Injecting higher charge states into the secondary accelerator may maximize the acceleration efficiency. High charge–states can be obtained using direct ionization or charge breeding in an EBIS or a ECRIS used as a charge-state amplifier by capturing a beam of singly-charged ions in its plasma. Considering the overall efficiency, yields of Tin isotope are estimated to be shown table III.4.3.2. One can see that the yields are comparable to the estimation of SPIRAL2 and all projects are now underway except for REX-ISOLDE.

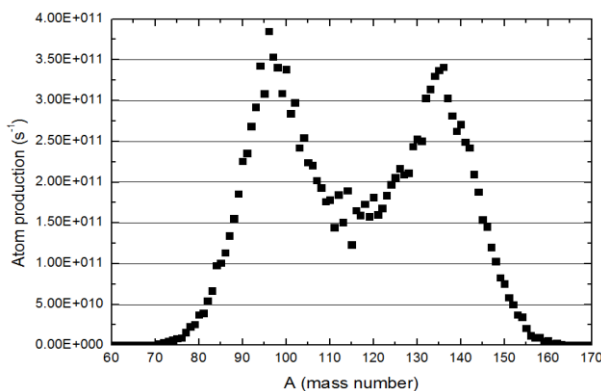


Fig III.4.3.1 Fission mass spectra yields

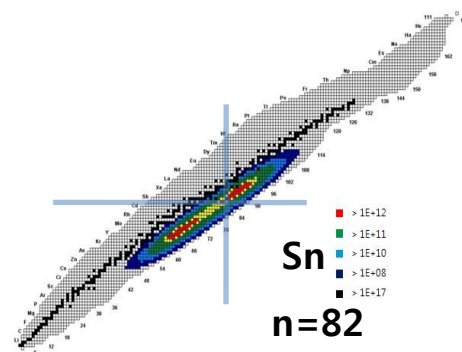


Fig III.4.3.2. Isotope production yield in the direct target via reaction of  $^{238}\text{U}(p,f)$ .

**Table III.4.3.1. Intensities calculated considering release, ionization, and acceleration efficiencies for different isotopes**

Isotope	Half-life	Yield of production target (pps)	Overall eff. (%)	Expected beam on the experimental target (pps)
<sup>78</sup> Zn	1.5 s	2.19 x 10 <sup>10</sup>	0.04	1 x 10 <sup>7</sup>
<sup>90</sup> Kr	32 s	1.99 x 10 <sup>12</sup>	1.00	2 x 10 <sup>10</sup>
<sup>94</sup> Kr	0.2 s	1.29 x 10 <sup>11</sup>	0.51	7 x 10 <sup>8</sup>
<sup>97</sup> Rb	170 ms	1.02 x 10 <sup>11</sup>	0.88	9 x 10 <sup>8</sup>
<sup>124</sup> Cd	1.24 s	4.98 x 10 <sup>11</sup>	0.02	1 x 10 <sup>8</sup>
<sup>132</sup> Sn	40 s	1.95 x 10 <sup>10</sup>	0.45	8 x 10 <sup>7</sup>
<sup>133</sup> In	180 ms	3.75 x 10 <sup>7</sup>	0.18	7 x 10 <sup>4</sup>
<sup>142</sup> Xe	1.22 s	2.84 x 10 <sup>10</sup>	2.08	6 x 10 <sup>8</sup>
<sup>144</sup> Cs	1.01 s	6.01 x 10 <sup>10</sup>	0.12	7 x 10 <sup>7</sup>

	Primary Beam	Power on target (kW)	Fission/s	<sup>132</sup> Sn rate (pps) @ Exp. Hall
KEK TRIAC	p 30 MeV, 3 $\mu$ A	0.09	10 <sup>11</sup>	3·10 <sup>5</sup>
ORNL HRIBF	p 40 MeV, 10 $\mu$ A	0.4	4·10 <sup>11</sup>	2·10 <sup>5</sup>
ORNL HRIBF up-grade	p 54 MeV, 20 $\mu$ A	1.8	10 <sup>12</sup>	5·10 <sup>5</sup>
CERN ISOLDE	P 1-1.4 GeV	3	4·10 <sup>12</sup>	10 <sup>7</sup> 5·10 <sup>8</sup> (1.4 GeV, 2.5 $\mu$ A, converter)
LNL SPES	p 40 MeV, 200 $\mu$ A	8	10 <sup>13</sup>	??
<b>RISP</b>	<b>p 70 MeV, 1 mA</b>	<b>70</b>	<b>10<sup>14</sup></b>	<b>~ 10<sup>8</sup></b>
GANIL SPIRAL2	d 40 MeV, 5 mA	200 (Convert.)	10 <sup>14</sup>	2·10 <sup>9</sup>

**Table III.4.3.2 Expectation yield of Sn Isotope at low energy experimental hall**

**[Reference III.4.3]**

[III.4.3.1] A. Mamdouh, J.M. Pearson, M. Rayet, E Tondeur, Nucl. Physics A, **644**, 389 (1998)

[III.4.3.2] J. Crank, The Mathematics of Diffusion, Clarendon Press (1956).

[III.4.3.3] H.L. Ravn et al., Nucl. Instrum. Meth. B, **88**, 441 (1994)

[III.4.3.4] B. Fogelberg et al., Nucl. Instrum. Meth. B, **70**, 137 (1992)

## III.5 ISOL Post Accelerator

### III.5.1 Charge Breeder

Charge breeder, which transforms externally injected ions with a charge state  $1+$  to a higher charge states  $n+$ , is necessary for multiplying the charge state of extracted rare isotopes (RI) from the ISOL target-ion source units for the efficient acceleration at the next stage. A charge breeder has to be capable of getting a high efficiency for the charge state breeding process in a short time compared to the half-life of the interest exotic nuclei. In addition, the higher intensities of RI beams up to  $10^{12}$  ions/s with a low level of background contaminants have to be handled by the charge breeder. In order to cover the various experiments planned in RISP, output beam should be in the charge state,  $+12$  to  $+25$  with  $Q/A > 1/9$ , and its emittance should be less  $0.35$  mm-mrad (normalized, 90 %) from singly charged various species ( $A = 80 \sim 160$ ) input beam.

The two types of breeders, electron beam ion source (EBIS) and electron cyclotron resonance (ECR) ion source, have distinct characteristic features. The advantages that make the EBIS attractive are a low level of background contaminants, fast charge breeding time and low  $A/Q$ . Many facilities including EURISOL, FRIB at MSU and BNL employed the EBIS system for their charge-breeding device. The weaknesses of the EBIS are the limited RI beam acceptance, system complexity, short cathode lifetime, and traits of pulsed mode operation. The limitation on RI beam acceptance can be overcome by increasing the electron beam current and density while at the same time shortening the required breeding times.

An EBIS can be used to produce high intensity of RI beams, and is an excellent choice for injection into a re-accelerator for ISOL Linac because the length of ISOL Linac is shorter than Drive Linac. An EBIS relies on a beam of electrons that collide with trapped ions, resulting in the stepwise ionization and production of highly charged ions. As the rate of

these collisions can be increased by creating a high density of electrons, the beam is compressed using a strong magnetic field. The total charge of ions extracted per pulse is proportional to the number of electrons in the trap. The maximum intensity of ion beams for ECR charge breeder will not exceed  $10^7$  per second. A charge breeder based on an EBIS will be up to  $10^9 \sim 10^{11}$  per second [1]. For the EBIS of BNL, it shows that intensity of  $\text{Au}^{32+}$  and  $\text{Fe}^{20+}$  are several times of  $10^9$  per second [2].

An EBIS composes an electron gun which generates electron beam, drift tube, and super-conducting solenoid, which traps electrons and ion beam, vacuum system and collector system. Because the intensity of ions is directly current of electrons times trap length, the EBIS is designed high current electron gun and long trap length. Avoiding background current, the chamber of EBIS is operation at Ultra High Vacuum (UHV). In order to offer UHV and long life time, a cathode of electron gun must to use dispenser cathode. High current and a very small diameter of electron beam leads to a low emittance of the extracted RI beam. The electron gun is required to have high compression ratio and this can be achieved by using super-conducting solenoid. The injected RI beams are radially trapped by space charge of an intense electron beam and then ionized by these electrons impact.

Ion accumulation process in EBIS is single and double ionization and charge exchange processes, radiative recombination, charge exchange between ions and neutral atoms, electron capture by a higher charged ion from a lower charged one, ion heating by electrons and ion escape from the trap. In order to increase breeding efficiency, A dedicated EBIS for charge breeding process has to be studied [3], [4].

A charge state breeder with the EBIS system was already carried out at several other facilities. The design parameters of the EBIS proceeded at other facilities are listed in Table III.5.1.1.

**Table III.5.1.1 Design parameters of EBIS at other facilities**

Parameter	CARIBU	BNL T-EBIS	REXEBIS
B field in trap	6 T	5 T	2 T
Electron beam current	2 A	10 A	460 mA
Current density inside trap	500 A/cm <sup>2</sup>	575 A/cm <sup>2</sup>	200 A/cm <sup>2</sup>
Cathode material	IrCe, CeB <sub>6</sub> , LaB <sub>6</sub>	IrCe, LaB <sub>6</sub>	LaB <sub>6</sub>
Beam Energy	10 keV	20 keV	6 keV

For the ECR charge breeder, the advantages are its ability to accept high fluxes of the incoming RI beams and minimized maintenance. The ECR charge breeder can also operate in CW or pulsed mode. The negative of the ECR charge breeder is the stable background produced by the source about nA range. The operating pressure of ECR charge breed affects significantly on the breeding efficiency. Multiple frequency operation helps the breeding efficiency as well as an improvement in the peak charge state with stable beam current. Relatively high level of background can be reduced by using high purity materials, sand blasting, and high pressure rinsing. Table III.5.1.1 shows the comparison of typical EBIS and ECRIS for charge breeder.

**Table III.5.1.2 Comparison of typical EBIS and ECRCB**

	REX-EBIS	JAERI-ISOL (ECRCB)
Efficiency	4~15 %	2~15 % - Broader charge state distribution
Breeding Time	13~500 ms	100~300 ms
A/Q	2~4.5	4~8
A	No real limitation	Injection difficult A < 40
Mode	Pulsed	CW or Pulsed
I <sub>max</sub>	A few nA	> 10 A
Acceptance	11 mm-mrad at 60 keV	> 55 mm-mrad at 18 keV

Emittance	15-20 mm-mrad at 20 keV	10 mm-mrad at 20 keV
Background	< 0.1 pA	< 1 nA
Reliability	Overall system complex	Robust and simple
Frequency		2.45 + 12 GHz

Both systems have complementary characteristics to each other as shown before. The ECR type is suited for producing high intensity RI beams while EBIS system is good for short lifetime isotopes and high purity RI beams. Using an existing 1+ to n+ scheme with both an ECR and an EBIS as a charge breeders will work up to what have been achieved in other labs worldwide. However, efficiency is everything in the production of RI beams. It would be nice to explore a 1+ to n+ scheme by finding a radiation-resistant magnet to construct an ECR ion source that can be located very close to the production target to product the n+ ions from the target neutrals with better efficiency. Again not all these options are required at the beginning but careful planning of the production area layout to account for future upgrade options is required. A ECR charge breeder based on the KAERI 14 GHz ECR ion source and KBSI 28 GHz ECR ion source may also be a good start to get the program started. The final decision on the charge breeder for RISP-ISOL will be taken according to the final evaluation of the facility layout, taking into account budget, performances and construction schedule.

**[Reference III.5.1]**

[III.5.1.1] P. Ostroumov et al., 2010 IOP Publishing Ltd and SISSA

[[III.5.1.2] J. Alessi et al., Proceedings of the 2003 Particle Accelerator Conference 89(2003)

[[III.5.1.3] S. Schwarz, G. Bollen et al., Nuclear Instruments and Methods in Physics Research B 266 (2008) 4466

[[III.5.1-4] I V Kalagin et al., Plasma Sources Sci. Technol. 7 (1998) 441

### **III.5.2 LEBT, RFQ, MEBT**

#### **III.5.2.1 LEBT**

The LEBT consists of solenoids and quadrupoles to provide transverse focusing for the rare-isotope beams from the charge breeder. To get a small longitudinal emittance, a buncher with 81.25 MHz is used at the entrance of RFQ. The location and the voltages for the buncher is optimized to match the beam longitudinally with RFQ and to obtain the high capture rate. The LEBT was optimized by the beams with the energy of 10 keV/u and a  $q/A$  of 0.2. The beam has a normalized rms transverse emittance of 0.2  $\pi$  mm-mrad and an energy spread of 0.2%. The beam is bunched and matched into a RFQ. Transverse emittance growth in the LEBT is not observed.

#### **III.5.2.2 RFQ**

Due to higher  $q/A$  of the beams from the charge breeder, the RFQ can accelerate the beam to higher energy of 300 keV/u compared to drive-accelerator and can result in improvement of performance in beam dynamics of the re-accelerator linac. As the beams are bunched at a buncher, RFQ can achieve higher acceleration efficiency. The growth of the transverse emittance in RFQ is small. As the energy spread can an impact on the longitudinal emittance from RFQ, it is important to achieve a small energy spread from the charge breeder.

#### **III.5.2.3 MEBT**

Same MEBT layout as the drive-linac will be used.

### **III.5.3 ISOL Superconducting Linac**

The ISOL post-accelerator is also a superconducting linac. As for the ISOL post-accelerator lattice choice, we are planning to share the same doublet lattice as the driver SC Linac to minimize types of accelerator components to reduce cost and R&D efforts. Cavities of the same types and betas will be used as well as the same type of cryomodules.

## Chapter IV Experimental Apparatus

### IV.1 KRS (Korea Recoil spectrometer)

As a main facility for studying nuclear structure, nuclear astrophysics, and super heavy elements search with low energy stable and radioactive ion beams, the Korea Recoil Spectrometer (KRS) has been proposed. The main purposes of the KRS facility can be summarized as follows:

- Direct measurement of the  $(p,\gamma)$  and  $(\alpha,\gamma)$  reactions of several pico( $10^{-12}$ )-barn cross sections with high background suppression and high detection efficiency (RMS mode);
- Production of exotic or more exotic beam through a certain reaction, which can be used to study more unstable nuclei existing near the drip line (IRIS mode);
- Search for super heavy elements ( $Z>116$ ) can be studied via hot fusion reactions ( $^{244}\text{Pu} + ^{58}\text{Fe} \rightarrow ^{299}\mathbf{120} + 3n$ ,  $^{238}\text{U} + ^{64}\text{Ni} \rightarrow ^{299}\mathbf{120} + 3n$ ) with high intense stable ion beams from SCL seg1 and ISOL post accelerator (SHE mode). For this purpose, KRS should have large angular acceptance to measure more dissipative reactions;

To perform such experiments, the facility satisfies the following requirements:

Parameters	RMS mode	IRIS mode
Maximum magnetic rigidity (Tm)	1.5	~1.5
Mass resolution ( $\Delta M/M$ )	~0.1 %	~0.5 %
Momentum resolution ( $\Delta p/p$ )	~0.05 %	~0.05 %
Angular acceptance	$\pm 70$ mrad	$\pm 100$ mrad
Background reduction	$< 10^{-12}$	N/A

The included detection system should be capable of beam tracking and particle and gamma ray detection.

- **Beam transport system**

- Two variable modes: Recoil mass separator (RMS), In-flight Radioactive Ion-beam Separator (IRIS).

- Two stages with six focal planes (F0 ~ F6): the end stage (F6) is movable, F1 and F5 are dispersive, and F0, F2, F3, and F4 are doubly achromatic

- Removable slit systems located at each focal point

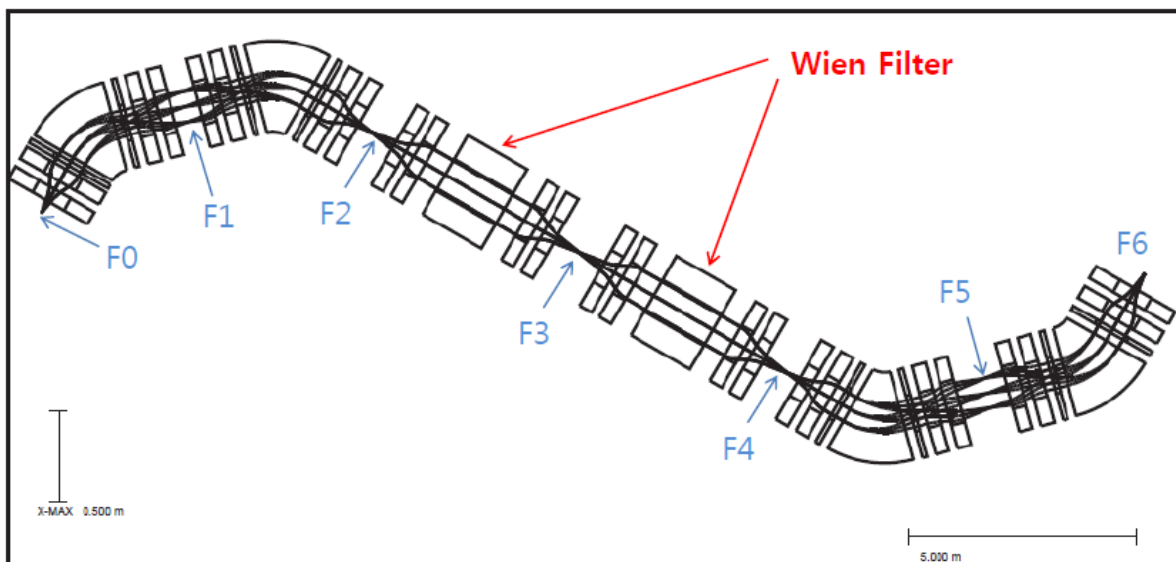


**Fig IV.1-1 Schematic representation of the KRS layout with typical ion trajectories.**

- **Target system**

- Supersonic jet gas target type for direct measurement experiments

- Plasma window gas target type for secondary beam production

#### ▪ **Detection system**

- Beam tracking: Multi-wired gas counters (ex, PPAC(Parallel Plate Avalanche Counter), MCP (Micro-Channel Plate))
- Particle detection: Ball-type scintillator array of CsI(Tl) crystals for low-energy ions, and  $\Delta E$ -E telescope array consisting of DSSD ( $\Delta E$ ) and CsI(Tl) scintillators (E)
- $\gamma$ -ray detection: Hybrid of LaBr<sub>3</sub>(Ce) crystals and highly-segmented Ge crystals applied with  $\gamma$ -ray tracking technique

### **IV.2 LAMPS (Large Acceptance Multi-Purpose Spectrometer)**

The Large Acceptance Multipurpose Spectrometer (LAMPS) is designed to explore the equation of state (EOS) of nuclear matter in a wide range of neutron-proton asymmetry. In order to achieve the physics goal, the low-energy (LAMPS-L) and high-energy (LAMPS-H) nuclear facilities are proposed to perform the collision experiments with the beam conditions outlined below.

#### ▪ RI beams

- Species:  $A > 120$ ,  $N/Z \geq 2$
- Energy: 250 MeV/u (maximum)
- Flux:  $> 10^7$  pps (for <sup>132</sup>Sn)

#### ▪ Stable ion beams

- Species: all possible ions ranging from H to <sup>238</sup>U
- Energy: 200 MeV/u (maximum) for <sup>238</sup>U, 250 MeV/u (maximum) for <sup>197</sup>Au
- Flux  $>$  larger than  $10^{10}$  pps for <sup>238</sup>U

#### **IV.2.1 Detector Design**

The spectrometer magnets and the detectors should effectively detect neutrons as well as charge particles (pions, proton, deuterons, and tritons), nuclear fragments and gamma

produced in the nuclear reactions. The optimal structure of the facility is outlined as follows.

#### IV.2.1.1 LAMPS-L

- Gamma detector
  - BaF<sub>2</sub> array
- Cluster detector
  - Ionization chambers + Silicon-strip trackers (Si+CsI)
- Neutron detector
  - Scintillators

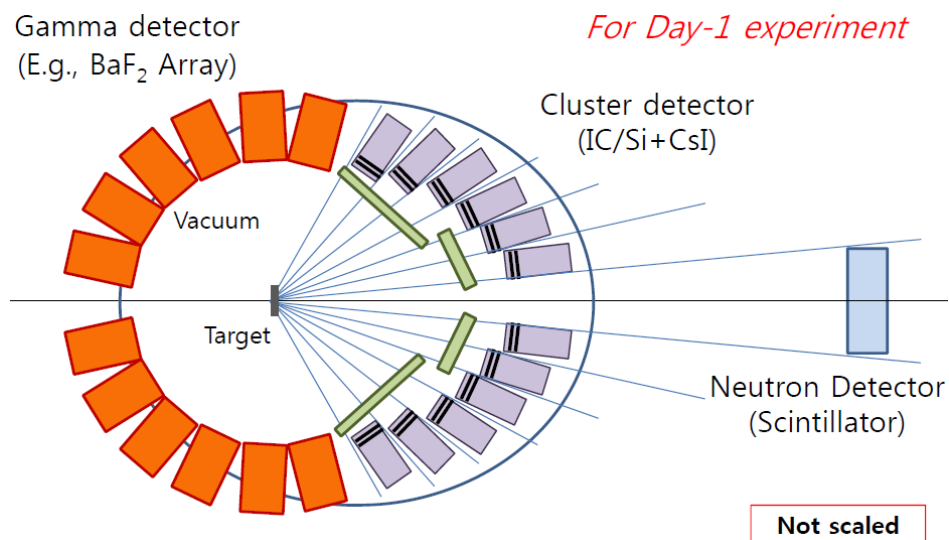


**Fig IV.2.1.1-1 LAMPS-L at RISP.**

#### IV.2.1.2 LAMPS-H

- Spectrometer magnet system composed of a solenoid magnet and a dipole magnet
  - Solenoid magnet for large-acceptance measurement of pions and high- $p_t$  nuclear fragments

: Field gradient = 2.0 T·m with B = 1.0 T

- Dipole magnet for precision momentum measurements of protons, deuterons, and tritons emerging at forward angles
  - : Field gradient = 1.1 ~ 1.5 T·m, maximum B field = 1.5 T
  - : Rotatable system, vacuum loaded in the active field volume
  - : Accuracy in field rigidity < 1/500
- Detector components
  - Silicon-strip trackers (Si+CsI): angle acceptance ~ 1.0 Sr
  - Time Projection Chambers (TPC): angle acceptance ~  $3\pi$  Sr
  - Dipole spectrometer arms equipped with TOF walls and tracking drift chambers
    - : Momentum resolution <  $10^{-3}$
    - : Accuracy in charge separation for light fragmentations < 0.3
  - A neutron calorimeter
    - : Energy resolution < 0.05 (for  $E_n < 100$  MeV) and < 0.10 (for  $E_n > 100$  MeV)

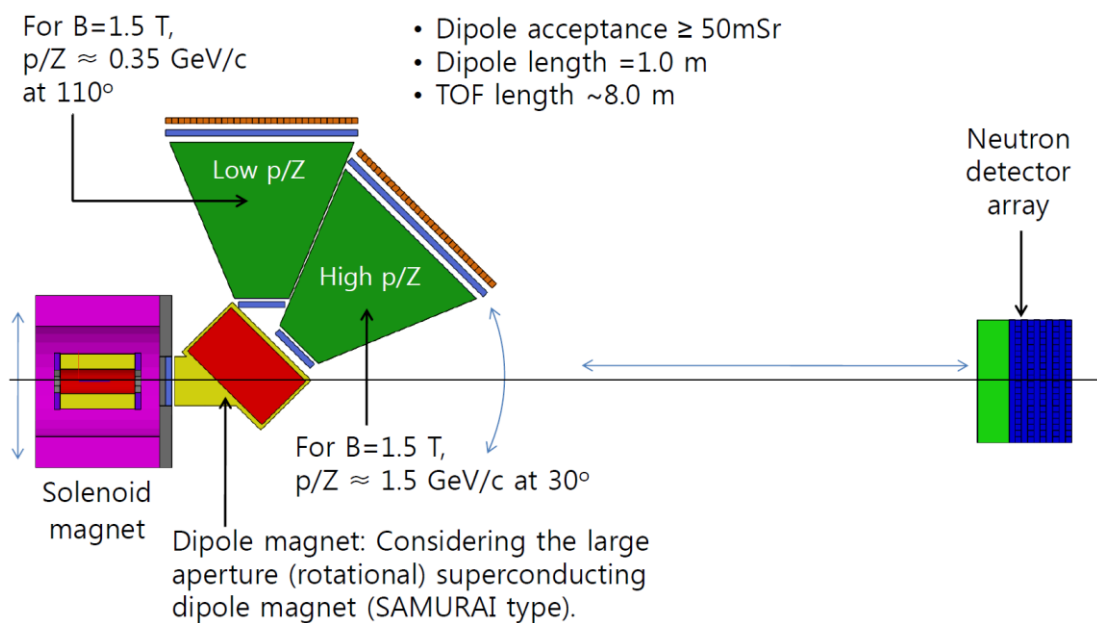


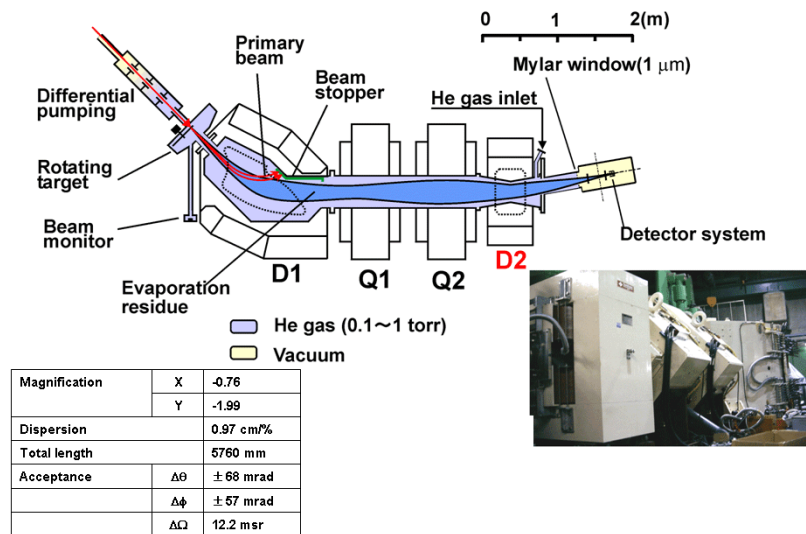
**Fig IV.2.1.2-1 LAMPS-H at RISP.**

### IV.3 Separator for SHE (Super Heavy Element)

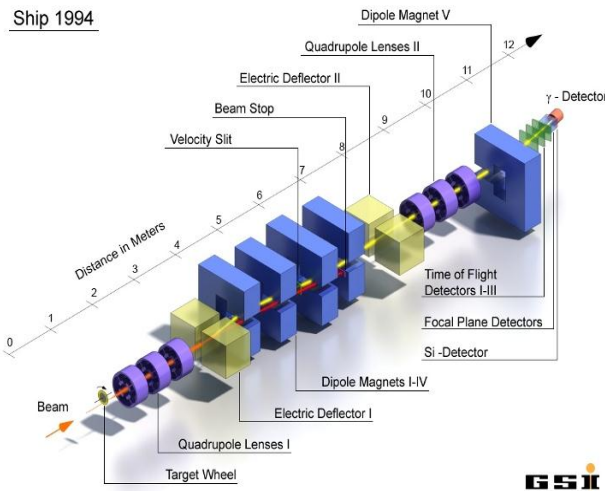
Search for Super heavy element (SHE) is one of main research field with intense stable ion beam extracted from the RISP facility. Now we are considering two types of separator for SHE research. One is a gas-filled separator such as FLNR at Dubna and GARIS at RIKEN. The other is vacuum type separator such as SHIP at GSI. Gas filled separator have advantage of a simple design with only magnetic elements. However, the high intensity beam loses a large amount of energy in the gas.

Figure IV.3-1 shows the GARIS separator and figure IV.3-2 show the SHIP with velocity filter at GSI. Detail design work will be done in phase of the technical design.

#### RIKEN GARIS(Gas-filled Recoil Ion Separator)



**Fig IV.3-1 GARIS at RIKEN**



**Fig IV.3-2 SHIP at GSI**

#### IV.4 High Resolution Spectrometer and ZeroDegree Spectrometer

- **High Resolution Spectrometer**

In order to study nuclear structure, we are considering experimental apparatus such as R3B at GSI. Figure IV.4-1 shows the High resolution Detector for Nuclear Structure measurement. High resolution Detector for Nuclear Structure measurement consists of large acceptance spectrometer (see IV.2 LAMPS) and high resolution spectrometer such as SHARAQ at RIKEN and S3 (Super Separator Spectrometer) at GANIL Spiral2.

Figure IV.4-2 shows the SHARAQ spectrometer. The SHARAQ spectrometer has a momentum resolution of  $\frac{\delta p}{p} = 15,000$  and an angular resolution of  $\Delta\theta < 1$  mrad for particle with magnetic rigidity of  $B\rho = 6.8$  Tm at maximum.

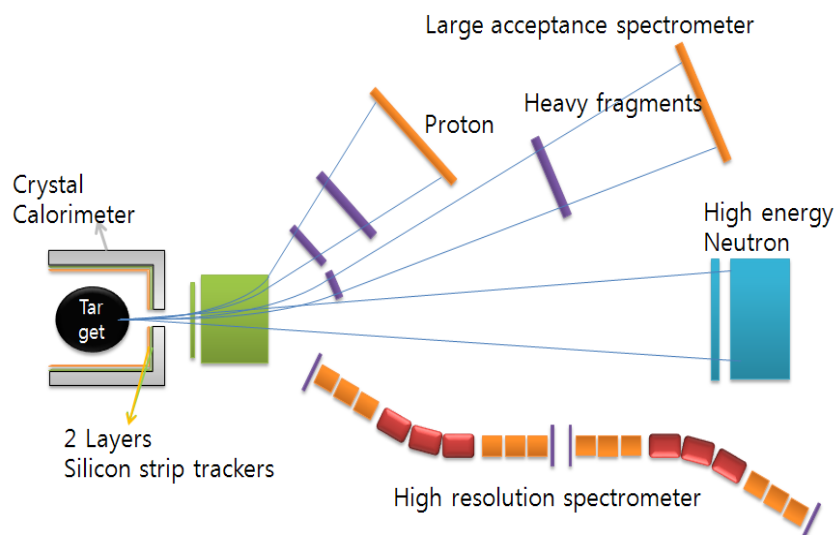


**Fig IV.4-1 Overview of High resolution Detector for Nuclear Structure measurement**

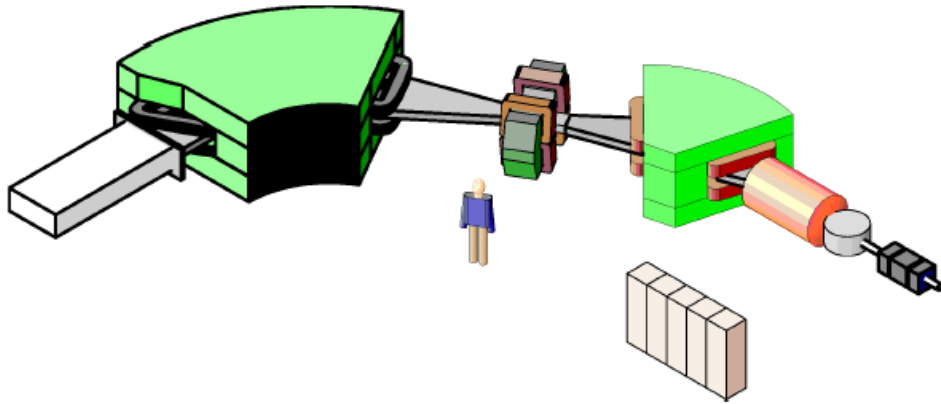


**Fig IV.4-2 Overview of the SHARAQ spectrometer**

Figure IV.4-3 shows the S3 separator at GANIL Spiral2. The S3 is a device designed for experiments with the very high intensity beam. The S3 has a two stage separator (momentum achromat) and spectrometer (mass spectrometer). The requirements of this separator are following.

- excellent primary beam suppression ( $10^{13}$  in most case)
- charge state acceptance :  $\pm 10\%$
- $B\rho$  acceptance for each charge state :  $\pm 10\%$
- maximum magnetic rigidity 1.5 – 2 Tm
- maximum electric rigidity 10 – 12 MV
- mass resolution of 1/300 (FWHM)

Detail design work will be done in phase of the technical design.

### S<sup>3</sup> Layout

Momentum achromat + mass separator

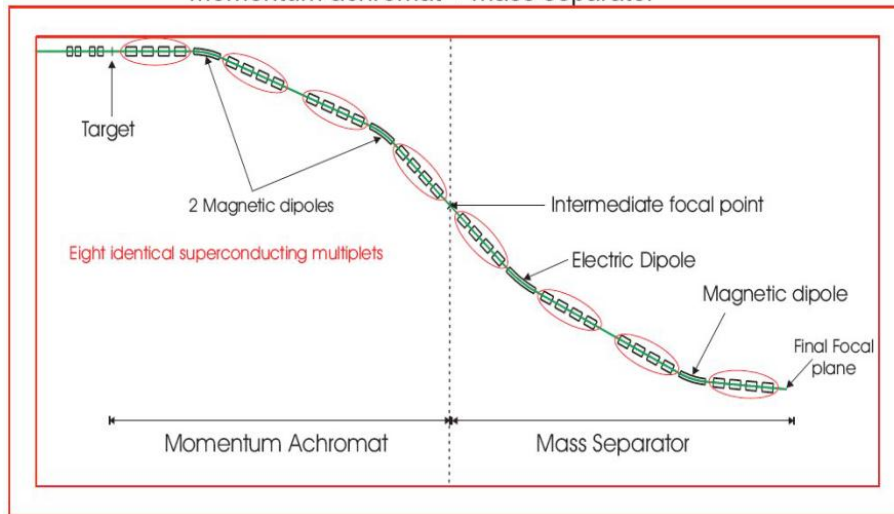


Fig IV.4-3 Overview of the S3 separator

#### ▪ ZeroDegree Spectrometer

Zero Degree Spectrometer can be placed after mass separator for studying of RI beam secondary reactions via inclusive/semi-inclusive measurements such as in-beam gamma spectroscopy, missing mass spectroscopy, and Iso-diffusion. Zero Degree Spectrometer is often operated with  $\pm 3\%$  of momentum acceptance and multi-modes:

- 1) Large acceptance mode has momentum resolution 1240 and angular acceptance  $\pm 45$  mrad in vertical and  $\pm 30$  mrad in horizontal
- 2) Moderate resolution mode has momentum resolution 2120 and angular acceptance  $\pm 20$  mrad in vertical and  $\pm 30$  mrad in horizontal
- 3) Dispersive mode has momentum resolution 4130 and angular acceptance  $\pm 20$  mrad in vertical and  $\pm 30$  mrad in horizontal [IV.4-1].

Detector system of Zero Degree Spectrometer is consisted of gamma detector array and missing mass detectors in between mass separator and Zero Degree Spectrometer. It is also combined of position sensitive beta detector and gamma detector at the end of Zero Degree Spectrometer. These detectors are able to measure angle-integrated cross section of gamma ray with identification of products.

#### **[Reference-IV.4]**

[IV.4-1] H. Sakurai, "RI Beam Factory Project at RIKEN", Nuclear Physics A 805 (2008) 526c-532c.

### **IV.5 Neutron science**

#### **IV.5.1 Beam line for fast neutron facility**

Beam line for the fast neutron facility consists of an accelerated p beam line and a neutron beam line. Protons accelerated by cyclotron are delivered to the neutron production target to produce neutrons. Thick targets such as Li, Be and C are used to produce neutrons. In case of thick target, the beam is stopped in the target. Neutrons produced by thick target go through collimators and react with experimental samples. There are 2 neutron beam lines at 0° and 30°. Neutrons passing through the experimental samples can be scattered from the wall of experimental hall. A neutron beam dump needs to be installed to absorb neutrons to prevent background. Figure IV.5-1-1 is the layout of the fast neutron experimental hall and beam lines inside the hall.

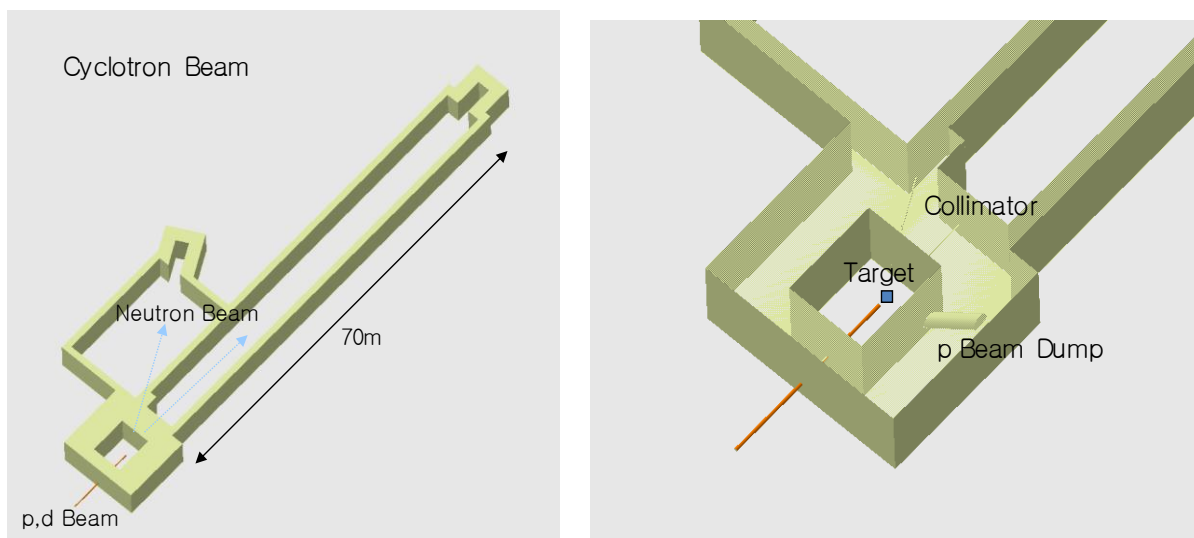


**Fig IV.5-1 Fast neutron experimental hall and beam lines**

Proton beams from the cyclotron are transported to the experimental hall for the fast neutron related nuclear data measurements. A few electric quadrupoles are installed to keep the beam focused until it hits the target. A few beam profile and emittance monitors are also installed to monitor the beam.

The main purpose of the neutron target on the basis of the 70 MeV proton is to provide fast neutrons by relying on knock-out and charge exchange reactions (p,n) with 70 MeV protons on light element targets such as Li, Be and C. The design goal of the target is to produce the fast neutrons, up to a few tens of MeV, intense enough for measurements of neutron-induced reaction cross-sections at the neutron time of flight facility. In target design, estimations of heat deposition, neutron yield and spectrum require 3-dimensional Monte Carlo simulations for particle transport and nuclear reaction calculations.

A nuclear data experiment system will be developed to measure neutron total cross section, neutron-induced fission cross section, neutron capture cross section, elastic scattering cross section and inelastic scattering cross section for the structure materials of new nuclear power plant and fuel materials.

Measurements of neutron total cross section, elastic scattering cross section, inelastic scattering cross section, capture cross section and neutron-induced fission cross section are performed coincidentally at two points by using n-TOF system with plastic detectors, liquid scintillators, a gamma-ray detection system with HPGe and the C<sub>6</sub>D<sub>6</sub> detectors, which has been used in GELINA [IV.5-1], fission chamber and several electronics. Neutron total cross section will be measured at 0° degree with respect to neutron beam direction and others will be measured at 30° coincidentally.

A ball detector with about 160 BaF<sub>2</sub> crystals is proposed to increase the efficiency of detecting gamma-ray for the accurate measurement of neutron capture cross section [IV.5-2].

#### **[Reference-IV.5]**

[IV.5-1] L.C. Mihailescu, A. Borella, C. Massimi, P.Schillebeeckx, "Investigations for the use of the fast digitizers with C<sub>6</sub>D<sub>6</sub> detectors for radiative capture measurements at GELINA", Nuclear Instruments and Methods in Physics Research A 600 (2009) 453-459.

[IV.5-2] C. Guerrero et al., "The n\_TOF Total absorption Calorimeter for neutron capture measurements at CERN", Nuclear Instruments and Methods in Physics Research A 608 (2009) 424-433.

#### **IV.6 Material science**

The material science facilities at RISP could include a β-NMR facility, PAC and EC facility, and μSR. The detailed design for β-NMR and μSR could be seen in following sections.

### IV.6.1 $\beta$ -NMR facility

The  $\beta$ -NMR facility consists of a beam polarizer, a beam line for transport of polarized RIBs,  $\beta$ -NMR/NQR spectrometers. Low energy RIBs provided from the ISOL is incident on the beam polarizer. The RIBs could be polarized with optical pumping method or tilted foil method. The optical pumping method is favored over the tilted foil method because of its high polarization efficiency. The polarized RIB is guided with electrical beam optics in order to maintain its degree of polarization, and is transported to the  $\beta$ -NMR/NQR spectrometer for the material analysis. The energy of RIB is low, any material something like window is not allowed on a beam path.

A polarizer consists of three parts, neutralizer, laser reaction region, re-ionizer. The neutralizer makes RIB neutral beam for optically polarizing the radioactive atom. The atoms in neutral beam collide with photons in the laser reaction region. In order to increase the photon absorption rate, photons in laser are circularly polarized and their frequency is tuned considering the Doppler effect due to velocity of atom. Nucleus becomes polarized by hyperfine interaction. The degree of polarization for  $^8\text{Li}$  reaches about 70% by using the optical pumping polarizer.

For guiding the polarized RIB, beam line consists of various beam optics components. Since the polarization axis of RIB can be perturbed by a Lorentz force within magnetic fields, all the optics components are electric. The beam line can be divided into several branches for conducting two or more experiments simultaneously. The polarized beam is divided time-sequentially by using a kicker that can immediately alter the beam direction. A re-ionizer can ionize polarized neutral atoms and then produces polarized RIB. The polarized RIB is separated with non-ionized atom beam by passing through an electric dipole. Polarized neutral beam is used for measurement of degree of polarization with a neutral beam monitor.

## IV.6.2 $\mu$ SR facility

In  $\mu$ SR spectroscopy, muons implanted into a sample come to rest at interstitial sites. With the measurement techniques of nuclear physics one can get the information about the internal magnetic fields in solids and their distribution and dynamics. In muon spin rotation the precession of the implanted muons in an external transverse magnetic field is observed. In muon spin relaxation, on the other hand, one observes the decrease of the muon spin polarization without an external field or in longitudinal fields. A muon decays into a positron (or electron) and neutrinos and the emission direction of the positron is related to the direction of the muon spin. Thus one can attain the information of the internal field and its dynamics by measuring a decaying asymmetry of the muons. The asymmetry can be determined by detecting the positrons (or electrons) with properly located detector system. Scintillation counters are extensively used for the detection of the positron (or electron) in  $\mu$ SR. The high energy positrons (or electrons) generate a lot of scintillation photons in the scintillation counters by losing their kinetic energy. The scintillation photons are converted into electric signal by using photon sensors such as photomultiplier tubes, silicon photodiodes, avalanche photodiodes, etc. The photon sensors tubes must not be influenced by the magnetic field which is essential for the muon spin rotation and muon spin relaxation experiments. In pulsed  $\mu$ SR, multiple of this detecting apparatus is deployed around sample space with maximum solid angle coverage for higher throughput of the experiments. The number of the detecting channels is directly related to the solid angle coverage in  $\mu$ SR experiments and it is better to have more detecting channels to increase the quality of experiment results. In the CW  $\mu$ SR, the multiple detector scheme is used mainly for the signal-to-noise enhancement but the proper spatial allocation of the detector apparatus is also very important for the experimental determination of the decay asymmetry. Also, higher coverage detector solid angle can be useful in CW  $\mu$ SR for the enhancement of detection efficiency. The electronic signal from the photon sensors is fed into the back-end

electronics unit and proper event signals are extracted and the signals which are not related to the muon decay in the sample are vetoed. After the extraction of the proper signal from the muon decay in the sample, signal processing electronics unit deduces the asymmetry of the muon decay and recorded as a result of the experiments. Because of the short life time of muon ( $\sim 2.2 \mu\text{s}$ ), the electronics units must process the signal at high speed for the high throughput of the experiments.

#### **IV.7 Ion trap and Laser spectroscopy**

The aim of this facility is to offer precise mass values and spectroscopic information of rare isotopes for the research fields of particle, nuclear, and astrophysics [IV.7-1].

For highly accurate mass measurement, we need intelligent manipulation of the ions using a cooler and buncher (RFQ), MR-TOF mass separator, charge breeder ion trap, q/A selector, preparation and measurement Penning traps, and other beam guiding optics. Each module should be precisely designed, manufactured, and tested separately for several years.

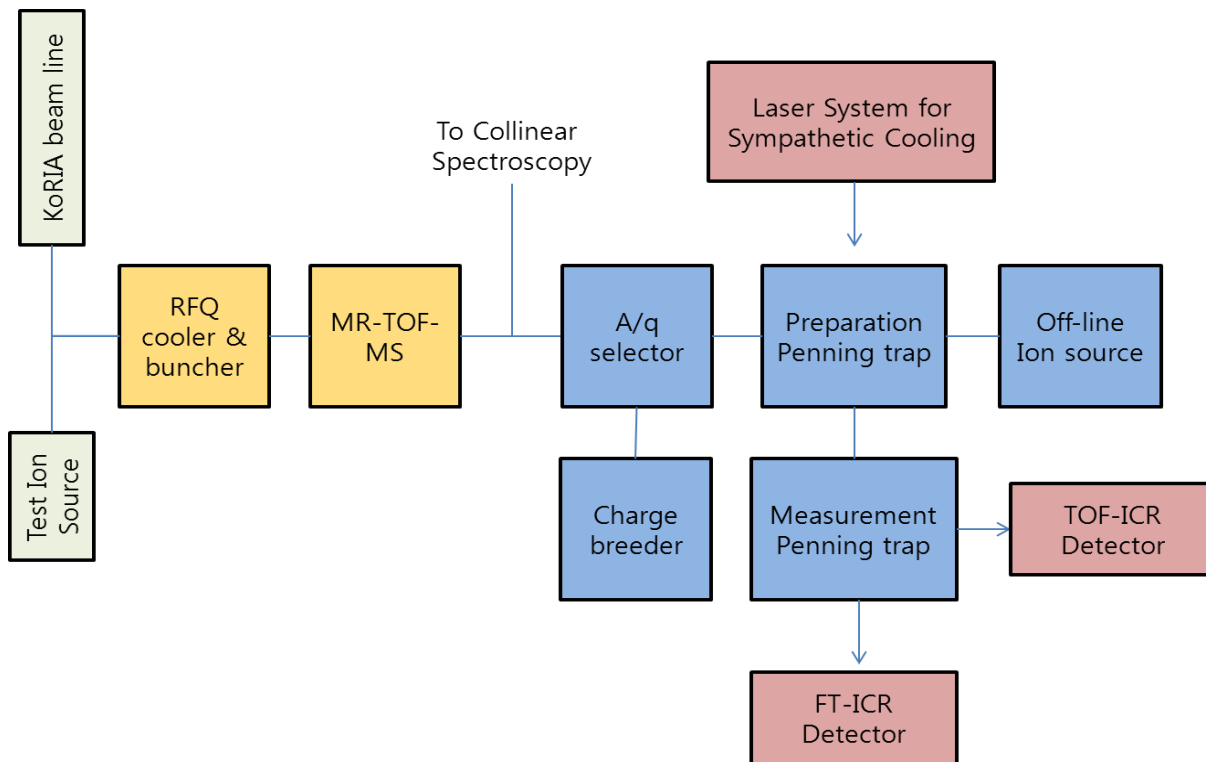


**Fig IV.7-1 Facility design for the mass measurement and laser spectroscopy module.**

The facilities for the mass measurement and laser spectroscopy module are drawn schematically in Fig IV.7-1. Starting with the injection into the RFQ cooler and buncher before a multi-reflection TOF-MS, the low energy ion beam splits into the dedicated experimental beam lines of mass measurement and laser spectroscopy. We are also considering a combined collinear laser spectroscopy setup using one common beam line as shown in Fig IV.7-2.

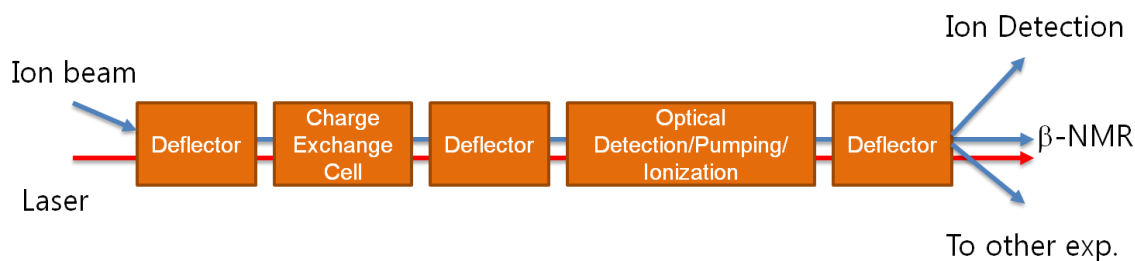


**Fig IV.7-2 Facility design for a combined collinear laser spectroscopy system at RISP.**

### **[Reference IV.7]**

[IV.7-1] H.-J. Kluge, Eur. J. Mass Spectrom. **16**, 269 (2010).

## **IV.8 Medical/Bio Science**

For the bio and medical science, the new understanding of the interaction between heavy ion beams and living cells has influenced radiation biology, and may result in a paradigm shift. For example, the discovery in 1953 of the double-helix model markedly increased our understanding of DNA structure and function. Therefore, several advances in biological science using heavy ion beams may have an innovative impact on the development of biological science. Medical science will result in improving human life quality by developing new cancer treatment methods and related fields (biology, physics, pharmacology and mechanical sciences, etc.).

- Developing new heavy ion beam therapy methods
- Imaging study of heavy ion beam dose distribution
- Radioresistance of cancer cells to heavy ion beams
- Discovery of new targets and drugs for improving heavy ion beam therapy
- Normal tissue damage to heavy ion beams
- RBE of heavy ion beam and oxygen dependence
- Genomic and proteomic research responsible to heavy ion beam
- Neoplastic transformation of cells by heavy ion beam
- Epigenetic change by heavy ion beam
- Effect of heavy ion beam on embryonic development
- Cellular and replica senescence induced by heavy ion beam
- DNA damage and repair induced by heavy ion beam
- Development of microbial genetic resource for biomass production
- Development of variant plant resistant to environmental stresses

The aim of medical/bioscience research is to improve human health and quality of life.

Requirements for the medical and bioscience study of world top level:

- Isotopes:  $^8\text{B}$ ,  $^9\text{C}$ ,  $^{12}\text{C}$ ,  $^{11}\text{C}$ ,  $^1\text{H}$ ,  $^{16}\text{O}$ ,  $^2\text{D}$ ,  $^3\text{T}$ ,  $^3\text{He}$ ,  $^4\text{He}$ ,  $^{14}\text{N}$ ,  $^{20}\text{Ne}$ ,  $^{36}\text{Ar}$ ,  $^7\text{Li}$ ,  $^9\text{Be}$ ,  $^{11}\text{Be}$ ,  $^{10}\text{B}$ ,  $^{27}\text{Al}$ ,  $^{115}\text{In}$ ,  $^{28}\text{Si}$ ,  $^{74}\text{Ge}$ ,  $^{32}\text{S}$ ,  $^{197}\text{Au}$ ,  $^{109}\text{Ag}$ ,  $^{56}\text{Fe}$ ,  $^{18}\text{F}$ ,  $^{35}\text{Cl}$ ,  $^{125}\text{I}$ ,  $^{131}\text{I}$ ,  $^{48}\text{Ti}$ , etc.
- Energy: 10 ~ 1000 MeV/u
- Intensity: 0.1 nA ~ 1  $\mu\text{A}$
- Beam size: 20  $\mu\text{mm}^2$  ~ 900  $\text{cm}^2$
- Beam direction: both of vertical and horizontal
- < 3% dose uncertainty at target position
- Dose rate: > 2 Gy/min

Facility design

- Low energy
  - Irradiation room: one room with horizontal beam, one room with vertical beam
  - Other research rooms: cell biology room, facility room, microbiology room, evaluation room
- High energy
  - Irradiation room: two rooms with both of vertical and horizontal beams, one room with horizontal beam for future gantry, one room with horizontal beam for beam test
  - Other research rooms: cell biology, facility, animal, evaluation and therapy research room

#### **IV.9 Elementary Particle Physics**

The aim of facility for the elementary particle physics is two-fold. First one is to establish a fundamental science with EDM search. Second is to look for lepton flavor violation with muons.

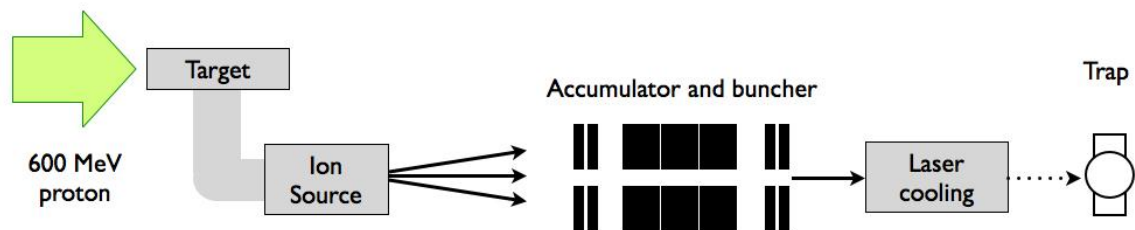


**Fig IV.9-1 Facility design for an EDM search with Ra isotope.**

- EDM search

The best strategy for EDM search with KoRIA is to study an atomic EDM, in particular, with Ra ion beam. Figure IV.9-1 shows a design for an EDM search using the laser cooling technique. It consists of a target station of protons, yielding approximately  $10^8$  (225) Ra ions/second [IV.9.1-1]. After passing accumulator and buncher, laser cooling technique is used to trap Ra ions. At this stage, if a high efficiency is maintained, a competitive EDM search with Ra ion beam can be achieved.

The main parameters to achieve are the high electric field at the trap region ( $> 100$  kV/cm) and the long coherence time ( $\sim 100$  s) of trapped Ra ions. The first atom trap of radium was realized using oven-based system [IV.9.1-2] and extensive R&D is required to achieve above parameters.

- Lepton flavor violation with muons

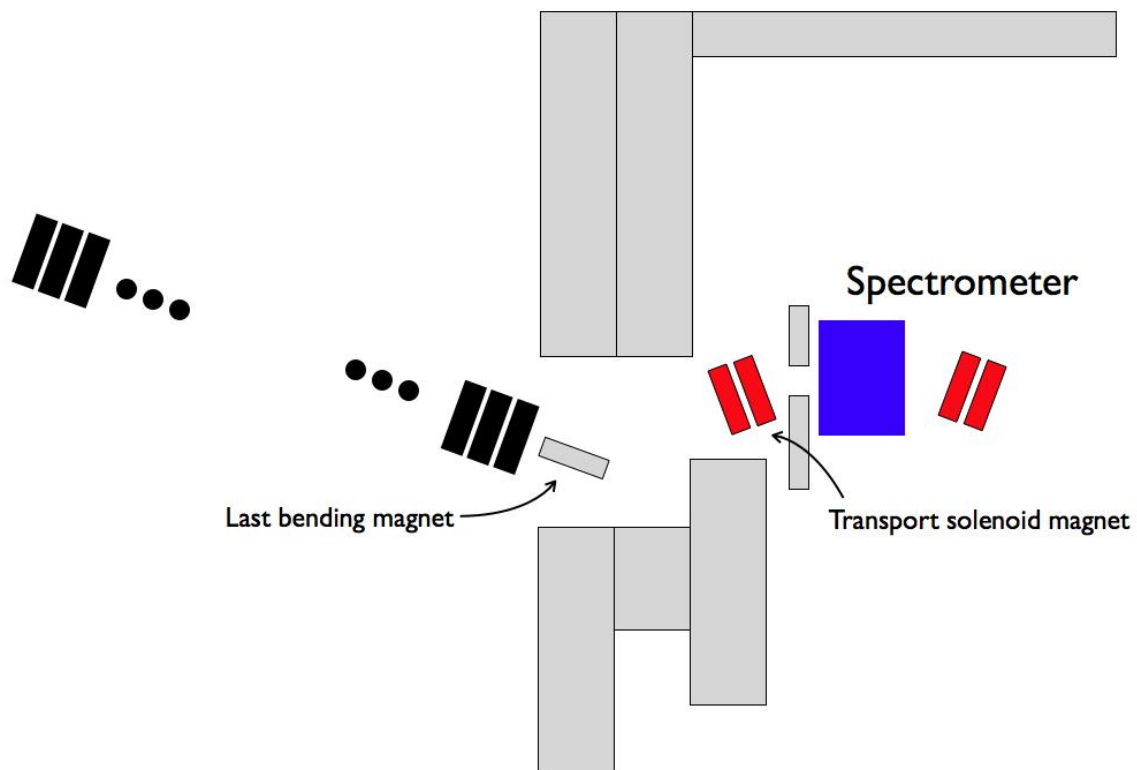


**Fig IV.9-2 Facility design for lepton flavor violation search muon transport.**

The best strategy for lepton flavor violation search with KoRIA is utilizing muon beams. For  $\mu \rightarrow e\gamma$  or  $\mu \rightarrow eee$  search, simplest muon beam structure can be obtained and a complicated and expensive design of solenoid can be avoided. Figure IV.9-2 shows a conceptual view of the experimental site with basic beam transport system indicated. Depending on which experiment is chosen to be running at a given time, the incoming muon flux has to be optimized. For example, in  $\mu \rightarrow e\gamma$  experiment, the random coincidence backgrounds are most severe therefore the muon flux has to be low enough to be a competitive experiment. In the case of  $\mu \rightarrow eee$  experiment, triple coincidence utilizing three charged tracks in the detector can suppress the backgrounds strong enough so that a substantially high muon flux can enter into the spectrometer.

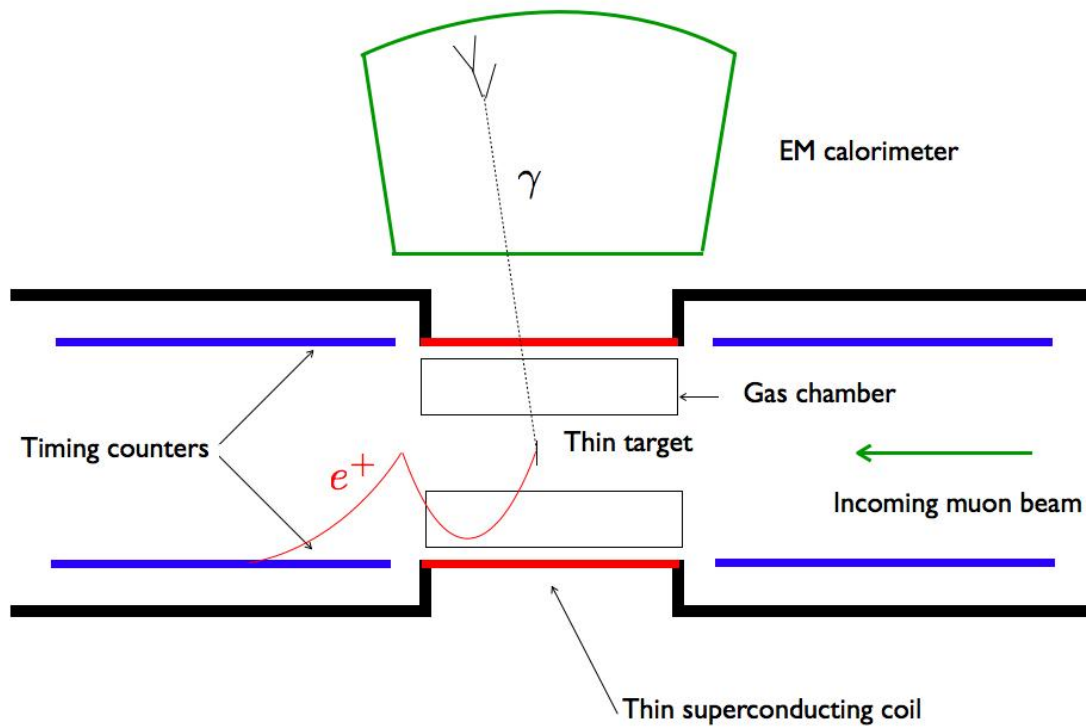


**Fig IV.9-3 Facility design for lepton flavor violation search spectrometer.**

For  $\mu \rightarrow e\gamma$  experiment, a calorimeter and tracking system with  $\Delta E_e/E_e = 0.8\%$ ,  $\frac{\Delta E_\gamma}{E_\gamma} = 4\%$ , timing resolution of (e,gamma) = 0.15 ns, angular resolution of (e,gamma) = 19 mrad is required in order to carry out a competitive physics program with  $\mu \rightarrow e\gamma$  experiment.

A conceptual idea on the spectrometer is shown in Fig. IV. 9-3 and a detailed study to be carried out for the optimization of the detector.

For  $\mu \rightarrow eee$  search, an excellent tracking system is required. A compact tracking system of silicon sensors or time projection chamber can be used to realize the experiment.

**[Reference IV.9]**

[IV9.1-1] Private communication with J. C. Yoon, IBS. Efficiencies in various stages are assumed to be 100%.

[IV9.1-2] Guest et al., Phys. Rev. Lett. 98, 093001 (2007)

## Chapter V Conventional Facilities

### V.1 Site

The accelerator complex will be located in Sindong area that is 14 km away from downtown of Daejeon city and 11km away from Sejeong special autonomous city. It is about 4km distance from the planned IBS headquarter. The aerial view of the complex site is shown in Figure V.1.



**Fig. V.1 The aerial view of the accelerator complex site, Sindong area**

The accelerator complex will be situated in the north side of the Sindong area and the total size of the area is  $1,049,504\text{m}^2$  ( $\sim 1,600\text{m} \times 660\text{m}$ ). The highest elevation point in the site is 124m (North West side) and the lowest point is 45m. A creek across the site runs

from west to east in the lowest elevation and a power line of 154kV is crossing in the west side of the site.

## V.2 Facilities

The complex should meet all scientific, functional, and operational requirements. It is comprised of two major areas because of the geographical feature of the site: the accelerator and experimental area located in the east side and the administration and supporting area in the west side. The well preserved forest area with a mountain top (124m) should remain as unaffected and it naturally isolates the office area from radiation area as shown in the Figure V.2.



Figure V.2 The layout of the accelerator site

Preliminary geotechnical data are collected by surface exploration and subsurface exploration of the site. Soil borings (total 20 points across the site) indicate that most of the accelerator and experimental area with elevation level of 75m is soft rock so that it provides solid foundations to linac tunnels and experimental halls. Because the accelerator tunnels and experimental halls will be positioned relatively high elevation of 75m without crossing a valley, a chance to encounter groundwater is very little. However further site survey and geotechnical investigations are required during preliminary design to meet project requirements. The facilities include accelerator buildings, experimental halls, office building, and support buildings as followings,

Main linac facilities include

- Injector area
- Linac tunnels
- Stripping area
- Linac support buildings and support utilities
- Target buildings

The ISOL and Re-Accelerator facilities include

- Cyclotron and target building
- ISOL area
- Post-Accelerator linac tunnel
- Linac support buildings and support utilities

The support facilities include cryogenic plant and system, high power test building, superconducting RF facility building, general assembly building, superconducting cryomodule assembly building, detector R&D and test building, power plant, and etc. There will be six experimental halls, three for the In-flight fragmented RI beam and three

for the ISOL RI beam, respectively. An administration and office building accommodates 240 persons including about 100 visitors. Additional 60 office spaces across the accelerator complex are considered in the linac support buildings and experimental halls. A guest house for 50 persons will be built in the supporting area. Guest houses at the IBS head-quarter can also be available for visitors. The planned buildings and their sizes are summarized in the following Table V.1.

Building Component	Gross Area (m <sup>2</sup> )
Main office	12,000
Dormitory	2,000
Experimental Halls	39,800
Support Buildings	48,350
Linac Tunnel (Main)	3,997
Linac Tunnel (Re-Accelerator)	3,033
Beam Line for IF	3,000
Linac Support building	18,352
Target Area (IF)	3,200
Target Area (ISOL)	1,600
<b>Total</b>	<b>135,332</b>

**Table V.1. Planned building sizes**

### V.2.1 Linac tunnel and linac support building

Several structural layouts of linac tunnels and its support buildings are considered and Figure V.2 configuration is adapted primary. Both driver and post-accelerator linac tunnels will be in the 14m underground. The linac tunnel will be constructed in cut and cover method and the gap between linac tunnel and RF gallery floor will be filled with 4m concrete and 4m soil. The linac supporting components will be positioned on the ground level so that both the structural and cost are optimal. The evaluation of RF and utility distribution will be performed in the Technical Design Report.

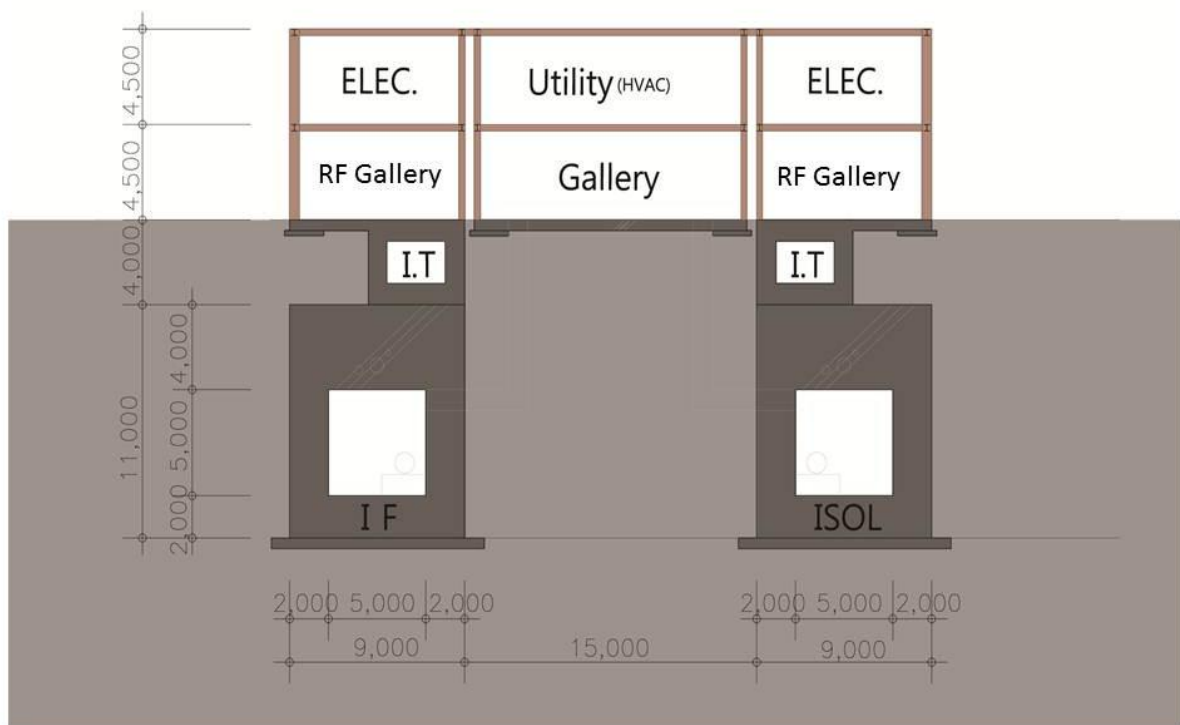


Figure V.3 Proposed linac tunnel and supporting gallery layout

### V.3 Cryogenic System

The cryogenic system has to be equipped to maintain the performances of superconducting (SC) cavities and SC magnets in the beam line and experimental facilities. The cryomodules provide the thermal insulations to SC cavities and SC magnets against the dynamic loads by the superconducting radio frequency (SRF) and the heat leakage from the surroundings. Major parts of the cryogenic system are the Helium Refrigeration System (He Ref), the distribution line and valve boxes, and the cryomodules. The cryomodules are connected to the He Ref via the vacuum shielded distribution lines. Fig. V.4 shows a basic concept of the cryogenic system for SC Linac.

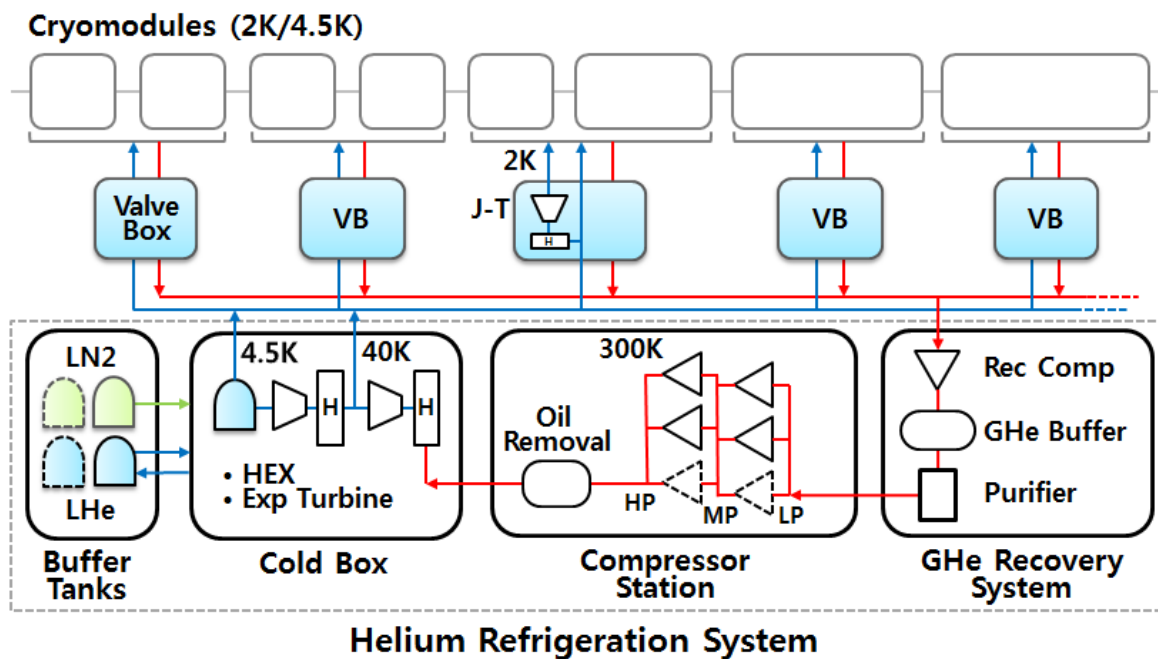


Fig. V.4 Cryogenic System Concept

The cooling capacity of He Ref will be decided by the estimated dynamic losses and the static heat leak from the surroundings into the cryomodules. Experimental results for prototype cavities are also needed. The static heat leak is calculated from the cryomodule design and the value will be verified by the prototype cryomodules.

The heat loads for all superconducting devices will be estimated and finally minimum He Ref capacity. Safety factor for the capacity will be at least 50 %. The helium inventory should be estimated, too. Approximately 50 % of helium will be stored in the cryomodules.

### **V.3.1 Helium Refrigeration System (He Ref)**

The He Ref is composed of gas helium recovery system, compressor station, cold box and Buffer Tank for liquid helium and liquid nitrogen. The He Ref supplies helium at several temperatures; 2 K and 4.5 K liquid helium for the linac cryomodules; 40 K helium gas for heat shields. Besides, 77 K liquid nitrogen will be used for the heat shields.

2 K helium is delivered by using 2 K modules which contains a 2K/4K heat exchanger and a Joule-Thomson (J-T) valve. These 2 K modules can be a central one located at the HRS or smaller modules located at the valve boxes near the cryomodules. The latter option is preferred by cryogenic experts. SNS have been used the heat exchanger at the cryomodules and those were proven to be reliable for several years.

Compressor station should be built in a separated building considering its noise level (around 100 dBA) and vibration. To absorb the vibration marshmallow spring mounted station will be used.

#### **V.3.1.1 Upgradable HRS option**

We should consider how to reduce the construction cost of the HRS due to limited budget status. In this point of view, upgradable HRS could be an option. For example, if whole superconducting devices need 15 kW total cooling power including safety margin, the option includes building 10 - 12 kW HTS firstly; and then attaching 3 - 5 kW upgradable system (cold box and compressor) secondly to the original one. Fig. V.5

shows the concept of the upgradable HRS option. Additional cold box (#2) and compressor (#3) will be added according to the increase of actual cryogenic needs.

Few leading companies in cryogenic industry (i.e. Linde, Air Liquide) can supply the large HRS (over 1 kW) and their competitions could make the HRS cost-effective. Final decision will be made after the cost analysis during the TDR.

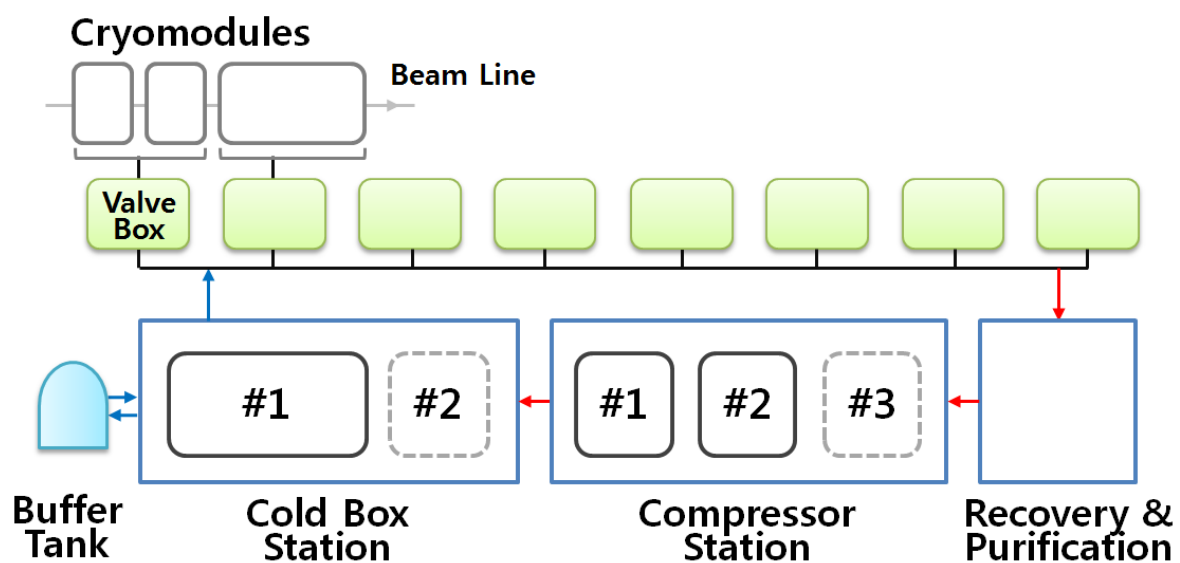


Fig. V.5 Upgradable HRS options

### V.3.2 Distribution Line and Valve Boxes

The cryogenic distribution line will run within the linac tunnel providing a connection between the HRS and the cryomodules. The distribution lines are shielded with MLI (Multi-Layer Insulation) and vacuum; and containing multiple cryogenic service lines. Several helium lines and valves are in the distribution line to control each cryomodule independently.

The valve boxes (VB) are connected to one or more cryomodules and the distribution line. The box contains several valves for each cryogenic line and, if needed, the heat exchanger and the Joule-Thompson valve for the 2 K helium supply.

### **V.3.3 Vacuum System**

The superconducting linac that is transporting heavy ions has cryomodules, each of which incorporates 1 or more niobium cavities. These cavities are submerged in a bath of liquid helium and are maintained at an operating temperature of 2 K or 4.5 K. This bath is surrounded by Multi-layer heat shields. The vacuum level near the beam paths of the heavy ions needs to be maintained at  $\sim 10^{-9}$  torr (with heavy ion beam, less than  $10^{-8}$  torr). To keep those ultra-high vacuum levels, a series of careful processes are needed, such as washing, cleaning, drying and degasing in a vacuum furnace etc. Assembly of the parts and storage should be done in the clean booth.

Specs of vacuum pumps are decided by the volume of vacuum tubes and the cavities, desired vacuum level and conductance.

### **V.4 Electric Power System**

Electrical power system for RISP, which will be technically designed with fixing the general design and P&ID, has been considered as 154kV electrical power receiving facility, AC power distribution, DC power /UPS, and earth / lightning protection.

- **154kV electrical power receiving facility**

154kV electrical power receiving facility provides the electrical power with the 3.3kV electrical power plant by reducing the electrical voltage to 3.3kV from 154kV lines delivered by Korea electrical power company (KEPCO). We have a plan to technically design by draw a circuit diagram, 154kV driving line, circuit breakers, and transformers

and to construct electrical devices, circuit breaker, and alarming system for monitoring /control for 154kV receiving facility, drawn by electrical logic diagram and connection.

- **AC electrical power distribution system**

AC electrical power distribution system provides 3.3kV, 480V, 220V Ac electrical power via a receiving transformer from 154kV electrical power plant. To minimize the cost from an abrupt accident and a power failure and assure the safety for operators, the diesel generator, connected to AC electrical power distribution system, will be designed to supply the essential load with emergency lines and UPS power sources.

- **DC electrical power supply and Uninterrupted Power Supply(UPS)**

DC electrical power supplying system, which provides the electrical power with the load needed to DC power, is composed of capacitors, DC distribution panel, and controls/monitors for operation. UPS supply the AC power to core elements such as control and monitors by an electrical power failure from a voltage instability, momentary power failure, and its accident. We have a plan to construct this sub system, composed of capacitors, rectifiers, invertors, static automatic or manual switch, variable transformers, and AC power panels.

- **Earth and lightening protection**

Earth and lightening protection system is to prevent the damage of the workers and instruments by lightening accident and earth loss in the site, and assure the protection system from the damaged system. Earth and lightening protection system can supply the

stable circuit voltage referred from the earth. Fixing earth type and earth line driving method divided by the instruments and facilities and setting the protective angle during lightning protection design process, lightning protection will be located in the storage of the explosive compounds.

## **V.5 Radiation Safety**

### **▪ Personal Protection System(PPS)**

Personal protection system assures the safety to prevent an abnormal operation and abrupt accident for the radiation workers and the ordinary person. This system is classified to an entrance level divided by a risky and alarming structure, and is based on the following conceptual requirement.

#### a) Reliability

All components of the PPS should be based on the performance quality assurance and be assured by a periodic inspection and a sound check of normal operation in advance.

#### b) Fail-Safe

PPS should be designed to assure the safety during electrical power failure, cable shortage, and its sensor failure.

#### c) Redundancy

Central control system and its electrical power of PPS should be constructed with redundancy.

d) Self-diagnostic function

PPS should be supported to an operating test, which can be used a manual or sequential mode, of each instruments and sensing lines.

e) Simplicity

PPS can be constructed for an easy maintenance and test by simplifying the structure of the control layer and cables.

f) Prevention to a breakdown of cable insulation

All cables should be inserted in the independent trays to prevent a malfunction of cables by a radiation and a cable failure by the workers mistakes.

g) Security instruments

The system cannot be modified without releasing the key lock which should be kept by the manager.

▪ **Radiation Monitoring System (RMS)**

Radiation Monitoring System can provide a monitoring function to access the facility and to read out operation status. RMS is composed of both an area monitoring system to observe the radiation level in the facility of the accelerator and experiment and environmental radiation monitoring system in the site boundary. We will design and construct the RMS as following process.

a) RMS should be designed to meet the radiation requirement, such as ALALA(as low as reasonably achievable), for the radiation workers and the ordinary person in the site area. We are considering the radiation guideline refer to the radiation safety regulations in Korea.

	Reference
①Site boundary	0.25 mSv/yr
②General area in the boundary	0.1 mSv/week (1 mSv/yr)
③Radiation area in the boundary	1 mSv/week (50 mSv/yr)

b) RMS should be monitor the typical system and area which can contain radioactive materials in the facility and the site boundary. Considering the specification of RMS can see the following table.

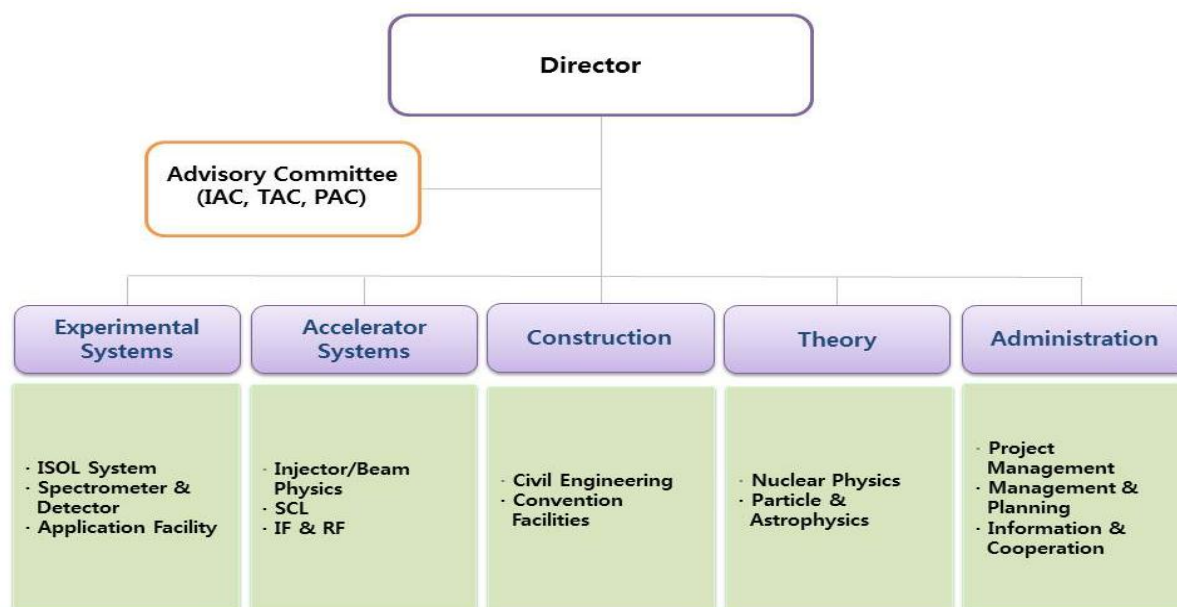
Detectors	Sensor type	Detecting energy	Radiation exposure
Neutron	3-He Proportional counter	0.025 eV ~ 12MeV	1 ~ 1E+4 uSv/hr
Gamma	Pressurized ion chamber	60 keV ~ 3 MeV	0.1 ~ 1E+5 uSv/hr

c) RMS should alarm and record at a high radiation level or electronics failure.

d) When a read out signal is higher than setting value of the radiation level, RMS should give some information to limit the access of the facility and to turn off the beam or shut-down the accelerator system.

## Chapter VI Organization

Currently the RISP is a project team in the IBS. Later, the RISP will evolve into an affiliated institute. Currently, the RISP consists of five divisions: Experimental Systems, Accelerator Systems, Construction, Theory, and Administration. The division of experimental systems consists of three teams: ISOL system, Spectrometer and Detector development, and Application facility teams. The division of accelerator system consists of three teams: Injector and beam Physics, Superconducting Linac (SCL), In-flight Fragmentation (IF) and RF teams. Three advisory committees advise the director: International Advisory Committee reviews the status of the overall project, project management, etc. Technical Advisory Committee (TAC) reviews the technical aspects of the design and construction of the accelerators, and the Program Advisory Committee reviews the experimental programs for the determination of the priority.



## VI.1 Work Breakdown Structure

Detailed scope of work is defined into a Work Breakdown Structure (WBS) and Figure VI.1 shows the RISP WBS through level 3. The WBS contains complete system elements of the RISP Project and is used to estimate the detailed cost for the project as well as schedule development.

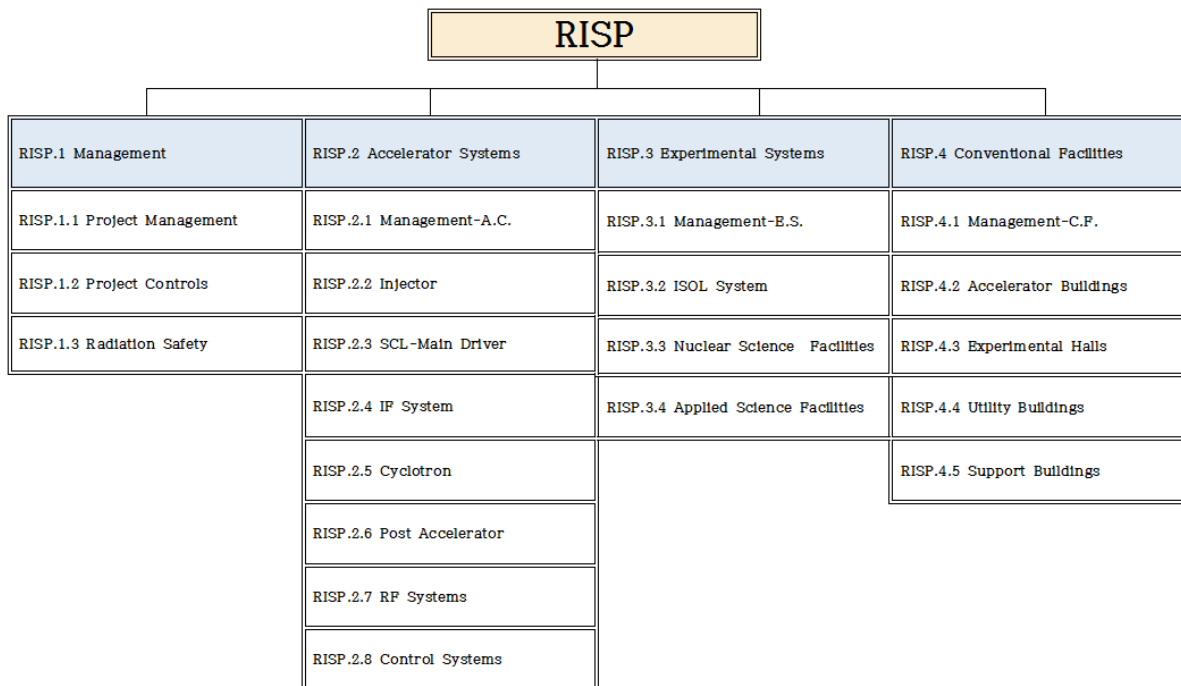


**Figure VI.1 Work Breakdown Structure of RISP**

Figure VI.2 and Figure VI.3 show the RISP WBS through level 4 for accelerator systems and experimental systems, respectively..

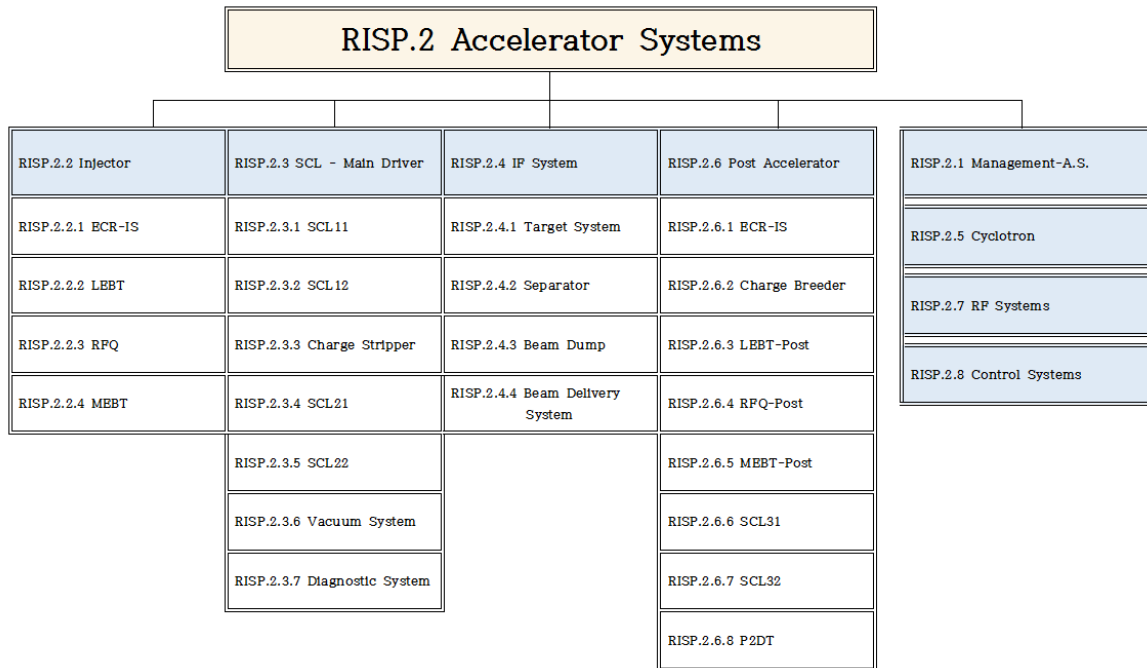


Figure VI.2 Work Breakdown Structure of Accelerator Systems

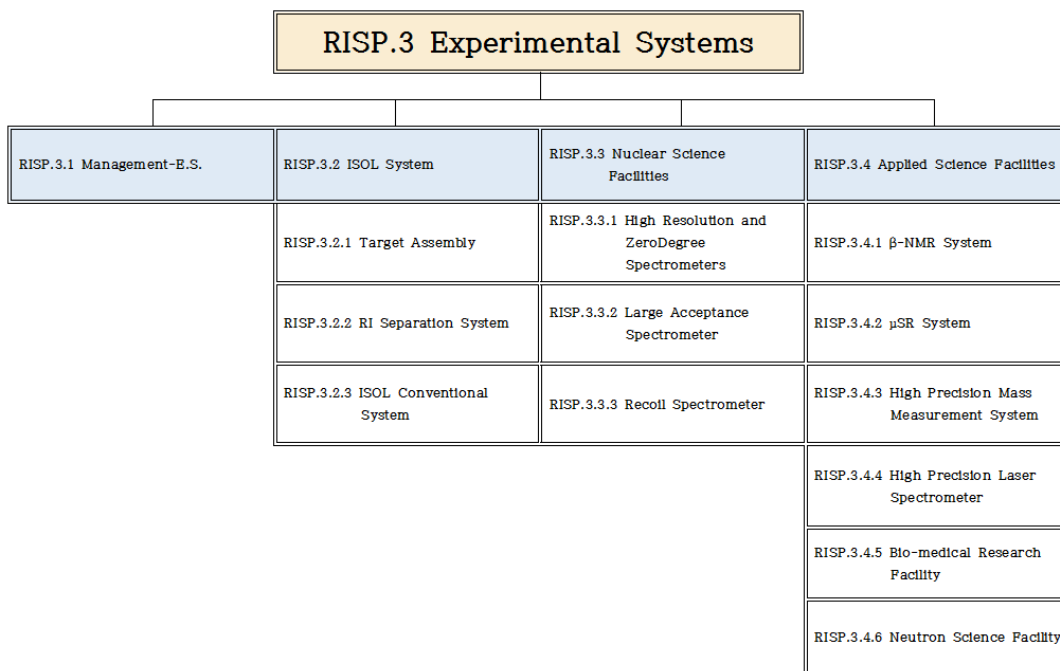


Figure VI.3 Work Breakdown Structure of experimental systems

## Chapter VII Costs and Schedule

This chapter summarizes the estimated construction costs for RISP. The projected total estimated cost for RISP is 460,400 million Korean won excluding lands, buildings and manpower.

RISP was started in December 2012 and the construction is expected to be completed by 2017. The schedule is based on the initial government proposal.

### VII.1 Costs

The total projected costs of the accelerator system including experimental setup are 460,400 million Korean won and the preliminary breakout is listed in the Table VII.1.

Cost Element	Cost (unit = MW, million Korean won)
SCL (Main and Re-accelerator)	197,000
Injector (ECR to MEBT)	24,700
ISOL System including driver	45,100
IF System (Target to experimental target)	18,000
RF and Control system	27,000
Cryoplant and system	18,000
Safety system and license	20,200
Experimental System	86,700
Management	21,700
<b>Total</b>	<b>460,400</b>

**Table VII.1 Preliminary cost breakout of the RISP accelerator system**

The costs for accelerator systems are estimated on the component basis. Costs for the experimental setup include the experimental equipment and major detectors for the science programs described in Chapter II and IV. The detailed cost estimation based on the single item will be provided in the Technical Design Report.

## VII.2 Schedule

The construction schedule is rather tight to complete civil construction and accelerator installation by February 2018. The construction schedule as shown in the Figure VII.1 is planned to achieve the goal.

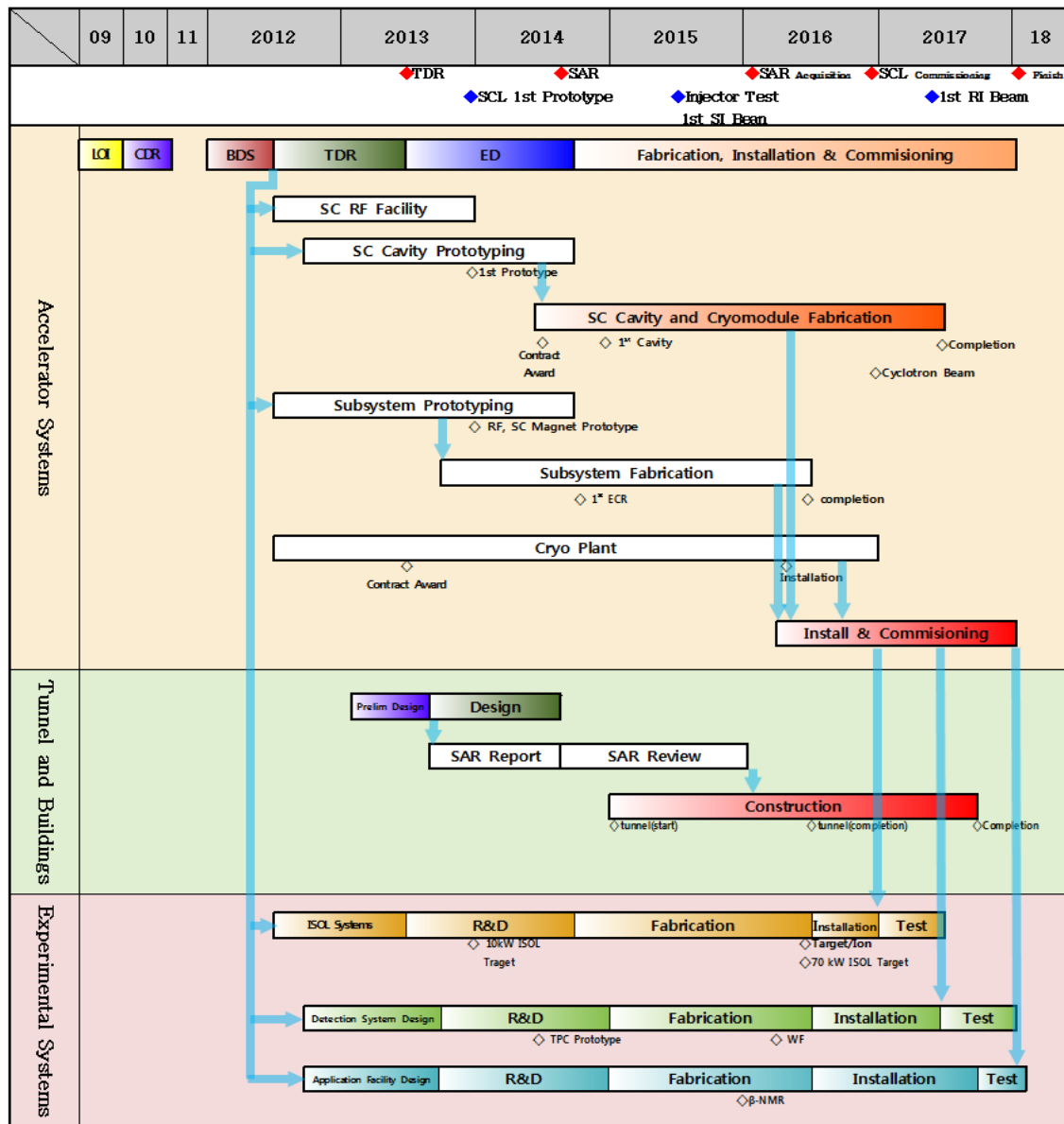


Figure VII.1 Construction schedules for RISP